JPRS L/9129

6 June 1980

USSR Report

EARTH SCIENCES

(FOUO 5/80)

FBIS FOREIGN BROADCAST INFORMATION SERVICE

NOTE

JPRS publications contain information primarily from foreign newspapers, periodicals and books, but also from news agency transmissions and broadcasts. Materials from foreign-language sources are translated; those from English-language sources are transcribed or reprinted, with the original phrasing and other characteristics retained.

Headlines, editorial reports, and material enclosed in brackets [] are supplied by JPRS. Processing indicators such as [Text] or [Excerpt] in the first line of each item, or following the last line of a brief, indicate how the original information was processed. Where no processing indicator is given, the information was summarized or extracted.

Unfamiliar names rendered phonetically or transliterated are enclosed in parentheses. Words or names preceded by a question mark and enclosed in parentheses were not clear in the original but have been supplied as appropriate in context. Other unattributed parenthetical notes within the body of an item originate with the source. Times within items are as given by source.

The contents of this publication in no way represent the policies, views or attitudes of the U.S. Government.

For further information on report content call (703) 351-2938 (economic); 3468 (political, sociological, military); 2726 (life sciences); 2725 (physical sciences).

APPROVED FOR RELEASE: 2007/02/08: CIA-RDP82-00850R000200090015-4

JPRS L/9129

6 June 1980

USSR REPORT

EARTH SCIENCES

(FOUO 5/80)

CONTENTS

METEOROLOGY

COMPLEX ACTIVE-PASSIVE SOUNDING OF CLOUD COVER

Leningrad TRUDY GLAVNOY GEOFIZICHESKOY OBSERVATORII: METODY AKTIVNOY I PASSIVNOY RADIOLOKATSII V METEOROLOGII No 411, 1978 pp 3-12

[Article by G. G. Shchukin, L. P. Bobylev , Ya. K. Il'in, A. I. Lyashko, N. F. Mikhaylov, N. I. Novozhilov, N. D. Popova]

[Text] The methods of active and passive radar sounding are being used successfully to solve an entire series of meteorological problems [7]. Both methods taken separately have their disadvantages and advantages, which is also determined by the specific nature of the problem at hand. Thus, when providing storm warnings the best results are obtained by the active radar method at the same time as when determining temperature and moisture profiles preference is given to the radiothermal location method. The fact that none of the remote methods of electromagnetic sounding provides sufficiently complete information about the physical state of the cloud atmosphere indicates the necessity for complex utilization of them. When estimating the parameters of the cloud atmosphere the characteristics of the reflected signal and the natural thermal radio wavelength emission of the investigated target must be obtained synchronously.

The complex utilization of the active-passive radar method appears to be the most prospective for diagnosing the state of cloud systems in order to estimate their suitability for the use of artificial means of regulating precipitation. It is expedient to use the same complex method also to monitor the results of the indicated active inputs.

To study the possibility of solving the above-enumerated problems, the GGO [Main Geophysics Observatory] has developed a model of an active-passive radar based on the MRL-2. In addition, a procedure has been developed for determining the parameters of the cloud atmosphere, and it has been checked out experimentally under field conditions.

Active-Passive Radar Complex

For complete matching of the thermal location and radar information in time and space, simultaneous operation of a radiometer and radar on one antenna is necessary. This operation is possible only under the condition of solving

the problem of electromagnetic compatibility inasmuch as the radiometer is a very highly sensitive instrument, and to eliminate interference from the powerful pulses of an active radar, decoupling of less than 120 decibels is required between them [4]. Another aspect of joint operation of the radiometer and radar is preference for a technical design which will not require significant alterations in either the radiometer or radar circuitry.

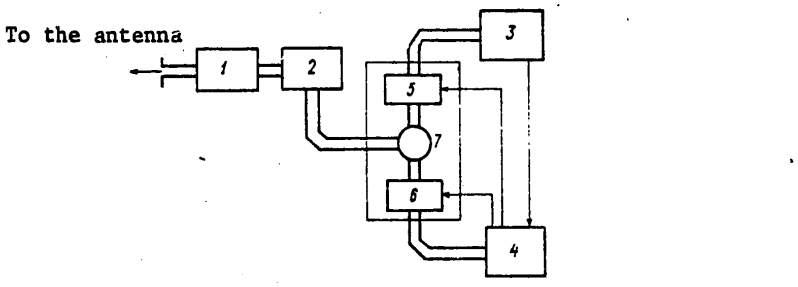

Figure 1. Block diagram of an active-passive radar complex operating on λ = 3.2 cm. 1 -- discharger (R), 2 -- MRL noise generator (GSh), 3 -- MRL receiver, 4 -- radiometer (RM), 5 -- pin I attenuator, 6 -- pin III attenuator, 7 -- commutator (K).

The Main Geophysics Observatory has developed a joint active-passive complex based on the standard MRL-2 mobile radar and a modulation radiometer operating on a wavelength of λ = 3.2 cm with a sensitivity ZK (sic) for a time constant of τ = 1 sec. The design of the complex follows.

A superhigh frequency commutator (K) based on pin-diodes on a double T-bridge (see Figure 1) is built in between the noise generator (GSh) of the MRL-2 radar and its receiver input. From one of the outputs of this commutator the signal goes to the input of the MRL-2 receiver; from the other output it goes to the input of the radiometer. The modulation frequency of the radiometer is equal to the sending frequency of the radar. The reference voltage of the radiometer is generated by a special generator which is synchronized by the MRL-2 start pulse and will permit a reference voltage phase shift.

The commutator (K) is controlled by the reference voltage of the radiometer. The reference voltage phase is established in such a way that by the time t_1 (see Figure 2) directly before the beginning of the pulse of the MRL noise generator, the radiometer input will be closed. In this case, the pin II attenuator is closed, and the signal from the antenna goes through the commutator (K) to the input of the MRL receiver, insuring normal functioning of the MRL. Here the decoupling of the radiometer and the MRL is defined as the sum of the attenuations of the pin II attenuator and the internal superhigh frequency commutator of the radiometer. Two of the type AP-5 pin-diodes, which are series included, and each of which introduces an attenuation of 40 decibels, are used as the pin II attenuator. The attenuation

introduced by the internal superhigh frequency commutator of the radiometer will be 30 decibels; consequently, the total decoupling of the radiometer and the MRL with respect to the wave guide channel will be 110 decibels. The additional decoupling of the radiometer and the MRL is achieved by selecting the frequency characteristics of the channels of the intermediate frequency amplifier of the radiometer and the MRL in accordance with the recommendations of [4], and it amounts to about 30 decibels. Thus, the total decoupling will be about 140 decibels, which, within the limits of accuracy of the measurements, completely excludes the effect of the MRL on the radiometer.

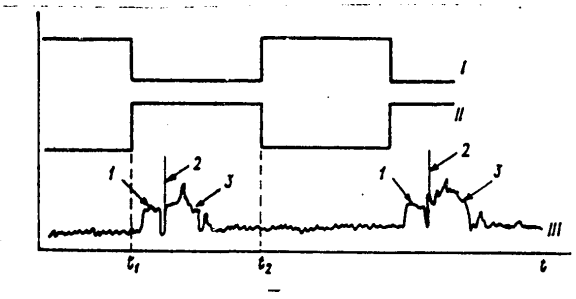

Figure 2. Diagram of the operation of the active-passive complex. I -- pin I voltage diagram, II -- pin II voltage diagram, III -- MRL and radiometer signal; 1 -- signal of the MRL noise generator, 2 -- MRL pulse, 3 -- echo.

At the time t_2($t_2 - t_1 = (1/2)T$, where T is the time between the two pulses of the MRL transmitter) the pin II attenuator opens, connecting the radiometer input to the antenna of the complex. In this case the attenuator pin I closes. The time t_2 corresponds to the MRL-2 range of 90 km where the echo is absent during operation of the complex in the near zone. Here the decoupling decreases to 30 decibels, but in view of the absence of the MRL echo, this is entirely adequate.

In order to eliminate the influence of the MRL discharger (R) in the preionization state on the radiometer, instead of a dc voltage of 700 volts, a 700 volt meander is fed to the discharger which coincides with respect to phase with the control voltage $U_{\text{pin II}}$ (see Figure 2).

This operating mode of the complex insures normal functioning of the modulation radiometer and the MRL-2 with reduction of the range of the latter to 90 km.

The advantages of the described complex are the following:

1) a high degree of decoupling of the radiometer and the MRL;

2) simplicity of structural design;

3) the possibility of using any radiometer in the three-centimeter range in the complex.

The deficiencies must include the following:

1) large losses in the wave guide channel of the MRL from the antenna to the input of the receiver (4.5 decibels), which leads to a noticeable decrease in the actual sensitivity of the radiometer;

2) high requirements on the phase stability of the reference voltage of the radiometer;

3) reduction of the MRL range to 90 km (the latter directly when operating in the near zone).

Estimation of the Water Reserve and the Water Content Profile of the Cloud Using the Active-Passive Radar Complex

By using an active-passive radar complex operating on a wavelength of λ = = 3.2 cm, it is possible to estimate both the water reserve of the cloud and the water content distribution in it in the direction of the maximum of the antenna radiation pattern. In order to determine the water reserve of a cloud during measurements of the radiothermal emission on one wavelength it is possible to use the method of radio brightness contrast. The radio-brightness contrast [1] is defined as the difference of the radio brightness temperature of the cloud atmosphere at the zenith angle θ and the radio-brightness temperature of the same atmosphere without considering the clouds. It is possible to measure this contrast directly only by using the radiometer, scanning by the antenna at a fixed zenith angle from the cloud to the section of clear sky. However, this does not always appear possible. Therefore in the given paper the radio brightness temperature of the pure atmosphere was calculated by the radio sounding data (the radio sounding station is located along side the radiomeasuring test area).

The radiobrightness contrast is related to the water reserve of the clouds by a correlation. In order to find this correlation, model calculations were performed on the BESM-6 computer. Models investigated in reference [3] were taken as the models of the cloud atmosphere. These models describe the real atmosphere of the northwestern part of the European Territory of the USSR. Data files on the pressure, temperature and humidity profiles obtained using radiosounding in Voyeykovo in the summer are used for the calculations. Each element of the given files (each specific situation of the cloud atmosphere) was randomly assigned values of the altitudes of the lower and upper boundaries of the cloud layer and also its water content (water content within the limits of the cloud layer was considered constant). The indicated parameters and also the water reserve of the cloud were calculated by the formulas:

$$w = \overline{w} + S_1 \sigma_w, \qquad (1)$$

$$Z_H = \overline{Z}_H + S_2 \sigma_{Z_H}, \quad (2)$$

$$Z_B = \overline{Z}_B + S_3 \sigma_{Z_B}, \quad (3)$$

$$W = w(Z_B - Z_H), \quad (4)$$

where w is the water content, g/m^3; Z_H, Z_B are the altitudes of the lower and upper cloud boundaries, km; W is the water reserve, kg/m^2. The bar over the symbol denotes average values, and the letter σ denotes the mean square deviations. The average values and the mean square deviations of the cloud cover parameters were selected in accordance with the type of cloud cover [3] which was observed for the given case of radio sounding. In formulas (1)-(3), S_1, S_2 and S_3 denote the quasirandom numbers distributed according to a normal law. In order to obtain them, a random number generator was used from the library of standard programs for the BESM-6 computer.

The calculation of the specific absorption coefficient which is needed for calculating the radiobrightness temperature was made using the procedure described in reference [2].

The radiobrightness contrast as a function of the water reserve of the clouds (in the vertical direction) for λ = 3.2 cm was calculated for 4 values of the zenith angle: θ = 70, 80, 85 and 89° (without considering refraction). This range of angles corresponds to the range of operation of the active-passive complex. As was noted, the correlation between W and ΔT_{bright} is linear. Since our problem is estimation of W by the measured values of the contrast $\Delta T_{bright}(\theta)$, the relation between the given values is conveniently found in the form

$$\hat{W} = (\varphi \pm \sigma_\varphi)\, \Delta T_{\text{a}}(\theta), \quad (5)$$

(a)

Key: a. bright

where ϕ is the regression coefficient, and σ_ϕ is the mean square deviation of this coefficient. The values of ϕ and σ_ϕ found by the least squares method are presented in Table 1. In order to have the possibility of estimating the water reserve with respect to the contrast measured at any angle from the investigated range it is necessary to know the coefficient ϕ for all values of θ. The dependence of ϕ on θ is linear. Consequently,

$$\varphi = \varphi_1 + \varphi_2 \theta. \quad (6)$$

It is easy to find values of ϕ_1 and ϕ_2:

$$\varphi_1 = 0{,}3436; \quad \varphi_2 = -0{,}0038. \quad (7)$$

Finally,

$$\hat{W} = [0{,}3436 - 0{,}0038\,\theta]\,\Delta T_s(\theta). \tag{8}$$

It is necessary to note that in the given case we have in mind the water reserve of the cloud in the vertical direction. In order to find the water reserve of a cloud along the direction of the maximum of the radiation pattern of the antenna, it is necessary to multiply the vertical water reserve by sec θ.

In order to restore the water content profile in the cloud it is possible to use the value of the water reserve obtained by the radiometer and the radar reflectivity profile obtained using the MRL [5]. The initial position is the known relation between radar reflectivity and the water content [6]:

$$Z = Aw^b, \tag{9}$$

where A and b are the unknown parameters. The parameter b can vary from 1 to 2 [6]. In reference [6] it is recommended that a value of b = 2 be selected for the cumulonimbus clouds which are the object of investigation of this paper. Hence,

$$\sqrt{Z} = \sqrt{A}w. \tag{10}$$

Knowing the reflectivity profile in the direction $\vec{\ell}$, it is possible to integrate expression (10):

$$\int_{\vec{l}} \sqrt{Z}\,dl = \sqrt{A}\int_{\vec{l}} w(l)\,dl = \sqrt{A}\,W_l, \tag{11}$$

where W_ℓ is the water reserve of the cloud in the direction $\vec{\ell}$. This makes it possible to find the value of the parameter A:

$$A = \left\{\int_{\vec{l}} \sqrt{Z}\,dl\right\}^2 \Big/ W_l^2. \tag{12}$$

Now, knowing the parameter A, it is possible to determine the water content at any point of the cloud in the direction $\vec{\ell}$ by the formula

$$w(l) = \sqrt{Z(l)}/\sqrt{A}. \tag{13}$$

Experiment and Analysis of the Results

During the summer of 1977 on the active-passive radar complex (λ = 3.2 cm) installed at the test area of the Main Geophysics Observatory in Voyeykovo, a series of observations were made on the cumulonimbus clouds (Cb). Radiosounding of the atmosphere was performed during the observations.

Table 1. Values of the regression coefficient and its mean square deviation as a function of $W = (\phi \pm \sigma_\phi)\Delta T_{bright}$ for $\lambda = 3.2$ cm

	$\theta°$			
	70	80	85	89
φ	0,081	0,043	0,024	0,009
σ_φ	0,008	0,004	0,002	0,001

Table 2. Experimental results using the active-passive radar complex ($\lambda = 3.2$ cm) on 3 July 1977.

Time		Coordinates		$T_{br.exp}$ K	$T_{br.clear}$ K	$\Delta T_{br.}$	W_l кг/м²	$Z_н$ км
hrs	min	azimuth	elevation					
9	08	165	7,5	68,7	28,4	40,3	10,50	0,24
9	12	187	10,0	53,3	19,7	33,6	8,35	0,24
13	52	36	20,0	59,6	10,2	49,4	11,75	0,57
14	21	133	20,0	82,7	10,2	72,5	17,25	0,40
14	21	133	30,0	68,7	7,02	61,68	14,80	0,40

Note. $T_{bright\ exp}$ is the experimental value of the radiobrightness temperature, $T_{bright.clear}$ is the value of T_{bright} for a clear sky, ΔT_{bright} is the radiobrightness contrast, W_ℓ is the water reserve of the cloud in the sounding direction, Z_H is the altitude of the lower cloud boundary.

The investigated thick Cb were selected using the MRL plan position indicator. In order to obtain the radar reflectivity, a signal from an oscillograph was recorded on photographic film using the FARM photo attachment. In order to avoid obtaining clipped signals, damping was introduced and the corresponding isoecho level was selected. The photography was done with each decrease in damping by 6 decibels. By the series of frames obtained for each sounding direction, graphs were constructed of the variation of reflectivity along the sounding beam.

In order to determine the antenna temperatures the radiometer was calibrated with respect to the "zenith." Here the calculation of the radiobrightness temperature of the clear sky when observing in the zenith was made by the radiosounding data. On the observation days, an analysis was made of the synoptic conditions and the nature of the cloud-forming processes.

For analysis of the experimental results a series of observations of the Cb on 3 July 1977 was selected. On that day a cold front passed in the morning

with low stratiformis dropping in places to 50 meters. During the day active convection, showers and thunderstorms were observed in the unstable air mass behind the front.

Table 2 gives the results of sounding the Cb on 3 July 1977. With respect to magnitude of the water reserve of the cloud along the sounding beam and with respect to the reflectivity profile, water content profiles were reproduced. Figure 3 shows the result of this reproduction for 0912 hours on an azimuth of A = 187° and with an elevation of β = 10°. The figure shows the profile of the logarithm of the radar reflectivity lg Z and the water content profile w, g/m^3. As is obvious from the figure, the course of the water content profile repeats the course of the lg Z profile. The values of the water contents themselves (maximum ≈4 g/m^3, average ≈1-1.5 g/m^3 correspond completely to the water content of the Cb which can be observed [3].

In order to coordinate the reproduced profile of the water content with the cloud Figure 4 gives the picture of the cloud system obtained using the IDV of the MRL-2 on the near azimuth (A = 164°). Of course, the difference in azimuth of 23° does not permit exact coordination of the reproduced water content profile with the cloud which was observed using the active-passive complex. However, it is possible nevertheless to make some defined remarks. The first three peaks of the water content profile are for cloud I. In the free space between clouds I and II, the water content in practice drops to zero. Then the growth of the water content with the local maximum for a distance of ≈10-11 km from the active-passive complex is observed. This maximum corresponds to cloud II. Then the water content gradually decreases, dropping to zero. This corresponds to the fact that the sounding beam (it is shown as a solid straight line in Figure 4) passes through the upper layers of the cloud at an altitude of 3-4 km. Either insignificant water content or crystalline phase is observed in these layers.

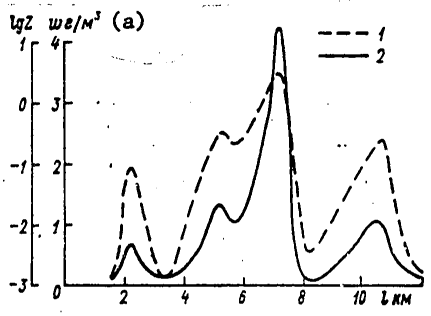

Figure 3. Profile of the logarithm of the radar reflectivity (1) and the reproduced water content profile (2) corresponding to the case of sounding the Cb on 3 July 1977.

Key: a. g/m^3

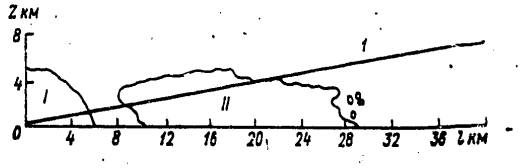

Figure 4. Diagram of a cloud system obtained on the IDV of the MRL on 3 July 1977 (0912 hours) on an azimuth of A = 164°. I -- first Cb cloud, II -- second Cb cloud, 1 -- direction of the sounding beam of the active-passive complex.

It must be noted that, unfortunately, during observations of the Cb using the active-passive complex, direct aircraft sounding to obtain direct data on the water content is impossible. This does not permit comparison of the reproduced water content profile with the actually existing water content profile in the cloud. Such a comparison can be realized, however, for the aqueous nimbostratus clouds (Ns), aircraft sounding of which is possible.

Conclusions

The experimental observations of the cumulonimbus clouds using the active-passive complex demonstrated that the proposed procedure for estimating the water reserve of the cloud and reproducing the water content profile along the sounding beam is prospective for the complex investigation of cloud systems. These cloud parameters are highly important when diagnosing the suitability of cloud systems for weather modification to regulate precipitation and monitor the results of these weather modification operations. However, the authors admit that the effect depends to a significant degree on the evolution of the clouds observed at the given time and the changes which occur in the moisture content characteristics themselves with time. In order to discover the cloud evolution, a special observation procedure is needed, above all a sufficiently high frequency of observations of the same cloud center inasmuch as another center (another mesosystem) can be in a different stage of development and undergo its own evolution. It is also necessary to include a procedure for estimating the integral water vapor content in the complex method in order to have the possibility of tracing the redistribution of two water phases in the cloud with time.

The development of the complex methods of cloud sounding considering the stated remarks and also the methods of analyzing the physical processes of cloud formation based on active-passive radar equipment is the next goal of the collective of authors.

BIBLIOGRAPHY

1. L. P. Bobylev, M. A. Vasishcheva, A. I. Novoselov, et al., "Study of the Water Content of Clouds Using the Three-Centimeter Radiometer," TRUDY GGO (Works of the Main Geophysics Observatory), No 328, 1975, pages 50-55.

2. L. P. Bobylev, M. A. Vasishcheva, G. G. Shchukin, "Determination of the Integral Moisture Content Parameters of a Cloud Atmosphere Directly by the Values of the Radiobrightness Temperature," TRUDY GGO, No 395, 1977, pages 59-67.

3. M. A. Vasishcheva, G. G. Shchukin, "Experimental Study of the Water Content of Clouds. Statistical Models of the Atmosphere," OBZOR VNIIGMI--MTSD, SER. METEOROLOGIYA (VNIIGMI Survey -- MTsD, Meteorology Series), Obninsk, 1976, 94 pages.

4. N. V. Gornostayev, A. I. Novoselov, V. A. Petrushevskiy, et al., "Active-Passive Radar for Studying the Atmosphere," TRUDY GGO, No 328, 1975, pages 120-124.

5. N. D. Popova, G. G. Shchukin, "Procedure for Determining the Water Content Profile in Clouds by the Passive-Active Radar Method," TRUDY GGO, No 395, 1977, pages 68-71.

6. V. D. Stepanenko, RADIOLOKATSIYA V METEOROLOGII (Radar in Meteorology), Leningrad, Gidrometeoizdat, 1973, 343 pages.

7. V. D. Stepanenko, G. G. Shchukin, G. B. Brylev, "Active and Passive Radar Sounding of Clouds, Precipitation and Thunderstorms," SOVREMENIYE FUNDAMENTAL'NYYE I PRIKLADIYYE ISSLEDOVANIYA GLAVNOY GEOFIZICHESKOY OBSERVATORII IM. A. I. VOYEYKOVA (Modern Basic and Applied Research of the Main Geophysics Observatory imeni A. I. Voyeykov), Leningrad, Gidrometeoizdat, 1977, pages 77-87.

10845
CSO: 8144/1073

SOME POSSIBILITIES OF USING THE SYNTHETIC APERTURES METHOD FOR OBSERVING METEOROLOGICAL TARGETS

Leningrad TRUDY GLAVNOY GEOFIZICHESKOY OBSERVATORII: METODY AKTIVNOY I PASSIVNOY RADIOLOKATSII V METEOROLOGII No 411, 1978 pp 107-112

[Article by Yu. A. Mel'nik]

[Text] One of the most significant achievements in radar theory and engineering in recent decades was the development of the synthetic apertures method which made it possible to increase the resolution of the radar systems for surveying the earth's surface to values commensurate with optical devices [1].

As is known, this method is based on using the a priori data on the law of variation of the signal phase where during the process of radar observation the target is shifted relative to the radar by a known law. For the harmonic sounding oscillation with a frequency ω the echo of the point target

(1)

turns out to be modulated. The variation of the amplitude S is usually neglected; the signal phase $\phi(t)$ is determined by the distance R to the target. If the law of displacement of the target R(t) is known, the received signal can be subjected to optimal processing which for the regular component of the signals is defined by the expression

$$Q(\tau) = \int_0^t s(t)\, s(t-\tau)\, dt. \qquad (2)$$

Its maximum value $Q_M = (1/2)S^2T$ is proportional to the signal energy for the observation time T.

The optimal processing leads to the "compression" of the signal insuring high resolution of the system. Thus, for example, it is known that in the radar for surveying the earth's surface the accumulation of the signal on the path of movement of the radar d_c is equivalent to the use of a large synthetic antenna of dimension d_c which at a range R_0 determines the linear

resolution $\Delta x = \lambda/d_c R_0$, where λ is the wavelength. The maximum possible path on which the signal is received in turn depends on the beam width of the real antenna (that is, on its aperture d), and it is $d_c = \lambda R_0/d$. From these expressions it follows that the admissible value of the resolution along the direction of movement is equal to the aperture of the real antenna installed on the aircraft.

The method of synthetic antennas can be extended to the case of a set of targets made up of particles which move by given laws. The processing system can be designed for isolation of the total signal of all the elementary reflectors, the parameters of motion of which $\nu_1, \nu_2, \ldots, \nu_n$ lie within certain limits $\nu_1 \pm \Delta\nu_1, \nu_2 \pm \Delta\nu_2, \nu_n \pm \Delta\nu_n$. The result of the processing for the observation time T is proportional to the energy of the signal characterizing the reflectivity of certain particles in the irradiated space, the parameters of which lie within the indicated limits. The set of these limits establishes the region of indeterminacy, inside which it is impossible to measure the specific values of the parameters.

The region of determinacy depends on the characteristics of the radar and the observation conditions. In the special case it can turn out that all the limits $\Delta\nu_i$, with the exception of one (for example, $\Delta\nu_1$) exceed the maximum actually possible variations of the corresponding parameters of motion. In this case the system for type-space coherent processing of the signals is the meter that measures the number of particles, the parameter of motion of which ν_1 is within the limits of $\nu_1 \pm \Delta\nu_1$. Being given various values of the parameter as a result of the time-space processing of the signal, it is possible to determine the particle distribution ν_1 by this parameter with the resolved interval $\Delta\nu_1$.

For the solution of the stated problem it is necessary to determine how the output effect of the optimal processing system varies if the parameters of motion of the elementary targets deviate from the given values. For this purpose it is expedient to introduce a generalized parameter in terms of which the deviations $\Delta\nu_i$ of the specific investigated values of ν_i can be expressed. The phase lead -- the increment of the signal phase for the observation time T -- is the generalized detuning parameter under certain assumptions easily made in practice.

Let us propose that under other invariant conditions the actual law of motion of the target differs somewhat from the given one, and the received signal is defined by the formula

$$s(t) = S\cos[\omega t + \varphi(t) + \varphi'(t)], \qquad (3)$$

where $\phi'(t)$ is the phase increment by comparison with the calculated $\phi(t)$. In this case the output effect of the system can be represented by the expression

$$Q = \frac{S^2}{2} \int_0^T \cos \varphi'(t)\, dt. \tag{4}$$

Let us define the relative value of the output effect $\psi = Q/Q_M$ considering that the deviation of the phase of the given law takes place linearly:

$$\varphi'(t) = \varphi' t/T \tag{5}$$

and at the end of the observation interval the phase lead reaches a value of ϕ'. Here the output effect of the processing system

$$\psi = \sin \varphi'/\varphi' \tag{6}$$

depends only on the phase lead. For a small phase lead where the processing system in practice is matched with the signal, the value of ψ is equal to one. As the phase lead increases (for $\phi' > \pi/2$) the output effect ψ assumes different values within the limits of zero to $1/\phi'$. The maximum of this value

$$\psi = 1/\varphi' \tag{7}$$

can be considered a response to the signal of the given detuned filter.

The phase lead is a function of the parameters of motion of the target. The variation of some parameter ν by comparison with the calculated value leads to the appearance of the phase lead ϕ' and attenuation of the output effect by $1/\phi'$ times. If we consider the output effect as a function of several parameters ν_1, ν_2, ..., ν_n, the deviations of these parameters from the calculated values (ν_1', ν_2', ..., ν_n') and the attenuation of the output effect caused by them are characterized by the indeterminacy function $\psi(\nu_1', \nu_2', \ldots, \nu_n')$. Geometrically the function can be represented by the indeterminacy body in the (n + 1)-dimensional space. The boundaries of the region of indeterminacy can be given by attenuation of the output signal to the level of ψ_0 or the resolved phase lead corresponding to it $\Delta\phi = 1/\psi_0$.

Thus, the region of indeterminacy is the cross section of the body of indeterminacy on the level $\psi_0 = 1/\Delta\phi_0$ and can be represented by the equation

$$\psi(\Delta \nu_1, \Delta \nu_2, \ldots, \Delta \nu_n) = 1/\Delta \varphi. \tag{8}$$

The small phase lead

$$\varphi' = 1/\psi(\nu_1', \nu_2', \ldots, \nu_n'),$$

which is a function of the small deviations of the parameters of motion ν_1', ν_2', ..., ν_n' from the calculated values, can be expressed in terms of these deviations as

$$\varphi' = \frac{\partial \varphi}{\partial \nu_1}\nu_1' + \frac{\partial \varphi}{\partial \nu_2}\nu_2' + \ldots + \frac{\partial \varphi}{\partial \nu_n}\nu_n'. \qquad (9)$$

This makes it possible to find the region of indeterminacy considering the effect of each parameter on the phase lead separately.

For illustration of the possibilities of the method let us consider the example of radar observation of the precipitation, assuming that the speed of the particles v is constant and is directed vertically. Let us find the region of indeterminacy when the observation is made by the ground coherent radar (see Figure 1), and the synthesizing is done as a result of the natural movement of the particles. With accuracy to the constant coefficients the expression (9) for this case can be represented in the form

$$\Delta h \frac{vT}{\lambda R_0} + \Delta v_T \frac{vT^2}{\lambda R_0} + \Delta v_r \frac{T}{\lambda} = 1, \qquad (10)$$

where Δh is the resolution with respect to altitude, Δv_r and Δv_T are the resolutions with respect to radial and tangential velocity, respectively.

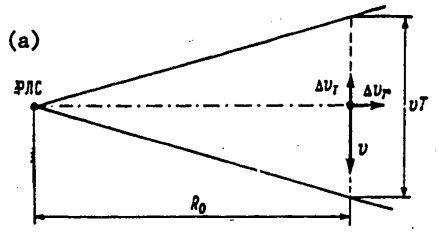

Figure 1. Synthesizing as a result of the natural motion of the particles of the ground coherent radar.

Key: 1. radar

The limiting values of each of the indicated resolutions (under the condition that the remaining parameters have rated values) are presented in Table 1. As follows from the data in the table, with small accumulation time the system is the standard meter of the radial velocity of the particles. However, for a large observation time there is sufficiently high resolution with respect to the tangential component of the velocity which is unusual for the existing doppler systems.

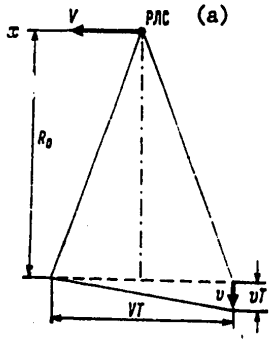

Figure 2. Synthesizing as a result of motion of the radar.

Key: a. radar

Table 1. Limiting resolution with respect to altitude (Δh) of the tangential (Δv_T) and radial (Δv_r) velocity of the particles as a function of the observation time T for the stationary ground radar with a distance R_0 = 300 km, wavelength λ = 3 cm and particle velocity v = 5 m/sec.

	T sec			
	0,1	1	10	100
Δh м	18000	1800	180	18
Δv_T м/sec	$1{,}8 \cdot 10^5$	1800	18	0,18
Δv_r м/sec	0,3	0,03	0,003	0,0003

Table 2. Limiting resolution along the path (Δx) and with respect to the particle velocity (Δv) as a function of the observation time T for radar moving with a velocity v = 7.5 km/sec for R_0 = 300 km, λ 3 cm and v = 5 m/sec.

	T sec		
	0,01	0,1	1
Δx м	80	8	0,8
Δv м/sec	3	0,3	0,03

Let us consider another, theoretically different case where the synthesizing is realized as a result of the movement of the radar. Let us propose that the speed of the carrier V = 7.5 km/sec, and the altitude from which the observation is made (R_0) is 300 km (see Figure 2). The equation of the

Table 3. Limiting resolution along the path (Δx), with respect to altitude (Δh) and velocity of the particles (Δv) as a function of observation time T for radar moving with a velocity of 700 km/hr for R_0 = 3 km, λ = 3 cm and v = 5 m/sec

	T sec		
	0,01	0,1	1
Δx м	50	5	0,5
Δh м	500	50	5
Δv м/sec	3	0,3	0,03

region of indeterminacy for this case can be approximately represented in the form

$$\Delta x \frac{VT}{\lambda R_0} + \Delta v \frac{T}{\lambda} = 1. \tag{11}$$

As follows from the data in Table 2 for a comparatively small time of signal accumulation there are quite high values of the resolution with respect to the speed of the particles (Δv) and the position of the observed volume along the direction of motion of the carrier (Δx). The system is not sensitive to the remaining parameters.

The resolutions of Δx and Δv can either be positive or negative. Therefore formula (11) defines four straight lines in the coordinates x;, v' with respect to the rated values of x and v. The region defined by these straight lines (see Figure 2) includes the set of parameters of motion of the particles, the signals of which are released by the processing system.

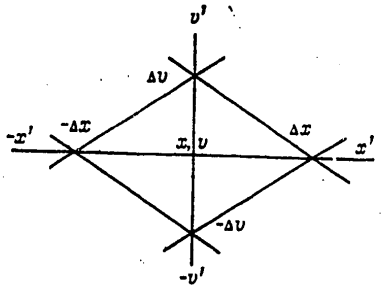

Figure 3. Region of parameters of motion of particles, the signals of which are generated by the processing system.

Analogously to formulas (10) and (11), the expression can be obtained for the region of indeterminacy where the observation is made from an aircraft. As

follows from the data in Table 3, the system has some resolution with respect to altitude which is explained by the comparatively small removal of the observed region.

Thus, the method of synthetic apertures is theoretically applicable for observation of meteorological targets. However, for determining the practical possibilities of its realization and estimating the effectiveness, special studies are required.

BIBLIOGRAPHY

1. A. P. Reutov, B. A. Mikhaylov, G. S. Kondratenko, et al., RADIOLOKATSIONNYYE STANTSII BOKOVOGO OBZORA (Side Viewing Radar), Moscow, Sovetskoye radio, 1970, 360 pages.

10845
CSO: 8144/1073

OBSERVATIONS OF FRONTS IN THE POLYMODE AREA

Moscow OKEANOLOGICHESKIYE ISSLEDOVANIYA in Russian No 30, 1979 pp 86-88

[Article by A. G. Zatespin, A. Yu. Krasnopevtsev, K. N. Fedorov]

[Text] The existence of fronts in the Sargasso Sea is a well-known fact [1, 2]. However, the subtropical convergence zone intercepting the Sargasso Sea is a large-scale front separating the more saline and warmer southern waters and the fresher and colder northern waters. The results obtained by A. D. Voorhis, et al. [2] indicate that the temperature fronts occur at the boundaries of the "tongues" of warm and cold water which are caused by affective transport by the geostrophic currents connected with the eddies. The opinion has been stated that the fronts in the ocean are well to be seen in the fall and winter period, and in the summer they are masked by warming of the upper layer. On the 25th trip of the "Akademik Kurchatov" scientific research ship, an effort was made to generalize this scattered information about the fronts which can be extracted from the data of synchronous density surveys, from direct measurements of the current velocities, towing of a thermistor and measurement by a thermal-salinity probe on the path of the ship in the region of expeditionary operations. As a result, it is possible to draw the following conclusions.

1. In spite of the masking effect of the summer warming, the fronts in the vicinity of the test area are comparatively easily detected by the temperature and salinity measurements in the surface layer of the ocean. The density survey also permits determination of the approximate position of the fronts. The sharpest fronts were in September, which is explained by sharpening of the zonal temperature and salinity gradients. These gradients were smallest in August. During the time of the operations in the test area, 13 cases of intersection of fronts by the ship were recorded. The temperature gradients on the fronts fluctuated from 0.2 to 2.0°C; the salinity gradients fluctuated from 0.2 to 0.4 parts per thousand. Gradients from 0.1 to 2.5 deg/km and from 0.1 to 0.2 parts per thousand/km corresponded to them. On the average the temperature gradient was 0.2 to 0.3 deg/km.

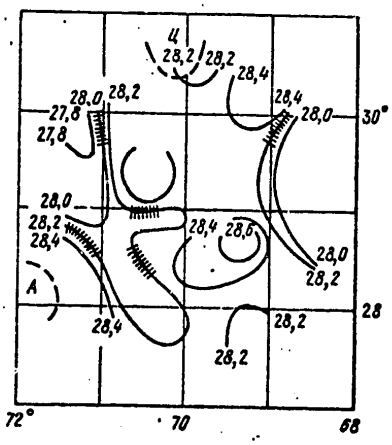

Figure 1. Temperature at a depth of 10 meters (September): Ц -- cyclone center; A -- anticyclone center. The regions of location of the fronts are cross hatched.

2. The fronts detected in the test area were characterized by positive correlation of the temperature and salinity gradients with far from complete compensation with respect to density. Here the density gradient was more frequently determined by the temperature contribution than the salinity contribution.

3. The data of the density and the XBT-surveys confirmed the results of A. D. Voorhis, et al. [3] pertaining to the existence of the warm and cold "tongues" of the advective origin connected with the dynamics of the eddies. We have noted an analogous picture also in the salinity distribution, that is, the "tongues" and "spots" of more saline and fresher water were detected. This structure of the temperature and salinity fields was correlated with the structure of the eddy field. Usually the fronts are located on the boundaries of the "tongues" and "spots." Fig 1 shows the temperature map on which the cyclone and anticyclone centers are indicated. The fronts were located in the crosshatched zones.

4. In the vertical sections the fronts are traced to the upper boundary of the layer of 18-degree water (100-200 meters) and obviously do not penetrate deeper. This is also confirmed by the T, S-diagrams of the vertical temperature and salinity distributions with respect to different sides of the fronts; they are analogous to the T, S-diagrams obtained in their time by E. J. Katz [1].

It is important to note that an explicit relation of the front positions to the structure of the eddy field and to the vertical thermochaline structure of the deep water has been detected. The fronts are located above the peripheral regions of the eddies where maximum deviations of the isotherms and isochalines of the principal thermocline are observed.

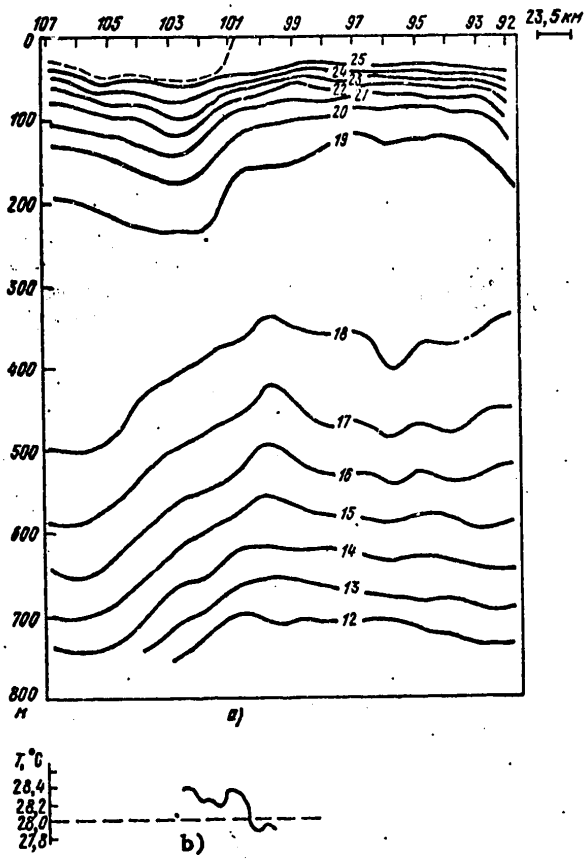

Figure 2. Vertical section in the temperature field according to the data from the XBT-survey (a), recording of the surface temperature (b)

As direct measurements show, these regions correspond to the maximum orbital current velocities in the eddies. Fig 2 shows the vertical section in the temperature field. In Fig 2 the curve reproducing the section of the analogous temperature recording recorded by the towed gauge indicates the position of the front on the surface in the scale of the section. The problem arises of whether the fronts are not characteristic "conductors" between the surface and abyssal layers which promote heat and mass exchange through the thermocline. According to the opinion of Voorhis, et al. [3], by means of the above-described "tongues" of water of advective origin connected with the eddies, horizontal heat transfer is realized. It is not excluded that the eddies have a significant influence also on the vertical transfer through the fronts occurring on their interaction. Hence, it is clear that the program for further

research should include the study of the vertical structure of the fronts and their interaction with the eddy field.

Abstract

The relation of the temperature-salinity fronts in the ocean surface layer to the large-scale surface temperature and salinity fields and the eddy field structure in a thermocline is analyzed.

BIBLIOGRAPHY

1. Katz, E. J. "Further Study of a Front in the Sargasso Sea," TELLUS, Vol XXI, No 2, 1969, pp 259-269.

2. Voorhis, A. D.; Hersey, j. B. "Oceanic Thermal Fronts in the Sargasso Sea," J. GEOPHYS. RES., Vol 69, No 18, 1964, pp 3809-3814.

3. Voorhis, A. D.; Schroeder, E. H.; Leetmaa, A. "The Influence of Deep Mesoscale Eddies on Sea Surface Temperature in the North Atlantic Subtropical Convergence," J. PHYS. OCEANOGR., No 6, 1976, pp 953-961.

[8044/0785-10845]

10845
CSO: 8044/0785

STUDY OF TEMPERATURE FLUCTUATIONS WITH INERTIAL AND DIURNAL PERIODS

Moscow OKEANOLOGICHESKIYE ISSLEDOVANIYA in Russian No 30, 1979 pp 89-92

[Article by L. I. Limanskaya, Ye. G. Morozov, A. S. Samodurov]

[Text] The measurements of the temperature fluctuations in the various parts of the ocean, as a rule, reveal the presence of energy peaks both on inertial and diurnal periods [1]. This is connected with the existence of different physical mechanisms exciting oscillations with the indicated periods. The temperature fluctuations with a period of 24 hours are caused by a baroclinic tide which obviously is caused by the interaction of the barotropic tide of the same period with unevennesses of the ocean floor or the coastal shelf [2-4]. The sources of the temperature fluctuations with an inertial period are less investigated. However, on the basis of the frequently noted fact of their alternation in space and in time it is considered that the nonuniformities in the wind field are responsible for generation [5, 6].

The region in which the studies are performed by the POLYMODE program has the negative peculiarity that the inertial period is close to 24 hours. The difference in the physical classes generating, on the one hand, the tidal fluctuations of the diurnal period, and on the other hand, the inertial fluctuations, has aroused interest in the effort to expand the temperature of the appearance of the two mentioned phenomena in natural series.

The spectral functions calculated by the numerous temperature realizations in the test area indicate the presence of a clearly expressed peak on a period of about 24 hours. It is possible to consider that this peak is caused by two processes -- the diurnal internal gravity waves (a period of 24 hours) and the inertial fluctuations with a period close to 24 hours (the local inertial period on a latitude of 30° is 24 hours, on a latitude of 29°, at the center of the test area, it is 24.75 hours, at the southern part of the buoy test area (buoy II), 25.85 hours).

As a result of such a small difference between the periods and insufficient length of the series these fluctuations are not separated by the spectral methods. Actually, the frequency difference on adjacent points of the spectrum is

$$\Delta f = 1/2M\Delta t,$$

where $M\Delta t$ is the maximum shift of the correlation function in units of time.

In order to separate the periods T_1=24 hours and T_2=25.85 hours, the frequency resolution must be

$$\Delta f = \frac{1}{T_1} - \frac{1}{T_2} = \frac{1}{2M\Delta t}.$$

The shift of the correlation function here is

$$M\Delta t = \frac{T_2 \cdot T_1}{2(T_2 - T_1)} \approx 168^{\text{ч}}. \quad (1)$$

Key: 1. hours

In order to insure 20° of freedom of the calculations the series must be no less than 1680 hours, that is, about 70 days. Here the values of the spectral functions on the frequencies of interest to us will correspond to the adjacent points of the spectrum with numbers 13 and 14 respectively. For reliable separation it is necessary that there be at least one point between the corresponding points of the spectrum, and this leads to an increase by twofold, that is, a five-month series is required.

In order to obtain preliminary ideas about the structure of the inertial and diurnal internal oscillations and their time variability, we made an effort to separate these oscillations using the method of complex demodulation first used in oceanology by V. Ye. Prival'skiy [7]. Thus, we studied these oscillations directly by the series of isolated harmonics of both periods. The filtration parameter here must be selected as follows (filtration by the sliding mean):

$$\frac{1}{l_\phi} = \frac{1}{T_1} - \frac{1}{T_2} = \frac{1}{335}\ ^{\text{ч}-1}, \quad (1)$$

Key: 1. hours^{-1}

that is, the filter parameter l_ϕ must be 335 hours. Selecting this filter and adjusting the calculation for one selected frequency, we completely suppressed the second.

The results of the calculation (that is, the harmonics of each of the periods) for the point II (the 50-meter horizon) are presented in Fig 1. The duration of the series is from 24 July to 26 September.

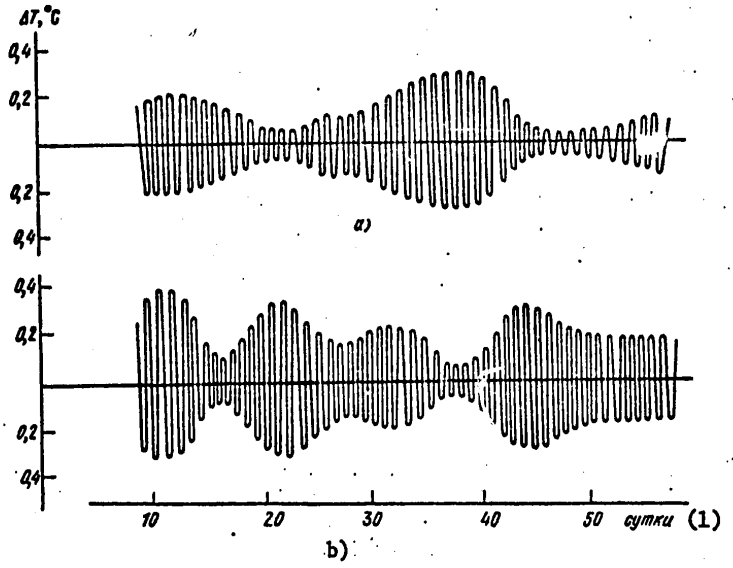

Figure 1. Inertial (a) and diurnal (b) harmonics of the temperature realization on the buoy II (horizon 50 meters) obtained by "gluing" of the series according to the data of two buoys operating in series with respect to time.

Key:
1. days

From Fig 1 it is obvious that the nature of the variability of each type of fluctuation is different. This indicates that this variability is determined by the nature of the fluctuations themselves and not by the variation of the vertical temperature gradient in time. For the inertial period the train structure is characteristic actually with one obvious oscillation train for the entire two-month observation period. The 24-hour fluctuation is characterized by 12-13 day variability which can be connected, on the one hand, with the synoptic processes [5], and on the other hand, with the semimonthly inequality of the barotropic tides generating the internal waves [8]. The result obtained can be considered somewhat unexpected. C. Day and F. Webster [9] performed measurements of the currents south of the Bermuda Islands at a latitude of close to 30°. The results of the investigations indicate that the energy of the fluctuations with a period of about 24 hours experiences significant variability in time. According to the data of the mentioned authors, on the 50-meter horizon this variability correlates quite well with the passage of storms over the east coast of the United States. The relatively smooth variation of the amplitude of the inertial temperature fluctuations with time discovered in this paper can be connected with the fact that weather conditions as a whole varied little during the period during which the measurements were taken. The recorded train of inertial oscillations

possibly is connected with the intensification of the wind in the test area to 10-11 m/sec observed in the last 10 days of August for 7 or 8 days.

By the measurement results during the first setup in July-August, the abyssal structure of the time variability of the diurnal and inertial fluctuations was analyzed.

Fig 2 shows the graph of the amplitude variation of the diurnal and inertial fluctuations in time for different horizons at the point II for a period of about 30 days in August. The nature of the variability of the inertial fluctuations with respect to depth is different. At individual times in certain horizons an increase in the oscillation amplitude is observed whereas on other horizons, a decrease in it occurs, which is connected with nonstationary regime and nonuniformity of the inertial fluctuations.

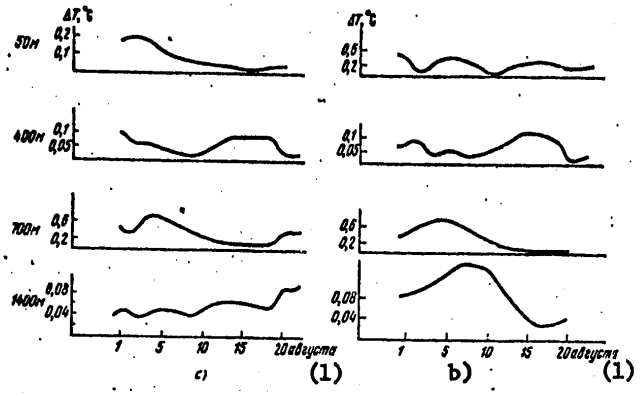

Figure 2. Variation of the amplitude of the inertial (a) and diurnal (b) temperature fluctuations for the 50, 400, 700 and 1400 meter horizons during August 1977.

Key:
1. August

This structure can be determined by the multimodal nature of the fluctuations or different sources generating oscillations at different depths. This can be determined also by a time delay in the different horizons of the disturbance propagated with respect to depth from the surface. An insufficient number of measurement horizons does not permit reliable confirmation of the latter. However, the disturbances are delayed with respect to depth. According to the rough estimates the average propagation rate of the disturbance downward is about 1.3 m/hr in the layer from 50 to 700 meters.

The amplitudes of diurnal temperature fluctuations vary at different depths according to different laws. However, the variability in the upper 400 meters is smaller. Their variability in the deep pair of horizons

at 700 and 1400 meters is also similar. Obviously, there are two different systems generated by different sources in the diurnal fluctuations. This possibility in this area was indicated previously in reference [10]. It is possible to propose that the diurnal fluctuations in the upper layer determined by the internal waves of the diurnal period are generated by the interaction of the barotropic tide with the coastal shelf of the nearby islands or continent [4]. The fluctuations in the basic thermocline can also be determined by the internal waves generated by the barotropic tide interacting with the unevennesses of the bottom [2, 3].

In conclusion it is necessary to note that the amplitudes of the temperature fluctuations on inertial and diurnal periods are approximately identical, and therefore they make an equal contribution to the formation of unseparated peak in the spectral densities of the temperature fluctuations.

Abstract

By means of complex demodulation the diurnal and inertial temperature fluctuations are distinguished as measured on buoy stations of the POLYMODE test area. The time and depth variability of each of the fluctuations is studied. Hypotheses are suggested for the mechanism of the fluctuations under the conditions of the test area.

BIBLIOGRAPHY

1. Ivanov, Yu. A.; Morozov, Ye. G. "Study of the Temperature Fluctuations on Tidal and Inertial Period," ATLANTICHESKIY GIDROFIZICHESKIY POLIGON-70 [Atlantic Hydrophysical Polygon-70], Moscow, Nauka, 1974.

2. Cox, C. S.; Sandstrom, H. "Coupling of Internal and Surface Waves In Water of Variable Depth," J. OCEANOGR. SOC. JAPAN, XX-TH ANNIV., 1962, pp 499-513.

3. Baines, P. G. "The Generation of Internal Tides by Flat-Bump Topography," DEEP SEA RES., No 29, 1973, pp 179-205.

4. Rattri, M. "Occurrence of Tides in the Coastal Zone," VNUTRENNIYE VOLNY [Internal Waves], Moscow, Mir, 1964.

5. Monin, A. S.; Kamenkovich, V. M.; Kort, V. G. IZMENCHIVOST' MIROVOGO OKEANA [Variability of the World Ocean], Lenlngrad, Gidrometeoizdat, 1974.

6. Pollard, R. T. "On the Generation by Winds of Inertial Waves in the Ocean," DEEP SEA RES., No 17(4), 1970.

7. Prival'skiy, V. Ye. "Complex Demodulation of Random Processes and its Application for the Analysis of Tides," MATERIALY XIII NAUCHNOY KONFERENTSII DVGU [Materials of the 13th Scientific Conference of the Far Eastern Hydrologic Administration], Vladivostok, Part 5, No 1, 1969.

8. Ivanov, Yu. A.; Morozov, Ye. G. "Semimonthly Inequality of the Internal Waves of the Tidal Period," DOKL. AN SSSR [Reports of the USSR Academy of Sciences], Vol 236, No 3, 1977.

9. Day, C.; Webster, F. "Some Current Measurements in the Sargasso Sea," DEEP SEA RES., No 12(6), 1965, pp 805-814.

10. Mirabel', A. P.; Morozov, Ye. G.; Plakhin, Ye. A. "Some Peculiarities of the Vertical Structure of the Temperature of the Tropical Part of the North Atlantic," IZV. AN SSSR. SER. FIZ. ATM. I OKEANA [News of the USSR Academy of Sciences, Physics of the Atmosphere and Ocean Series], Vol 9, No 9, 1973.

[8044/0785-10845]

10845
CSO: 8044/0785

SEPARATION OF SEMIDIURNAL TEMPERATURE FLUCTUATIONS DETERMINED BY THE BAROTROPIC TIDE AND INTERNAL WAVES

Moscow OKEANOLOGICHESKIYE ISSLEDOVANIYA in Russian No 30, 1979 pp 78-81

[Article by Ye. G. Morozov, A. S. Samodurov, L. P. Filatova]

[Text] As is known, in the ocean there are always two types of fluctuations of an identical time scale -- this is the semidiurnal barotropic tide and the internal baroclinic gravity wave with the same period. The spatial scale of these oscillations is distinguished by approximately an order. However, when studying the fluctuations of the hydrological characteristics of the 12-hour period using time realizations of the temperature and current at a point, the spatial scale cannot manifest itself. Therefore, both types of oscillations are taken as a united whole.

Inasmuch as barotropic tide in practice causes no vertical shift of the water particles, the temperature fluctuations caused by it are insignificant. The temperature fluctuations are determined basically by the internal gravity waves having a vertical velocity component. Therefore the tidal internal waves are studied by the temperature fluctuations.

In many papers, in particular, in [1] it is demonstrated that the horizontal coherence of the current fluctuation on a 12-hour period is small. This is explained by the fact that both the barotropic tide and the baroclinic tide make contributions to the current fluctuations approximately in equal proportions. In addition, from the general physical arguments it is clear that the coherence of the fluctuations must be relatively high.

In reference [2], by averaging the Fourier coefficients vertically, an effort was made to separate the velocity field into barotropic and baroclinic tides. In this study another procedure was used. For the separation of these fluctuations, just as in reference [2] the property of the barotropic tide was used -- invariability of the horizontal current velocity vertically. In the region encompassed by the POLYMODE program (at point D) a buoy was installed with current velocity meters from the surface to the bottom. The BPV-2 and BPV-6 instruments were installed

at the 100, 700, 1400, 3000 and 4500 meter horizons at an ocean depth of 5200 meters, and at the 25, 50, 100, and 700 meter horizons temperature recorders were suspended. The autonomous buoy station operated for 9 days with a measurement spacing of 1 hour. Using the complex demodulation procedure [3], the 12-hour harmonic was isolated from the realizations (actually a band was isolated with a period of 12±2 hours). The realizations of the U and V components, the velocity modulus and temperature were subjected to this processing. Thus, in the current fluctuations band that has been isolated, both batotropic tide and internal wave were present. The internal wave will make a basic contribution to the temperature fluctuations, for the temperature variations caused by advection of the horizontal nonuniformities of the temperature by the barotropic tide are small, especially deeper than the seasonal thermocline layer. Below, a detailed study was also made of the temperature fluctuations.

After isolation of the narrow-frequency band from the series of currents for separation of the internal and barotropic tides the currents measured every hour on one vertical were averaged. The series obtained was an approximation to the velocity series (components and modulus) caused by the barotropic tide. The word "approximation" was used inasmuch as the five measurement horizons selected at the characteristic points of the vertical is the minimum number of horizons for which such an operation is justified. The approximation to the barotropic tide that was obtained is further interpreted by us as the barotropic tide. Increasing the number of current meters naturally should improve the result. However, even for such a small number of observation horizons the expected result was obtained. The isolated averaged series of velocities (orbital velocities of the particles of the barotropic tide) varied in time with a period of 12 hours. The difference on each horizon between the initial series which is the sum of the barotropic and the baroclinic tides and averaged vertically, which is the barotropic tide, gives a series for the orbital velocity of the particles in the internal wave. Let us denote these three series by U_{Σ}, U_{bt}, U_{iw} respectively. In all horizons the series U_{iw} also fluctuate with a 12-hour period. It is necessary to indicate the values of the oscillation amplitudes of the velocity modulus: for the series U_{Σ}=10, U_{bt}=~5-6, U_{iw}=~5-6 cm/sec at depths to 1000 meters and 2-3 cm/sec at depths of more than 1000 meters for all variables.

Thus, during the semidiurnal fluctuations of the currents the barotropic tide and the internal wave in the upper layers make an approximately equal contribution; in the deep layers the barotropic tide makes the primary contribution.

It is interesting to note that C. Wunsch [4] estimates the energy of the semidiurnal baroclinic tide on the whole throughout the ocean as 10-15% of the barotropic of the same period.

Using our data, it is possible to calculate the ratio of the energy of the baroclinic tide to barotropic in the vicinity of the investigated test area by the expression

$$k=\frac{\Delta^{(1)}_{\text{вв}_{100}}\cdot h_1+\Delta^{(1)}_{\text{вв}_{700}}\cdot h_2+\Delta^{(1)}_{\text{вв}_{1400}}\cdot h_3+\Delta^{(1)}_{\text{вв}_{3000}}\cdot h_4+\Delta_{\text{вв}_{4500}}\cdot h_5}{\Delta^{(2)}_{\text{бт}}\cdot H},$$

Key: 1. iw=internal wave
2. bt=barotropic tide

where Δ_{iw} is the dispersion of the current fluctuations caused by the baroclinic tide on the corresponding measurement horizons; Δ_{bt} is the dispersion of the current fluctuations caused by the barotropic tide; h_i is the layer thickness; H is the depth of the ocean; $H=\sum_{i=1}^{5}h_i$.

A similar estimate for the relative energy of the internal tide in our calculations gives the value about 60%. This is insignificantly greater than the value obtained by Wunsch.

Let us consider the results of analyzing the barotropic tide wave. Using the method of determining the direction of the wave adopted by N. P. Fofonov [5] and A. Ye. Filonov [6], by the mutual spectral analysis of the components U and V of the barotropic tide current we obtain its direction equal to 8°. It is determined from the formula presented in the paper by Filonov [6] with accuracy to 180°:

$$\theta_N=\frac{1}{2}\operatorname{arctg}\frac{2Co_{UV}}{S_{VV}-S_{UU}},$$

where Co_{UV} is the cospectrum of the components U and V; S_{VV} and S_{UU} are the spectra of the components V and U respectively. The calculations of the tidal wave M_2 executed in references [7, 8] agree well with this result.

The calculation performed in this way for the internal wave gave the following directions on the different horizons: 100 meters, 270°; 700 meters, 263°; 1400 meters, 261°; 3000 meters , 290°; 4500 meters, 213°.

The closeness of the direction of the internal waves on the different horizons is a consequence of the semidiurnal internal fluctuations on all horizons belonging to one system, that is, the fluctuations are close to unimodal.

Let us consider the results of the mutual analysis along the vertical. Inasmuch as when measuring the currents by the BPV instrument the noise level is large, in particular for the velocity components, as a result of the absence of averaging of the direction we made a decision to use only the velocity modulus for the mutual analysis. As should be expected, the vertical coherence between the series $|U|_{\Sigma}$ is small. Thus, for the pair of series $|U|_{\Sigma}$ at 100-7000 meters the coherence is 0.32. For the same pair of series $|U|_{iw}$ the coherence is appreciably higher; it is 0.69.

In the deep layers of the ocean the inverse piecture is observed. For the pairs of horizons of 3000 to 4500 meters the coherence of the series $|U|_{\Sigma}$ is 0.96; the fluctuations take place in practice in one phase. For the pairs of series $|U|_{iw}$ the coherence is 0.22.

Thus, in the upper layer of the ocean where the internal tidal wave is well developed, the addition of the internal and barotropic tides leads to worsening of the mutual analysis functions. The internal wave separated from the barotropic tide is well coordinated vertically.

In the deep layers where the amplitudes of the internal waves are small, the fluctuations on a period of 12 hours almost completely are determined by the barotropic tide; therefore the total series is well correlated vertically, and the internal wave is poorly correlated as a result of small amplitudes.

Let us consider the results of mutual analysis between the currents and the temperature. The coherence between the temperature fluctuations on the 100-meter horizon with series $|U|_{\Sigma}$, $|U|_{iw}$, $|U|_{bt}$ is 0.11, 0.30, 0.40, respectively; on the 700-meter horizon, 0.29, 0.48 and 0.27 respectively.

In the layer close to the seasonal thermocline (100 meters) the coherence for the total series is small, but it increases significantly on separation of the series into the internal wave and barotropic tide. Here quite high coherence occurs for the two series of currents $|U|_{iw}$ and $|U|_{bt}$.

The high coherence vertically is regular for the internal waves inasmuch as the fluctuations of all the characteristics in it are functionally related. The quite high temperature coherence of the barotropic tide in the layer of the seasonal thermocline is obviously explained by the fact that the barotropic tide carries over the horizontal nonuniformity causing the temperature fluctuations at the recording point. The amplitude of these temperature oscillations can reach the amplitudes determined by the internal waves with respect to order of magnitude inasmuch as the coherence in both cases is similar. Acting jointly, these processes are accumulated one on the other, lowering the coherence. In the layer of the principal thermocline on the 700-meter horizon the picture is different. Here the fluctuations are basically determined by the internal wave, and the barotropic tide appears in the role of noise, lowering the coherence of the total phase. When determining the internal wave from the barotropic tide the coherence between the current fluctuations caused by the internal wave and the temperature increases to 0.48.

In this paper an effort is made to consider the contribution of each of the indicated types of fluctuations to the variability of the physical characteristics of the ocean. The performed calculations gave hopeful results. Further studies in this area will permit, on the one hand, deepening of the knowledge of the structure and the mechanisms of the generation of the internal tides, and on the other hand, availability of the required material for improvement of the calculation schemes for

constructing the tidal charts of the World Ocean. In the future it is expedient to increase the number of measurement horizons, to locate them at equal distances and increase the length of measurement series.

Abstract

A velocity time series caused by the barotropic tide is formed by vertical averaging of the hour-values of the 12-hour harmonics of moored velocity measurements. The remaining part of the series is defined by internal gravity waves. The cross analysis of currents caused by internal waves as a function of temperature and the interaction among themselves is shown to give better results than the original series. The direction of waves of the barotropic tide is calculated which correlates well with the theoretical estimates.

BIBLIOGRAPHY

1. Ivanov, Yu. A.; Morozov, Ye. G. "Study of the Temperature Fluctuations on Tidal and Inertial Periods," ATLANTICHESKIY GIDROFIZICHESKIY POLIGON-70 [Atlantic Hydrophysics, Poligon-70], Moscow, Nauka, 1974.

2. Fahrbach, E. "Einige Beobachtungen zur Erzeugung und Ausbreitung interner Gezeiten Wellen am Kontinentalabhang vor Sierra Leone," METEOR FORSCHUNGSERB, A, No 18, 1976, pp 64-77.

3. Prival'skiy, V. Ye. "Complex Demodulation of Random Processes and its Application for the Analysis of Tides," MATERIALY XIII NAUCHNOY KONFERENTSII DVGU [Materials of the 13th Scientific Conference of the Far Eastern Hydrologic Administration], Vladivostok, Part 5, No 1, 1969.

4. Wunsch, C. "Internal Tide in the Ocean," REV. GEOPH., SPACE PHYS., Vol 13, No 1, 1975.

5. Fofonoff, N. P. "Spectral Characteristics of Internal Waves in the Ocean," DEEP SEA RES., No 16, Suppl., 1969.

6. Filonov, A. Ye. "Determination of the Parameters and Spectral Characteristics of Internal Waves by the Current Observation Data," PROMYSLOVAYA OKEANOLOGIYA I PODVODNAYA TEKHNIKA [Industrial Oceanology and Underwater Engineering], Moscow, TsNIITERKH, No 14, 1972.

7. Pekeris, C. L.; Accad, Y. "Solution of Laplace's Equations for M_2 Tide in the World Ocean," PHILOS. TRANS. ROY. SOC., Leningrad, A 265, 1969, pp 413-436.

8. Zahel, W. "Die Reproduction Gezeitenbedinger Bewegungsvorgange im Weltozean mittels des hidrodinamisch-numerischen Verfahrens," MITTEIL. INST. MEERESKUNDE, Hamburg, No 17, 1970, pp 1-50.

[8044/0785-10845]

10845
CSO: 8044/0785

STUDY OF THE DIURNAL AND SEMI-DIURNAL TEMPERATURE FLUCTUATIONS

Moscow OKEANOLOGICHESKIYE ISSLEDOVANIYA in Russian No 30, 1979 pp 63-73

[Article by Ye. G. Morozov, A. S. Samodurov, L. I. Limanskaya, L. P. Filatova]

[Text] A characteristic feature of the temperature fluctuations in various parts of the World Ocean is the presence of high oscillation amplitudes in the inertial and tidal periods [1, 2]. When processing the temperature series obtained on the buoy stations in the region of operations under the POLYMODE program, special attention was given to the study of the fluctuations with indicated periods as the most energy-bearing mesoscale processes.

The region of investigation is characterized by the presence of powerful eddy formations which moved a noticeable distance during the observation time. The presence of eddies at each observation point is manifested in the existence of currents that are variable with respect to magnitude and with respect to direction in time and space. The average transfer in the research area was small.

There is still another fact which distinguishes the test area. It is that the test area is located in the direct proximity of 30° latitude which is critical for the internal waves of diurnal period. The inertial period here is 24 hours.

In our opinion, the presence of synoptic eddies and the proximity of the region of investigation to the critical latitude caused the singularities detected in the behavior of the long-period internal waves.

Brief Characteristics of the Hydrologic Situation. The vertical distribution of the hydrologic elements is characterized by the following. The upper quasiuniform layer is thin (20-30 cm). The seasonal thermocline layer is expressed sharply at depths from 40 to 70-80 meters and it is traced to 150-200 meters. Then comes a quite powerful quasiuniform layer of "18°" water, the lower boundary of which is at depths of about

500 meters. The layer of the principal thermocline reaches 900 meters. The maximum gradients are observed in the 700-800 meter layer. The abyssal water with small vertical gradients is located still deeper. The vertical temperature distributions T, provisional density distribution σ_t and the Brent-Vaisälä frequency N are presented in Fig 1. The Vaisälä-Brent frequency profile with depth, just as should be expected, is characterized by two peaks in the seasonal and basic thermocline layers. The corresponding periods ($\tau=2\pi/N$) for these layers are close to 5 and 20 minutes. The period that is the inverse of the Vaisälä-Brent frequency is about 2 hours for the 18° water.

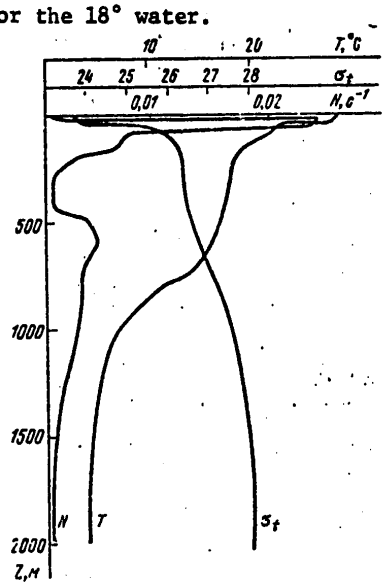

Figure 1. Vertical temperature distribution (T), provisional density distribution (σ_t), and Brent-Vaisälä frequency (N)

When performing the experiment the temperature gauges were installed on the 50 and 100 meter horizons -- in the seasonal thermocline layer; 400 meters in the "18°" water layer; 700 meters in the principal thermocline layer; the current meters were periodically also installed in the 1400-meter horizon.

Survey of Spectral Density Functions. The spectral density functions were calculated without filtration by the series with discreteness of 1 hour. These series were transformed from the initial ones with smaller discreteness by low-frequency filtration with subsequent selection. The spectra were calculated by the Fourier transform of the correlation function, the maximum shift of which was 1/10L (L is the length of the series) so as to insure 20 degrees of freedom of the calculation.

Fig 2 shows the spectrum of the temperature fluctuations characteristic of the investigation region. It was constructed by the realization of two series of a month each at the 50-meter horizon at the point II.

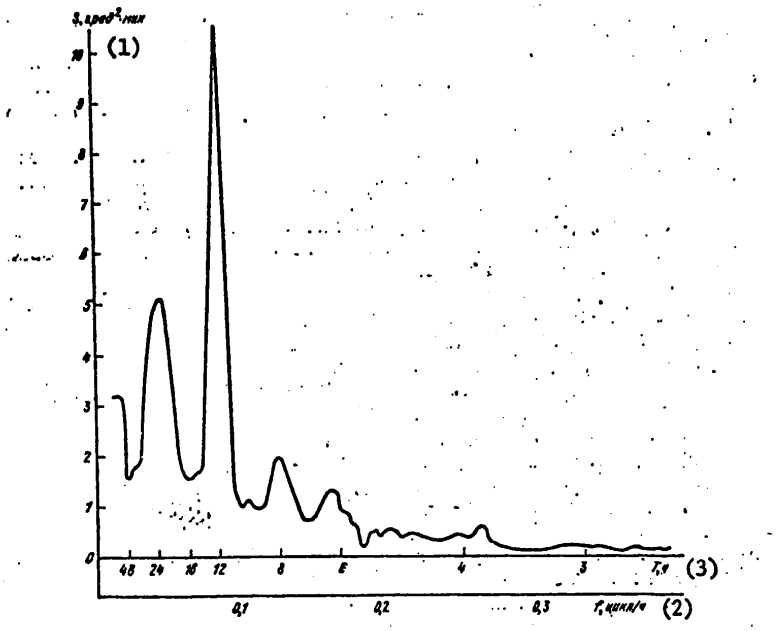

Figure 2. Spectral density of the temperature fluctuations for the point II (50-meter horizon). The calculation was performed by the 2-month series made up of two realizations

Key:
1. S, deg^2-min
2. f, cycles/hr
3. T, hr

Fig 3 shows the spectral density for various horizons of point C. Inasmuch as the measurements at the 1400 meter horizon at point C were not performed, the magnitude of the spectral function for this horizon was taken at point B. The level of the values of the spectral density of the temperature is determined on the one hand by the amplitude of the vertical movements of the liquid, and on the other hand, by the vertical temperature gradient. Beginning with this fact, it is possible to substantiate the difference in level of the spectral "energy" vertically.

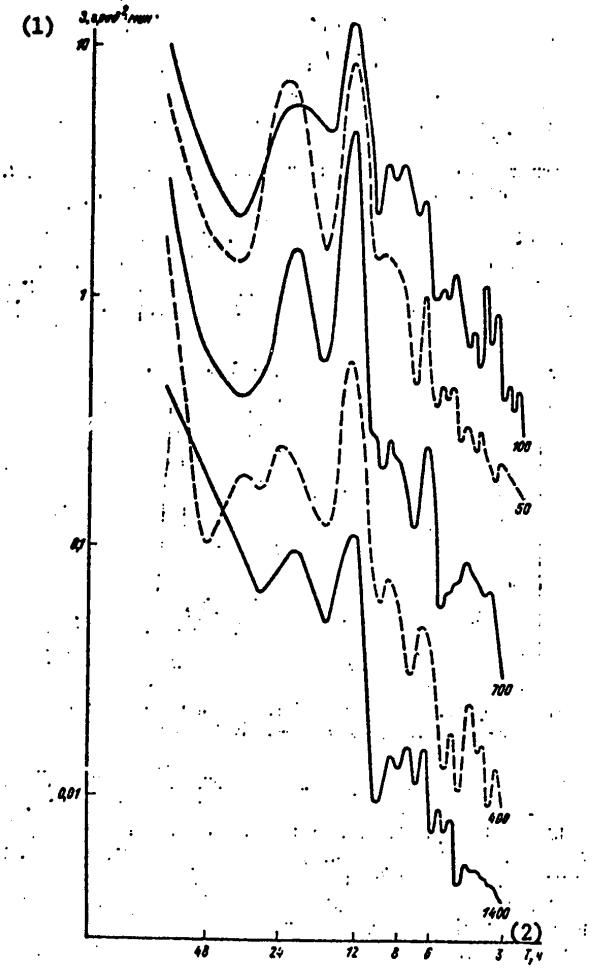

Figure 3. Spectral density of the temperature fluctuations for the points C (horizons 50, 100, 400, 700 meters) and B (horizon 1400 meters). Series of 1-month duration.

Key:
1. S, deg^2-min
2. T, hr

At the 50 and 100-meter horizons the vertical fluctuations cannot reach high amplitudes, for they are limited by the proximity of the ocean surface. However, inasmuch as these horizons are in the seasonal thermocline layer with large vertical temperature gradients, the amplitudes of the temperature fluctuations are quite large here. In addition, in the upper layer the temperature fluctuations can be explained not only by the internal waves, but to a significant degree also by the advective transfer of the horizontal temperature gradients by the currents.

At the 400 and 700-meter horizons the amplitudes of the vertical fluctuations must be of the same order or higher than in the upper layer. The differences in values of the spectral density are determined by a significant difference in vertical temperature gradients in the quasiuniform "18°" layer and in the layer of the principal thermocline.

The differences in the values of the spectral densities with respect to horizontal are less significant. However, their variability in this region is much greater than in the other parts of the World Ocean. With respect to the horizontal it is characterized by the predominance of peaks at different periods depending on the measurement point. For example, in Fig 4 there are several spectral density functions for different points of the test area.

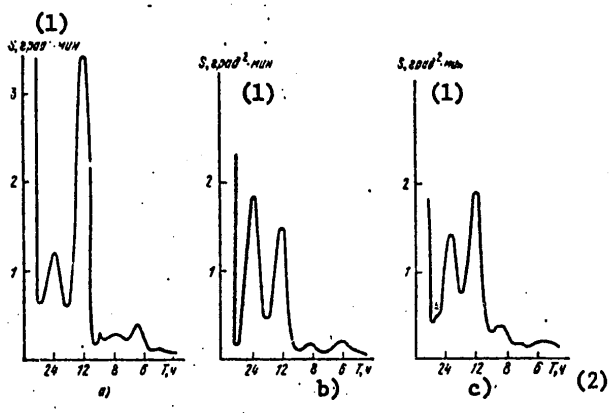

Figure 4. Variability of the spectral density functions with respect to the horizontal (700 meters):
a -- point B - 1; b -- point П - 1; c -- point T - 1

Key:
1. S, deg^2-min
2. T, hr

A significant time variability of the spectral functions is also characteristic of the region of investigation. It is characterized by the same peculiarities as the variability with respect to the horizontal. Fig 5 shows the variability of the spectra in time for the point L (at a 700-meter horizon). The spectra are presented by the measurements in August and September.

Analyzing the space and time variability of the spectral functions, it is possible to note that the large differences are noted in the location of the peaks with respect to the frequency axis. The spectral energy peaks are grouped near the periods equal to 24 and 12 hours. This is caused by the fact that the inertial and tidal periods carry significant energy. The series at our disposal are insufficient to separate the 24-hour barocline tide from the inertial movement; therefore these fluctuations merge into one common peak.

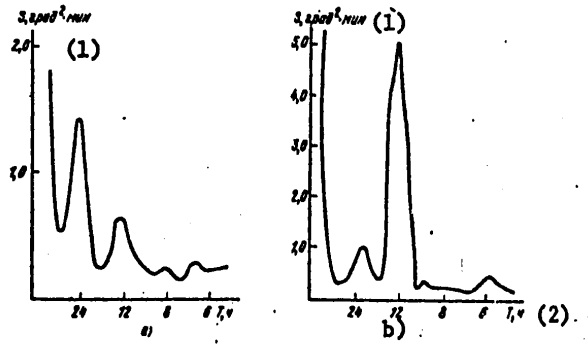

Figure 5. Variability of the spectral density functions in time (horizon 700 meters): a -- point L - 1, August; b -- point L - 2, September

Key:
1. S, deg^2-min; 2. T, hr

In addition to the presence of two basic peaks, in the spectral densities there are a number of deviations. The most important of them is the shift of one of the peaks to the left or right along the frequency axis. In addition, on the spectra quite frequently additional peaks appear along with the principal one (Fig 6). In some cases, quite rare, one of the basic peaks is not observed at all (Fig 7, a). It is possible to consider that more than half of the series have at least one of these deviations.

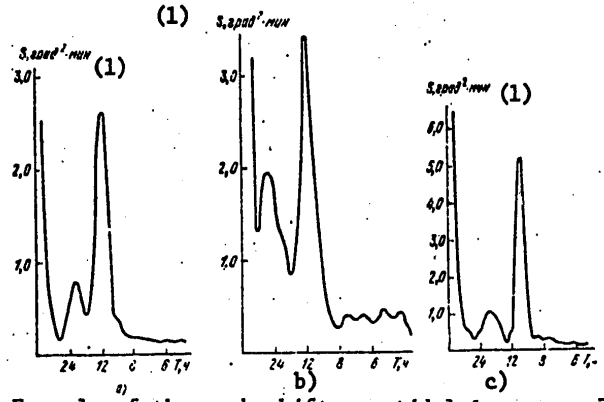

Figure 6. Example of the peak shifts on tidal frequency 700 meter horizon): a--right (point B-1), b--left (point H-1), c--right (point Y-1); a significant number of surges of the spectral function to the right in two periods--24 and 12 hours--are noted.

Key: 1. S, deg^2-min; 2.

The shifts in the position of the fluctuation energy peaks with respect to the time axis of tidal periods can be caused by the following causes. Let the measurements be taken at a fixed point in space. Let us propose

that the wave of period T_0 having phase velocity C_ϕ is propagated in the flow with velocity component along the direction of movement of the wave u. Then as a result of the Doppler effect, the measured wave period T_1 will differ from the true one. The relation between them is subordinate to the radio

$$T_1 = \frac{T}{1 + \frac{u}{c_\phi}}.$$

Depending on the sign u the recorded period will either be greater than T_0 or less than. From the observed current velocities on the order of 30 km/sec, the phase velocities of the wave 83 cm/sec (for 24 hours) and ~360 cm/sec (for 12.4 hours) the intervals of variation of the periods will be 38-18 and 13-11 hours respectively. They can be, however, even greater. For example, for a velocity of 50 cm/sec characteristic of the upper horizon the indicated intervals are equal to 60-15 and 14-10.8 hours. A discussion will be presented below of the estimate of the phase wave velocities. The internal waves of diurnal period are more subject to the Doppler effect than semidiurnal ones. This is connected with the fact that the phase velocity of the internal waves of diurnal period is approximately 4 times less than the semidiurnal inasmuch as the diurnal waves are characterized by a high mode number.

On the basis of the difference in the velocities of propagation of the inertial and diurnal tidal waves, splitting of the corresponding blips as a result of the Doppler effect is possible. In Fig 7, b one of these spectra is depicted for the point I-1 (50-meter horizon). The point was located in the anticyclonic eddy in the zone of effect of strong currents. In this sense the spectrum of the temperature fluctuations at the 50-meter horizon at the point I-1 located near the critical latitude (north of it) in the vicinity of the strong cyclonic eddy currents caused by splitting of the energies in the spectrum is characteristic. The spectrum for this point is depicted in Fig 7, c, from which it is obvious that the diurnal peak is split into two. This is characteristic to a different degree of many spectra of the investigated regions. It is necessary to give attention to one characteristic feature of the depicted spectrum. The harmonics of the diurnal oscillation up to 6 orders are noted in it in the absence of a peak in the 24-hour period. This fact was not recorded once for inertial waves [3].

The absence of the principal blips in the spectra noted very rarely and only on the upper horizons, can be explained by the fact that the amplitudes themselves of the vertical movements in the upper layers are small. In addition, the joint effect of the internal wave and the transfer of horizontal gradients by the tidal currents can be put together so that when operating in opposite phases they mutually cancel each other.

Results of the Dual Analysis of a Temperature Realization. During the course of the first buoy installation, as a result of technical failures many of the temperature recorders uniformly distributed with respect to space did not respond or only partially responded. Therefore it was very difficult to perform the dual analysis. However, the study of the

material advantageous for the solution of the stated problems has still made it possible to draw sone entirely defined conclusions.

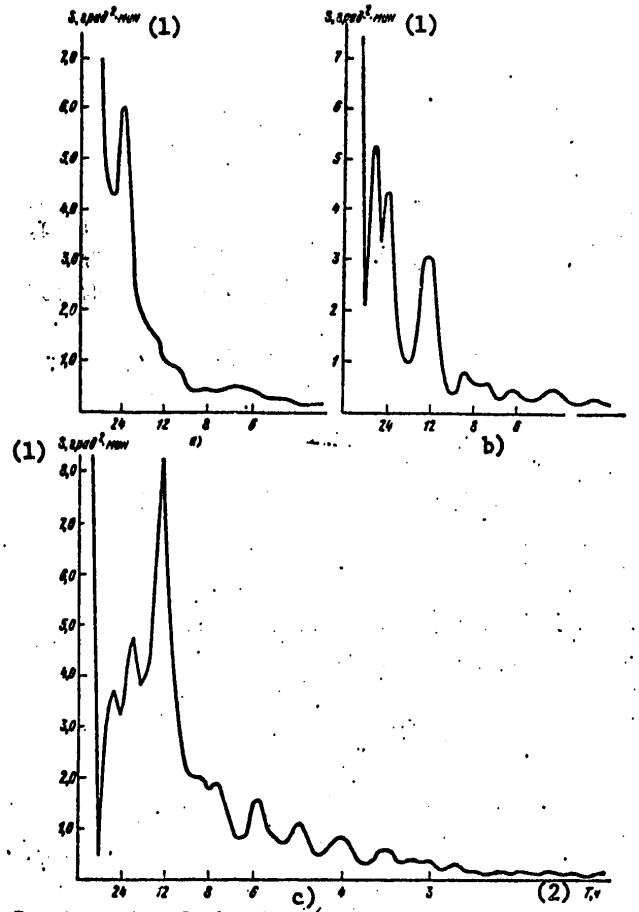

Figure 7. Example of the distortion of the spectral density functions: a -- spectral density function for the point A-1 (horizon 100 meters); blip in the semidiurnal period absent; b -- Г-1 point (50-meter horizon); blip in the spectral density on a 24-hour period split into two; c -- point I-1 (50-meter horizon); diurnal peak split into two; the harmonics of the diurnal fluctuation are present to 6 orders.

Key:
1. S, deg^2-min; 2. T, hr

The coherence of the fluctuations on 24 and 12.4 hour periods, as a rule, is not very high vertically. Nevertheless, on the majority of pairs of realizations it is close to the confidence value. With an increase in

distance vertically, it decreases. For the example, all of the coherence calculations* in 12 hour-period for the D-3 buoy on which the number of temperature meters vertically was increased, are presented in Table 1.

Table 1

Coherence of the Temperature Fluctuations Between Various Horizons

Horizons, meters	50	100	400	700
25	0.13	0.07	0.05	0.04
50		0.29	0.34	0.20
100			0.10	0.10
400				0.41

As is obvious from the table, the coherence in the deep layers (400-700 m) is very high -- this is characteristic for measurements at the majority of points. The coherence of the deep horizons with the horizons in the upper layer is somewhat lower, especially on the 25-meter level where the activity of the upper layer introduces significant noise. This fact was noted for this region also earlier [4]. The structure of the fluctuations here is two-layer as a result of the presence of the powerful quasiuniform layer of 18-degree water. The coherence with respect to the horizontal between the temperature fluctuations in the POLYMODE region is appreciably lower than in the other parts of the World Ocean in which studies were previously performed.

Apparently this result is connected with the intensive eddy activity in this region. As a result of the spatial variability of the current field in the test area the Doppler effect on the fluctuations is different at various points of the test area. The mutual analysis was performed by series lasting no less than 10-12 days and frequently up to 25 days, that is, in a quite long time interval so that the eddies moved noticeably in space. Accordingly, the Doppler frequency shift varies also in time. The indicated time-space variability of the average conditions with sufficiently dense packing of the eddies in the test area also led to the fact that the horizontal coherence is absent in many pairs of realizations.

Considering these arguments, we performed a mutual analysis for the pairs of realizations obtained under approximately identical average conditions, that is, for example, when both realizations are obtained from buoys located in one eddy formation or when both buoys are located in the deformation between the eddies. In this case, as a rule, the coherence turned

*The coherence was calculated by the formula $H=(C_0^2+Q^2)/9S^2_x \cdot S^2_y)$, where C_0 and Q are the mutual spectral, S_x and S_y are the autospectra.

out to be appreciably greater than the confidence coherence. The most reliable results were obtained in the principal thermocline layer in the 700-meter horizon. In the seasonal thermocline probably the noise caused by the activity of the upper boundary layer is large. In the quasiuniform layer at a depth of 400 meters on the basis of smallness of the vertical gradients, the useful signal is also small, on the basis of which the coherence frequently turns out to be below the confidence level.

We made an effort to estimate the parameters of the internal wave with respect to the phase relations [5]. It must be noted that under the above-indicated average conditions the proposition that the waves are planar is highly provisional; therefore, the results obtained must be considered very rough. It is for this reason that the phase diagrams are not closed in many of the calculated triangles.

The parameters of the internal waves with periods of 12.4 and 24 hours were estimated by the available data. It was possible to establish only the general directions of the wave propagation. In Fig 8, as an example, phase diagrams are presented for the results of calculating the directions of propagation of the waves which was performed by three series of measurements in one horizon. The estimates of the wave lengths in the region of investigation turned out to be as follows: for the 24-hour period, 72 km; for the 12.4-hour period, 154 km; the estimates for the phase velocities are 83 and 360 cm/sec respectively.

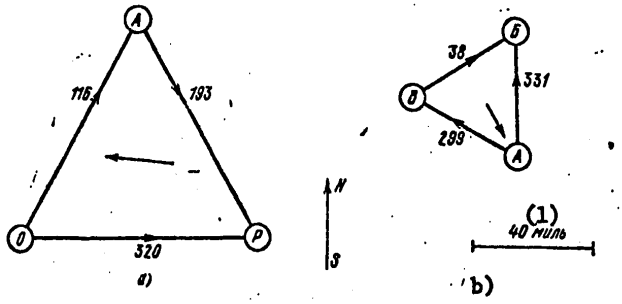

Figure 8. Phase diagrams for calculating the parameters of the internal waves by the buoy triangles: the arrows inside the triangle are the directions of propagation of the wave. The numbers on the vectors are the magnitudes of the phase shift in degrees; the arrows are the positive direction of the phase shift; a -- the triangle of buoys A-O-P, wave period 12 hours, horizon 700 meters, wave length 84 miles; b -- buoy triangle A-B-V, wave period 24 hours, horizon 700 meters, wave length 39 miles.

Key:
1. 40 miles

Numerical Integration of the Internal Wave Equation. In order to compare the wave length and phase wave velocities obtained with the calculated estimates for the actual conditions of the test area, we performed a numerical integration of the equation for the internal waves

$$\frac{d^2w}{dz^2} + \frac{N^2}{g}\frac{dw}{dz} + \frac{N^2-w^2}{w^2-f^2}k^2w = 0$$

for zero boundary conditions and the selection of the inertial period equal to 24.75 hours, which corresponds to the central point of the test area. The results of the calculations for certain periods are presented in Table 2. The density distribution was taken as the real density distribution, according to the hydrologic series data. The calculation was performed by the density distribution measured in the deformation field between eddies.

In order to estimate the limits of the variations of the wave parameters under various hydrologic conditions of the cyclone and anticyclone, a calculation was also made as applied to the first mode of the semi-diurnal oscillations in the central parts of the indicated formations. The wave lengths obtained are equal to 140 km for the cyclone and 153 for the anticyclone, respectively.

Table 2

Wave Lengths of the Internal Oscillations of Different Periods and Different Modes (km)

Mode No	Period, hours											
	2	4	6	8	10	13.4	14	16	18	20	22	24
1	20	42	65	89	115	149	176	215	265	334	443	684
2						55						252
3						43						197
4						29						135
5						24						109
6						20						92
7						16						76
8												67

Fig 9 shows the eigenfunctions of the first three modes of the semi-diurnal internal waves. The calculation was performed for the velocity W. The extraordinarily high peaks of the second and third modes obviously cause strong differences in the wave lengths of the first mode from the second and third.

From Fig 9 it is also obvious that the amplitudes of the fluctuations in the upper layer (50 and 100 meters) are very small, which in certain cases could cause the absence of a blip on the spectra.

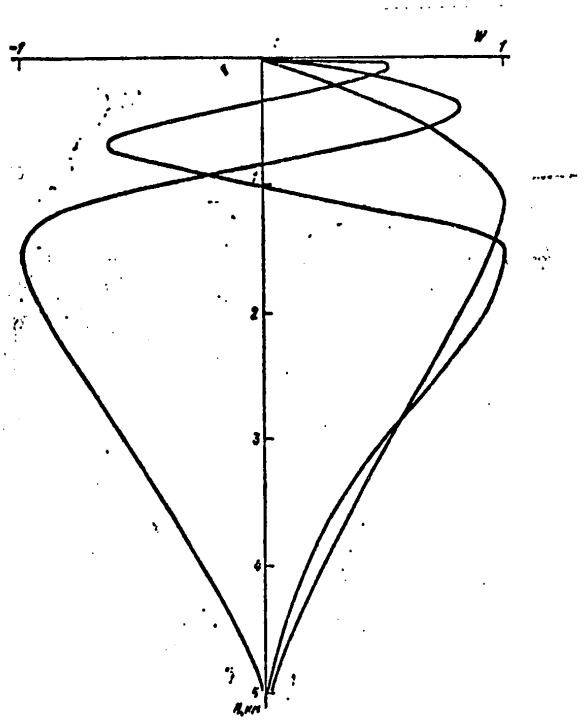

Figure 9. Eigenfunctions of the first three modes of the semi-diurnal vertical velocity fluctuations. The functions are normalized for maximum value vertically.

As is obvious from the presented theoretical calculation, the wave length of the first mode of the semidiurnal oscillation agrees well with the experimental estimates. Therefore it is possible to consider that the semidiurnal internal wave of the first mode predominates in the test area.

Comparing the results of the calculation by the phase relations with the theoretical estimates for the diurnal wave, it is possible to conclude that the primary contribution to the temperature fluctuations of diurnal period is made by the internal waves characterized by the high mode number (~7-8). The plausible explanation of this phenomenon is illustrated by Fig 10. It depicts the dispersion curves for the internal waves in a rotating liquid with the Coriolis parameter equal to f. The vectors have projections (ω, k) where ω is the oscillation frequency, k is the wave number of the corresponding harmonic. A study is made of the case where all of the wave vectors are colinear. It is found that in the internal wave system nonlinear triple-wave interactions are possible where the resonance conditions are satisfied [6]:

$$\omega_1 \pm \omega_2 \pm \omega_3 = 0,$$
$$k_1 \pm k_2 \pm k_3 = 0. \qquad (2)$$

The system investigated by us indicates that the internal wave of diurnal period having high mode number can be excited on interaction of the semidiurnal and diurnal internal waves having low mode numbers. The absence of the signs of the diurnal internal wave of the low mode among the results of the mutual analysis can be explained by the fact that in the region of investigation it has low amplitude.

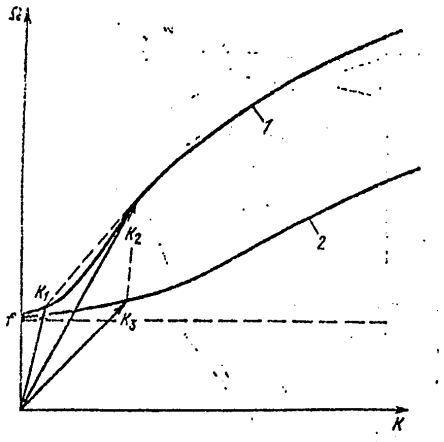

Figure 10. Qualitative picture of the triple-wave interaction: 1 -- dispersion curve of the first mode, 2 -- dispersion curve of the second mode, K_1 -- wave vector of the diurnal wave of the first mode, K_2 -- wave vector of the semidiurnal wave of the first mode, K_3 -- wave vector of the diurnal wave of the high mode.

In conclusion it is possible to draw the conclusion that when investigating the internal waves in the POLYMODE region we encountered effects which were not manifested so clearly in other areas, and therefore they had not received attention. Whereas previously we considered that the variability of the average conditions is basically determined by the seasonal behavior of the hydrologic characteristics, in the vicinity of the test area the fluctuations of the average conditions were determined by passage of synoptic eddies which greatly complicated the picture.

Abstract

The diurnal and semidiurnal temperature fluctuations are investigated by moored temperature measurement data. The frequency shift of the spectral peaks is shown to be cause by the Doppler effect due to intensive currents in the region under investigation. The parameters of the internal waves are defined which appear to be close to the theoretical estimates.

BIBLIOGRAPHY

1. Ivanov, Yu. A.; Morozov, Ye. G. "Investigation of the Temperature Fluctuations on Tidal and Inertial Periods," ATLANTICHESKIY GIDROFIZICHESKIY POLIGON-70 [Atlantic Hydrophysical Poligon-70], Moscow, Nauka, 1974.

2. Morozov, Ye. G.; Plakhin, Ye. A.; Shapovalov, S. M. "Study of Temperature Fluctuations in the Northwestern Part of the Pacific Ocean in the Frequency Range of the Internal Gravity Wave," OKEANOLOGIYA [Oceanology], Vol 16, No 1, 1976.

3. Titov, V. B. "Some Peculiarities of the Mesoscale Movements in the Ocean," OKEANOLOGIYA, Vol 13, No 6, 1973.

4.. Morozov, Ye. G.; Neyman, V. G.; Plakhin, Ye. A. "Peculiarities of the Thermal Structure in the Vicinity of the Antilles-Guiana Countercurrent," OKEANOLOGICHESKIYE ISSLEDOVANIYA, NO 25 (ANTILO-GVIANSKOYE PROTIVOTECHENIYE) [Oceanological Research. No 25 (Antilles-Guiana Countercurrent)], Moscow, Nauka, 1977.

5. Byshev, V. I.; Ivanov, Yu. A.; Morozov, Ye. G. "Study of the Temperature Fluctuations in the Frequency Range of the Internal Gravity Waves," IZV. AN SSSR. SER. FIZ. ATM. I OKEANA [News of the USSR Academy of Sciences. Physics of the Atmosphere and Ocean Series], Vol 7, No 1, 1971.

6. Phillipps, O. M. DINAMIKA VERKHNEGO SLOYA OKEANA [Dynamics of the Upper Layer of the Ocean], Moscow, Mir, 1969.

[8044/0785-10845]

10845
CSO: 8044/0785

STUDY OF ABYSSAL TEMPERATURE AND DENSITY STRUCTURE AND THE VELOCITY PROFILES IN AN ANTICYCLONIC EDDY

Moscow OKEANOLOGICHESKIYE ISSLEDOVANIYA in Russian No 30, 1979 pp 32-35

[Article by A. S. Samodurov, V. G. Kort, Ye. G. Morozov, S. M. Shapovalov]

[Text] A large number of papers have been published on the materials of the American MODE experiment in which certain peculiarities of the behavior of the synoptic ocean eddies in the southwestern part of the Sargasso Sea are discussed. The first expedition by the POLYMODE program put the richest material to study the eddy activity in the investigated program in the hands of the oceanologists. Without touching on many of the important aspects in the structure and eveolution of the indicated formations, let us only discuss one detail which deserves attention. The first area surveys already demonstrated that there are certain anomalies in the vertical distribution of the horizontal temperature gradients. Thus, whereas the isotherms are concave in the lower horizons in the anticyclone, they are convex in the upper horizons. Thus, in the anticyclone there is a lens of water with a temperature of about 18°, the horizontal axis of which is at a depth of 200-250 meters. A similar phenomenon was noted in this part of the ocean [1] by the materials of the XBT-sections, that is, when investigating only the temperature data. As for the structure of the cyclones, in them, on the contrary, with greater convexity of the isotherms, thinning of the layer of 18-degree water is observed.

During the work of the "Akademik Kurchatov" scientific research ship in the first phase of the POLYMODE expedition, we observed the anticyclonic eddy located in the southern part of the test area. This eddy was traced by the data of several large-scale test area surveys and during the observation it moved significantly in the westerly direction. For the eddy that we investigated it is characteristic that the isotherms and isopycns in the upper 200-meter layer are convex upward, and below this layer, concave downward. That is, if we judge only by the shape of the density isoline distribution, the impression can be created that in the upper part the eddy is cyclonic, and in the lower part, anticyclonic. The current measurements on the buoy stations of the southern group which were located in

the eddy during its drift across the test area indicate that it is anticyclonic with respect to its entire depth.

For a detailed investigation of the temperature field distribution, salinity and density in the anticyclonic region in the southwestern part of the territory, two mutually perpendicular hydrologic sections were created with installation of a buoy. The position of the hydrologic stations is shown in Fig 1, from which it is obvious that they were executed with continuous horizontal step size. In the region where the buoy was installed, the depth of the stations was greater. The series were performed to 1200 meters, and along the edges and in the center of the sections, to 2000 meters. The depth of occurrence of the 15° isotherm is presented in the same figure according to the data of the performed survey. By the position of the isolines it is possible quite precisely to determine the center of the eddy. When making the meridional section, we were oriented by the survey data of the "Akademik Krylov" scientific research ship. The error in determining the eddy drift velocity reduced to the fact that this section cut the rear part of the anticyclone in its central part. The operative data processing from the first section made it possible to correct the position of the second section in time; it passed in practice through the center of the eddy.

Fig 2 shows the temperature distribution (a) and the density distribution (b) in the zonal section through the eddy. In the lower layer (400 m deep) a dip of the isotherms and isopycns that is characteristic of an anticyclone is observed. The difference in depth of occurrence of the isotherms at the center of the anticyclone and on its periphery is highly significant. Thus, for the 18° isotherm it reaches 150 meters. In the upper layer of the central part of the anticyclone the isotherms and isopycns are convex upward and are submerged toward the periphery of the eddy. Thus, the layer of small gradients in this section is significantly thicker (to 375 meters)than along the edges (200 meters).

As is obvious from the performed analysis, the bend in the isolines in opposite directions is characteristic both for the temperature and for the density. The fact that this direction remained for at least 3 months is significant. Therefore, it is impossible to explain this effect by the eddy activity of the adjacent layer of the atmosphere.

The causes of this eddy structure still are unclear. However, whatever the mechanism of its formation, it appears that an important role is played by the hydrology of this region itself, and more precisely the quasi-uniform layer of the 18° water located within the limits of the depths from 100 meters to 400 meters. Without excluding other explanations, let us state some arguments with respect to causes of formation of the layered structure of the observed anticyclone.

Let us propose that initially the anticyclone had the usual structure, that is, all of the isolines were concave. Let us also propose that on the whole it is stable and subject to geostrophic relations. The presence

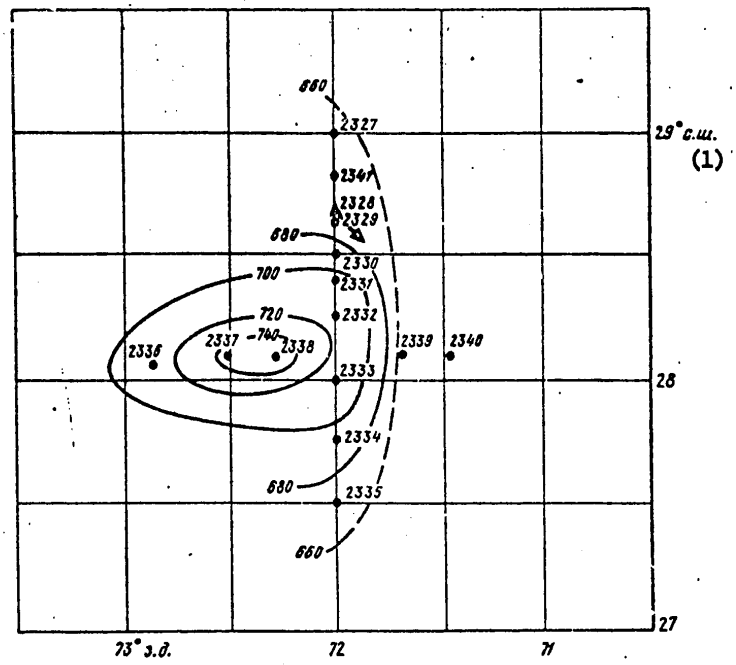

Figure 1. Diagram of the arrangement of the hydrologic stations:
Isolines -- depths of the current of the 15° isotherm;
Triangle -- position of the buoy station at the point Y;
The arrrow -- predominant current direction in all horizons

Key:
1. north latitude

of the quasiuniform layer of 18-degree water can cause the following phenomenon. It is known that in the flow of a uniform liquid with transverse velocity gradient (having an inflection point), the exchange between layers moving with different velocities is possible. Let us assume that on the periphery of the anticyclone such exchange has led to the reduction of the velocity in the quasiuniform layer of 18-degree water. Then one of the possible paths of restoration of the geostrophic equilibrium is the occurrence of the compensation flows leading to lowering of the isopycn of the upper layer with a change in sign of the horizontal density gradient. This density is caused by the known equation following from the geostrophic relations:

$$\frac{du}{dz} = \left(\frac{g}{f - \frac{2u}{r}}\right)\frac{1}{\rho}\frac{\partial \rho}{\partial x},$$

here r is the eddy radius. Actually, in the uniform layer of the geostrophic flow du/dz=0; with a decrease in velocity on the vertical

profile u, the minimum appears, which can be compensated for by the appearance of a horizontal density gradient.

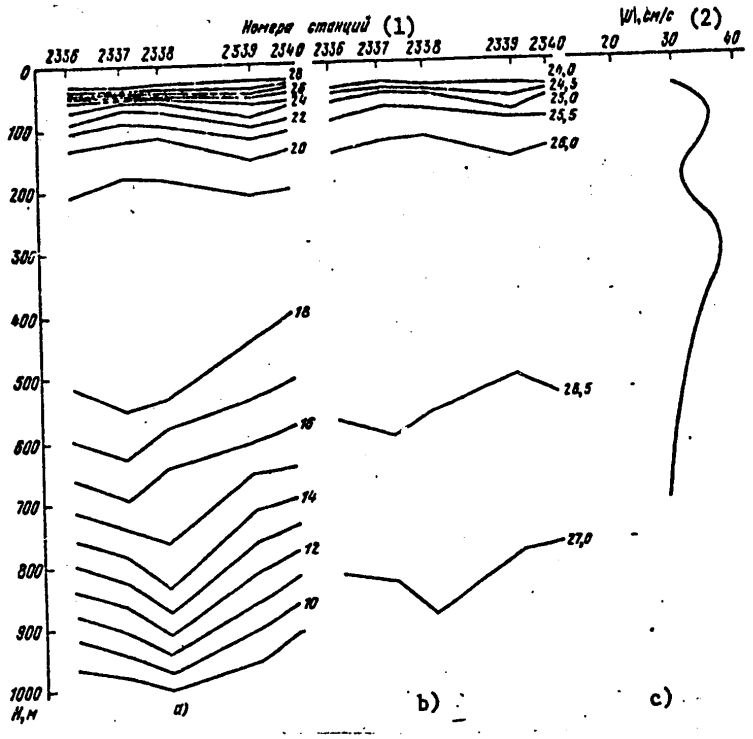

Figure 2. Distribution of the hydrologic characteristics in the sections and vertical velocity diagram. Temperature distribution (a) and provisional density distribution (b) in the zonal section; diagram of the velocity modulus at the point Y by the BPV measurements (c)

Key:
1. Station number
2. |U|, cm/sec

An autonomous buoy station (buoy Y) which operated for 36 hours, was installed to study the vertical distribution of the horizontal velocity in the northeastern peripheral part of the eddy. The current meters are located in the 50, 100, 200, 250, 300, 400 and 700 meter horizons. Fig 1 shows the position of the buoy and the direction of the current (the arrow), which for all the measurement horizons is in practice invariant and was within the limits of 140 to 150°.

Fig 2, c shows a diagram of the velocity modulus in the anticyclone by the BPV measurement data. From the figure it is obvious that the minimum velocity at the 200-meter horizon is quite obvious. Thus, the direct measurements of the currents confirm the theoretical proposition of the presence of a minimum velocity in the vicinity of the uniform layer, that is, where the direction of the convexity of the isopycns changes.

Abstract

An an anticyclonic eddy observed in the POLYMODE area, the temperature and density isolines are shown to be displaced upward in the upper 200-meter layer and downward in the lower layers. This leads to a minimum in the velocity profile that is confirmed by direct measurements of the currents.

BIBLIOGRAPHY

1. Leetmaa, A. "Recent Observations of Eddies Southwest of Bermuda," POLYMODE NEWS, No 10, 1976.

[8044/0785-10845]

10845
CSO: 8044/0785

POLYMODE INTERNATIONAL LARGE-SCALE OCEAN EXPERIMENT

Moscow OKEANOLOGICHESKIYE ISSLEDOVANIYA in Russian No 30, 1979 pp 5-9

[Article by V. G. Kort]

[Text] An interdepartmental expedition to the central part of the Atlantic Ocean provisionally called "Poligon-70" was made in 1970 under the direction of the Oceanological Institute imeni P. P. Shirshov of the USSR Academy of Sciences (IOAN SSSR). Continuous observations of the variability of the basic hydrophysical characteristics (current, temperature, salinity, and so on) over an area of 120x120 nautical miles were performed for 6 months from expeditionary ships and autonomous oceanographic buoy stations. The results of these unique studies of ocean dynamics turned out to be very interesting. Large eddy disturbances of the current velocity vector resembling atmospheric cyclones and anticyclones were detected in the open sea, in the vicinity of quasistationary currents (the Northern Tradewind Current). The characteristic scale of these ocean eddies was on the order of 100 to 200 km. They were traced to depths of 1000 to 1500 meters. In the vicinity of the test area, the eddies moved in a westerly direction with mean diurnal velocity to 5 cm/sec with an average orbital velocity at depths of 200-300 meters of 20-25 cm/sec. The detection by the Soviet scientists of such powerful eddy disturbances in the ocean stimulated the development of similar studies in other countries. Thus, in 1972 American researchers began to study eddy disturbances in the southwestern part of the North Atlantic under the Middle Ocean Dynamics Experiment Program -- MODE -- which is also called the MODE Program in Russian. The results obtained by American researchers confirmed the existence and the great variety of the eddy movements in the ocean with respect to scale and genesis.

The discovery of the synoptic eddies in the ocean has great scientific significance; it has introduced basic changes into our concepts of the internal dynamics of the ocean and it has directed theoretical and experimental dynamic oceanology toward the study of the processes of synoptic eddy formation and the interaction of eddies with large-scale processes. It appears very important to consider the fact of the existence of synoptic eddies when performing research with respect to many areas of oceanology

such as acoustics of the ocean, the hydrochemical structure of water, biological productivity, pollution and propagation of a passive admixture, and so on, and to tie the results to the hydrologic and kinematic structure of the ocean formed by the processes of synoptic eddy formation.

Considering the important role of eddy disturbances in the dynamics of the water of the World Ocean and also the great complexity and tediousness of studying them in 1974 the scientific program for Soviet-American cooperation in the study of the World Ocean was developed and adopted. This program -- the International Large-Scale Ocean Dynamics Experiment -- is a logical development of the research under the Poligon-70 and MODE programs, and it is provisionally called POLYMODE (POLIMODE in Russian). The scientific research ships of Great Britain, Canada, France and the Federal Republic of Germany are also participating in this program which is planned to last 5 to 6 years.

The basic scientific goals of the research under the POLYMODE program are the following:

1. The kinematic and statistical study of the ocean eddy field, including the interaction of the eddies with each other on significantly larger time-space scale than in the preceding studies.

2. Determination of the local dynamic balance in the most typical parts of the ocean.

3. Determination of the role of the eddy transfer of momentum and energy; the variation of this transfer in space and time; interaction of eddies with the average motion.

4. Study of the mechanisms of the occurrence, transfer and dispersion of energy in eddies.

5. Study of the large-scale currents in the research area and their variability with respect to depth and time.

6. Study of mesoscale phenomena in the ocean (internal waves, inertial currents) and the processes in the upper layer of the ocean and their interrelation to synoptic eddies.

7. Study of the lower layer of the atmosphere and the possible influence of atmospheric processes on synoptic ocean eddies.

8. Development and checking of the numerical models of the medium-scale and overall ocean circulation considering medium-scale eddies.

The satisfaction of these goals permits us to create a scientific basis for short-period and long-period oceanographic forecasts and it will offer the possibility of constructing a combined dynamic model of the ocean-atmosphere system required for further improvement of the weather forecasting methods.

The POLYMODE program provides for Soviet research from July 1977 to August 1978 in the hydrophysics test area located in the southwestern part of the North Atlantic Ocean. The center of the test area 300x300 miles is bounded by the coordinates of 29° north latitude and 70° west longitude. This region is characterized by significant velocities in the eddy field and a wind mode that is comparatively favorable for long-term operation of the oceanographic buoy stations with surface buoyancy. The American researchers continued the work started in 1976 on the oceanographic buoy stations to the north, northeast and southeast of the Soviet test area and performed a local synoptic experiment near the main test area.

The schedule for the international expeditionary studies by the POLYMODE program is presented in the table. In addition to the expeditionary work, this plan provides for theoretical studies and numerical experiments on hydrodynamic models of ocean eddies. The work is being participated in by the leading Soviet and American theoretical oceanologists. The head institutes with respect to execution of the POLYMODE program are the following: the Oceanology Institute of the USSR Academy of Sciences in the USSR, and Woods-Hole Oceanographic Institute in the United States.

The studies by Soviet oceanologists under the POLYMODE expeditionary program began at the end of June 1977. Six scientific research vessels participated in the first phase of the research (June-October 1977): "Akademik Kurchatov" (Oceanology Institute of the USSR Academy of Sciences), "Akademik Vernadskiy" (the Marine Hydrophysics Institute of the Ukrainian SSR Academy of Sciences), "Akademik Krylov" (Hydrographic Service), "Petr Lebedev" and "Sergey Vavilov" (Acoustics Institute of the USSR Academy of Sciences) and "Viktor Bugayev" (GOIN Institute).

In the test area the following were performed: the installation and adjustment of the autonomous oceanographic buoy stations; controlling of them with oceanographic observations on the side; quasisynchronous hydrologic surveys on different scales; oceanographic observations in microtest areas (on the scale of one eddy formation); meteorological and geophysical observations with respect to the routes of ships.

In accordance with the recommendations of the Soviet organizational committees for POLYMODE the work in the test area was performed on four scales (figures):

1) The quasisynchronous large-scale hydrologic surveys using losable temperature buoys (XBT)* throughout the body of water involved in any test area with a uniform grid step size of 17 miles;

---

* The XBT probes (iosable bathythermosondes) with starting recording device were provided by the American scientists.

Schedule of International Research Under the POLYMODE Program

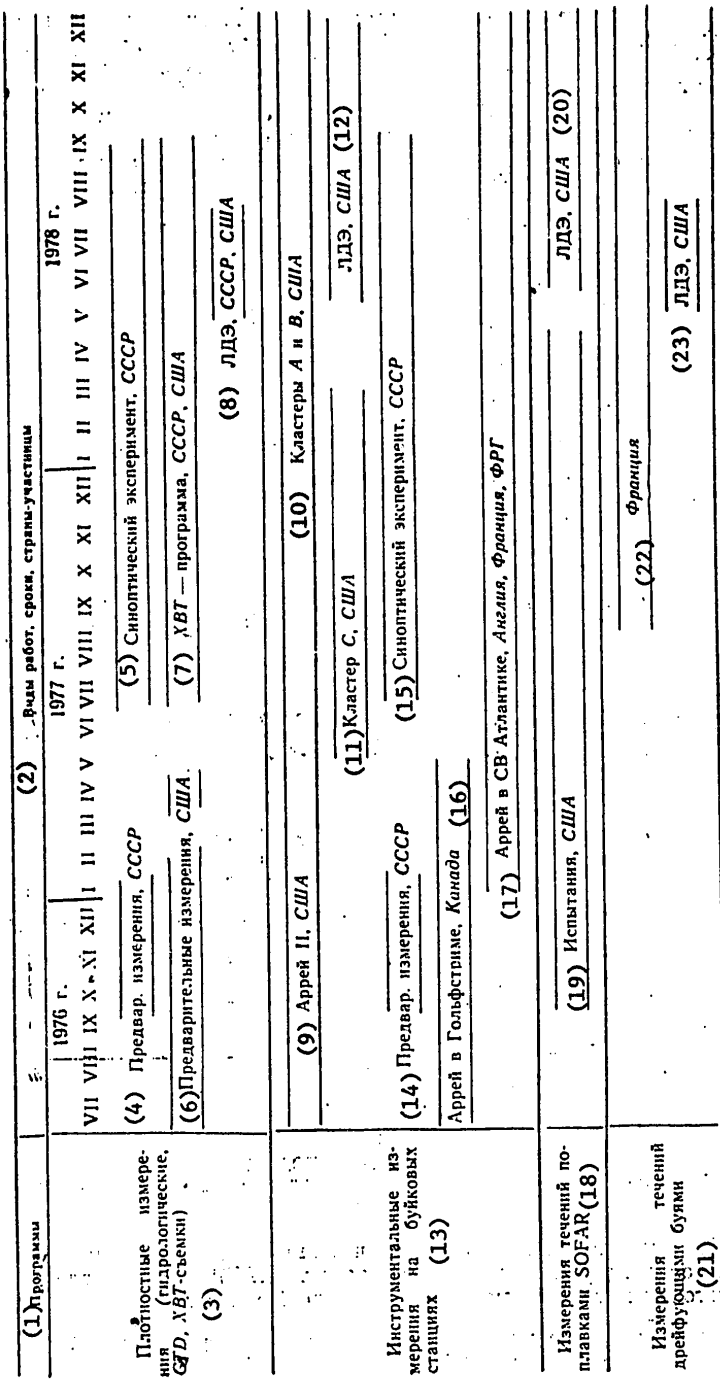

[See key on following page]

[Key to table "Schedule of International Research under the POLYMODE Program"]:

1. Programs
2. Types of operations, times, participating countries
3. Density measurements (hydrologic, CTD, XBT-surveys)
4. Preliminary measurements, USSR
5. Synoptic experiments, USSR
6. Preliminary measurements, USA
7. XBT-program, USSR, USA
8. LDE, USSR, USA
9. Array II, USA
10. Clusters A and B, USA
11. Cluster C, USA
12. LDE, USA
13. Instrument measurements on buoy stations
14. Preliminary measurements, USSR
15. Synoptic experiment, USSR
16. Array in the Gulf Stream, Canada
17. Array in the Northeast Atlantic, England, France, Federal Republic of Germany
18. Current measurements by the SOFAR floats
19. Tests, USA
20. LDE, USA
21. Current measurements by drifting buoys
22. France
23. LDE, USA

LDE -- local dynamic experiment; array -- a group of waves in one line; cluster -- a group of buoys clustered together.

2) Quasisynchronous mesoscale hydrologic surveys using XBT probes, salinity temperature probes (ISTOK, AIST) and bathometric measurements in the inside part of the test area with the same station grid spacing;

3) Long-term oceanographic observations at 19 autonomous oceanographic buoy stations installed at the corners of equilateral triangles (39 miles on a side) on the inside body of water of a test area 134x154 miles with its center at the coordinates 29° north latitude, 70° west longitude;

4) Oceanographic observations in microareas on the scale of individual eddy formations.

Bottom depths in the water of the test area vary from 5100 to 5400 meters. The current and temperature recorders were installed on the 50, 100, 400, 700, and 1400 meter levels. The observations by the XBT probes were made to a depth of 750 meters, the ISTOK and AIST probes and the bathometric series, to 2000 meters.

The selection of the mentioned observation levels by the autonomous buoy stations arose from the following arguments: 50 meters -- this is the layer of active interaction with synoptic processes in the atmosphere; 100 meters -- seasonal thermocline; 400 meters -- layer of 18-degree water of the Sargasso Sea; 700 meters -- 700 meters -- principal thermocline; on this level observations are being made in accordance with the American program using the SOFAR acoustic floats; 1400 meters -- depth of pure barotropic synoptic current fluctuations. The TsIITT digital integrating

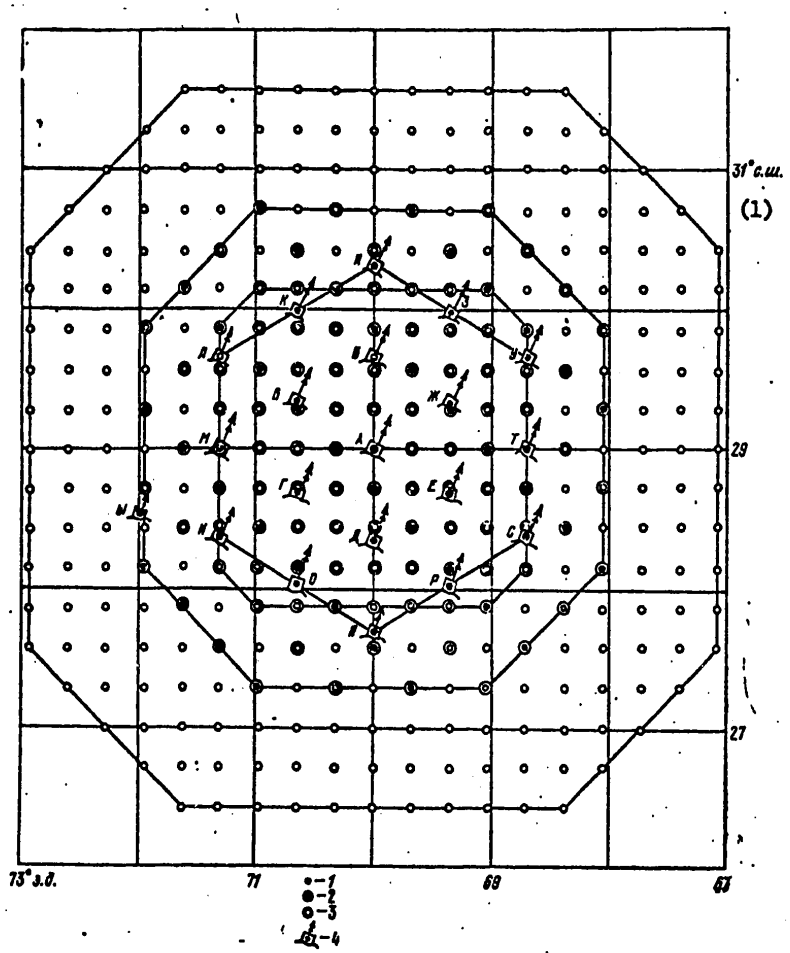

Diagram of the POLYMODE expedition:
1 — XBT-sounding; 2 -- hydrologic series; 3 -- STD-sounding;
4 -- autonomous buoy stations

Key:
1. 31° north latitude

automatic recorders developed and manufactured at the IOAN Institute (designed by Valovskiy), the TsITT-3 meters (designed by Shekhvatov) and the BPV-2 recorders (designed by Alekseyev) were used to measure the velocity vectors of the currents and the water temperature.

During the period from 11 July to 3 October 1977, the expeditionary ships conducted five large-scale and three mesoscale surveys and also observations in several microareas. During the same time the "Akademik Kurchatov" scientific research ship conducted 66 installations and 46 surveys of the autonomous oceanographic buoy stations.

During the first phase of the work in the test area, about 1 million recordings were made of the current velocity vector components, 463,000 water temperature recordings, observations at 1800 hydrologic stations and temperature sounding stations. All of the data went through primary processing.

The materials of this and the subsequent stages of the expedition will be published in the collections of articles OKEANOLOGICHESKIYE ISSLEDOVANIYA [Oceanological Research], Nos 31, 32, and so on.

Abstract

The Soviet-American POLYMODE proram, the goals of the experiment, the ship measurement program and structure of the test areas in the south-western part of the North Atlantic are described. The main types of the studies to be performed during the expedition and the time-space scales to be studied are analyzed.

[8044/0785-10845]

10845
CSO: 8044/0785

STUDY OF THE TRAIN STRUCTURE OF SHORT-PERIOD TEMPERATURE FLUCTUATIONS

Moscow OKEANOLOGICHESKIYE ISSLEDOVANIYA in Russian No 30, 1979 pp 93-96

[Article by A. S. Samodurov, Ye. G. Morozov]

[Text] There are a significant number of studies in which it is noted that the short-period (T~1 hour) internal gravity waves exist in the ocean in the form of individual groups separated by sections of relative quiet [1-4]. Most frequently the groups (or trains) of waves are detected in defined phases of the larger scale internal waves, as a rule, tidal. However, the distinguishing feature of the indicated measurements is the fact that they basically were performed in the coastal shallow region where the amplitudes of the long-period waves are maximal. In the case where the regime of the large-scale wave is close to critical it was demonstrated [5] that the wave train is formed in the vicinity of the point $u=c_\phi$, where u is the orbital velocity in the wave, c_ϕ is the phase velocity.

The present study was undertaken in order to discover how much the train structure of the short-period internal waves is characteristic for the open sea and also to determine the periodicity of the appearance of the trains. It must be noted that experimentally the train structure of the short-period fluctuations was also noted in the open sea [6-7], but its existence was determined by the series lasting no more than 8-10 days, that is, it was not confirmed statistically. Therefore it is difficult to judge the periodicity of the appearance of the trains. The performed experiment made it possible to obtain continuous series of long duration with small discreteness.

We have used series lasting about a month with a discreteness of 6 minutes. With respect to the successive 2-day segments of this series spectral functions were calculated for determining the clearly expressed energy-bearing period τ in the high-frequency region of the spectrum. The number of degrees of freedom was 20 everywhere. An example of this series of spectra is presented in Fig 1, from which it is obvious that on periods close to 1 hour from time to time high energies appear. However, after a short time these fluctuations cease to give blips on the spectra.

It must be noted that the 50-meter horizon that we selected for investigation is the most characteristic by the variability of the fluctuation spectra in time and also the large vertical temperature gradients inasmuch as it is located in the seasonal thermocline layer. Let us note that on other horizons the variability of the spectra in time also occurs. The measurements performed with such small discreteness at a depth of 1400 meters indicate the presence of very strong variability also at this depth.

By using the method of complex demodulation [8], from the initial realization fluctuations were isolated in a narrow range of periods $\tau \pm \Delta\tau$. The value of $\Delta\tau$ in all cases was 5 minutes. The period τ was selected by the spectral analysis, that is, τ is also the period in the high-frequency region of the spectrum at which high-energy blips appeared. After processing the series by the method of complex demodulation, the harmonic of the desired period was obtained with amplitude variable in time. From this harmonic, a series of amplitudes were compiled. Its discreteness was equal to the period τ respectively. Thus, the series obtained is the envelope of the harmonic isolated after complex demodulation. The spectrum was again calculated by the formed series. The location of the peaks on the constructed spectrum (let us call it ψ) indicates the most probable periodicity of the appearance of groups of high-frequency internal waves.

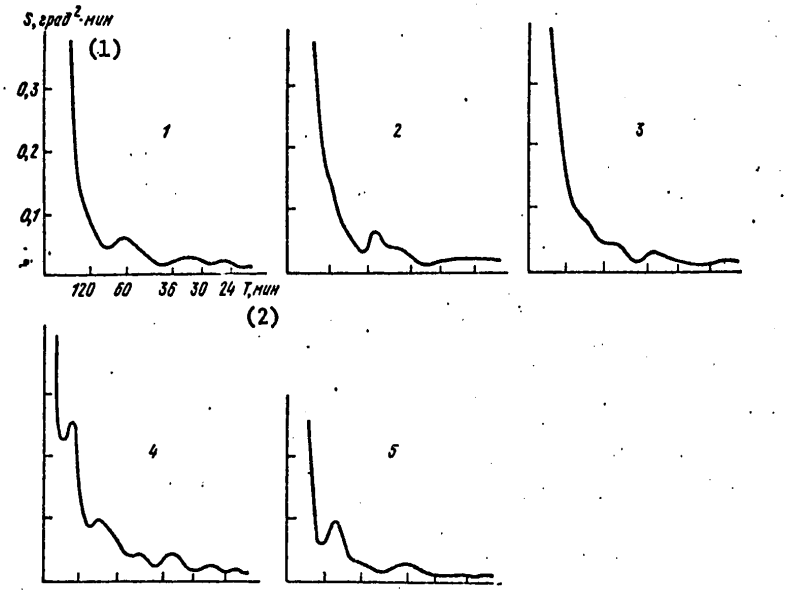

Figure 1. Five functions of the spectral density calculated by the successive two-day series on the buoy M (50-meter horizon). The graphs indicate the time variability of the temperature fluctuations. The numbers are the numbers of the realizations.

Key:
1. S, deg^2-min; 2. T, min

Before we proceed to a discussion of the results, let us note that the region in which the measurements were made is distinguished by a complex system of currents caused by the passage of the powerful ocean eddies.

In reference [9] it was demonstrated that as a result of the Doppler effect existing here the tidal and inertial peaks in the temperature spectra can shift with respect to frequency, which frequently also occurs in reality. For the conditions of the test area the shifts can be highly significant. Thus, if the currentswith a velocity of 30 to 50 cm/sec and a propagation rate of the observed wave of diurnal period are directed in opposite directions, the corresponding peak shifts to the vicinity of the periods of 38-60 hours. The described phenomenon turned out to be significant for the results of this paper.

In Fig 2, a, d, spectral functions ψ are depicted for four points of the test area. According to the data of the spectral analysis for the series obtained at the points M, H, П, K the periods τ of the isolated oscillations were selected equal to 60, 48, 50 and 60 minutes respectively.

From Fig 2 it is obvious that at two points M and П there is a blip on a period of about 24 hours; at the points H and K there are quite strong peaks in the 40-hour range; at the point П, a blip of about 50 hours. As for the semidiurnal period, on the presented graphs it in practice does not appear.

In our opinion, the peculiarities in the behavior of the function ψ are caused by the following causes.

The groups of short-period internal gravity waves are formed in defined phases of the internal tidal waves. This process occurs as follows. If the short-period waves have a group velocity equal to the phase velocity of some large-scale wave, the nonlinear resonance interaction occurring in the system leads to growth of the small-scale disturbances [10-12]. This mechanism must be manifested most strongly in the vicinity of the defined phase of the long wave where as a result of the peculiarities of the vertical distribution of the velocity intensity (the Richardson number is minimal) the occurring small-scale wave disturbances are suppressed to the least degree.

As an illustration in Fig 3 we have the temperature fluctuations with a period of 24 hours isolated from the initial series using the method of complex demodulation and variations in time of the fluctuation amplitude with a period of 48 minutes at the same point. It is obvious that the peaks of the lower curves frequently occur for the same phase of the diurnal wave. It is interesting to note that the amplitude of the latter in the indicated phase is zero. This means, in particular, that the time behavior of the amplitude of the short-period oscillation is caused by aperiodic variations of the mean temperature gradient caused by the diurnal wave.

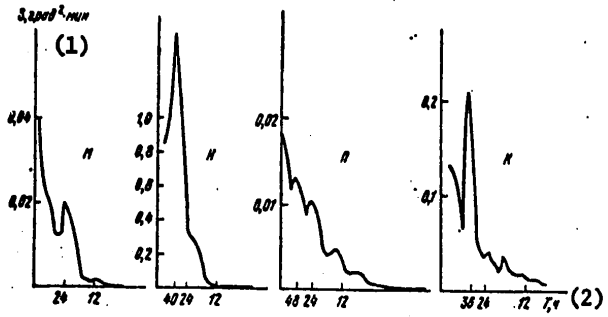

Figure 2. Spectral density functions Ψ constructed by the series of amplitude peaks after processing the series by the method of complex demodulation according to the data of buoys M, H, П, K (50-meter horizon)

Key:
1. S, deg^2-min
2. T, hours

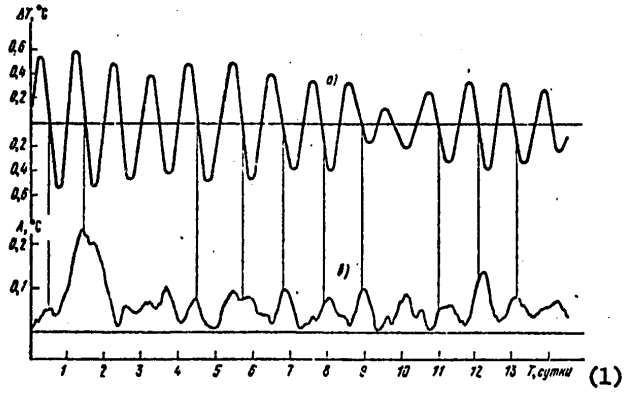

Figure 3. Time variability of the diurnal temperature fluctuation and temperature fluctuations with a period of 48 minutes (50 meter horizon): a -- diurnal fluctuation harmonic, b -- amplitude of the fluctuation with a 48-minute period. The lines join the amplitude peaks with a period of 48 minutes for defined phases of the diurnal fluctuation.

Key:
1. T, days

The appearance of the groups of high-frequency waves with periods greater than 24 hours is caused by the Doppler effect as a result of which the parameters of the diurnal internal wave vary [9].

The "energy" of the groups of waves appearing with diurnal periodicity is greater than the "energy" of the trains of semidiurnal period inasmuch as the parameters of diurnal wave are such that in them the occurrence of the trains of short-period waves has greater probability. The internal wave with a 24-hour period is characterized by large mode number [9]. This means that the vertical scale of the diurnal wave is less than semidiurnal and, consequently, here for equal amplitude large vertical velocity gradients are formed. In addition, for equal amplitudes the diurnal wave is steeper than the semidiurnal as a result of the fact that for a large mode number the wave length is shorter. This leads to instability of the wave and the formation of a packet of short-period waves.

The increase in "energy" of the trains on periods of 38-60 hours is explained by the fact that the corresponding gradients of the quasi-stationary current are superposed on the vertical velocity gradients in the diurnal wave. This implies an increase in the overall velocity shift and promotes more intense growth of the short-period disturbances.

Abstract

The periodicity of the short-period internal wave trains is studied. The wave trains are shown to occur with the period of the diurnal tidal wave due to the instability of the latter.

BIBLIOGRAPHY

1. Ziegenbein, J. "Short Internal Waves in the Strait of Gibraltar," DEEP SEA RES., Vol 6, No 5, 1969.

2. Gade, G.; Eriksen, F. "Notes on the Internal Tide and Secondary Oscillations in the Strait of Gibraltar," ARBOK UNI V. BERGEN, MAT.-NATUR. SER., No 9, 1969.

3. Hecht, A.; Hughes, P. "Observations of Temperature Fluctuations in the Upper Layers of the Bay of Biscay," DEEP SEA RES., Vol 18, No 7, 1971.

4. Byshev, V. I.; Ivanov, Yu. A.; Morozov, Ye. G. "Study of Temperature Fluctuations in the Frequency Range of the Internal Gravity Waves," IZV. AN SSSR. SER. FIZ. ATM. I OKEANA [News of the USSR Academy of Sciences. Physics of the Atmosphere and Ocean Series], Vol 7, No 1, 1971.

5. Samodurov, A. S. "Generation of Internal Wave Trains in the Ocean," ISSLEDOVANIYE IZMENCHIVOSTI GIDROFIZICHESKIKH POLEY V OKEANE [Study of the Variability of the Hydrophysical Fields in the Ocean], Moscow, Nauka, 1974.

6. Sabinin, K. D. "Some Peculiarities of Short-Period Waves in the Ocean," IZV. AN SSSR. SER. FIZ. ATM. I OKDEANA, Vol 9, No 1, 1973.

7. Morozov, Ye. G.; Plakhin, Ye. A.; Shapovalov, S. M. "Study of the Temperature Fluctuations in the Northwestern Part of the Pacific Ocean in the Frequency Band of the Internal Gravity Waves," OKEANOLOGIYA [Oceanology], Vol 16, No 1, 1976.

8. Prival'skiy, V. Ye. "Complex Demodulation of Random Processes and Its Application for Tide Analysis," MATERIALY XIII NAUCHNOY KONFERENTSII DVGU [Materials of the 13th Scientific Conference of the Far Eastern Hydrologic Administration], Part 5, No 1, Vladivostok, 1969.

9. Morozov, Ye. G.; Samodurov, A. S.; Limanskaya, L. I.; Filatova, L. P. "Study of the Diurnal and Semidiurnal Temperature Fluctuations," see the present collection, p 63.

10. McIntyre, M. E. "Mean Motions and Impulse of a Guided Internal Gravity Wave Packet," J. FLUID MECHAN., No 60, 1973, pp 801-811.

11. Grimshaw, R. "The modulation and Stability of an Internal Gravity Wave," MEM. SOC. ROY. SCI., Liege, 6th Series, No X, 1976, pp 299-314.

12. Grimshaw, R. "The Modulation of an Internal Gravity Wave Packet and the Resonance with the Mean Motion," STUD. IN APPLIED MATHEM., No 56, 1977, pp 241-266.

[8044/0785-10845]

10845
CSO: 8044/0785

UDC 528.516;621.396.962.21

PHASE RADIOGEODETIC SYSTEMS FOR MARINE RESEARCH

Moscow FAZOVYYE RADIOGEODEZICHESKIYE SISTEMY DLYA MORSKIKH ISSLEDOVANIY (Phase Radiogeodetic Systems for Marine Research) in Russian 1979 signed to press 11 Nov 79 pp 2, 152-153, 162-163

[Annotation, conclusion and table of contents of book by A. M. Agafonnikov, Izdatel'stvo "Nauka," 1,000 copies, 164 pages]

[Text] Annotation. In this book the author generalizes and systematizes information on phase radiogeodetic systems operating in the range 1.5-3 MHz. Their circuitry is described, as is the instrumentation itself and the methods for using it. Information is given on the propagation of radio waves. The problems involved in increasing the accuracy of systems and the prospects and directions of their development are considered. The monograph is intended for scientific workers, graduate students, engineers and students specializing in the field of marine geodesy and radionavigation. Tables 2, figures 77. Bibliography of 184 items.

Conclusion. As already confirmed by the enormous experience in their use, phase radiogeodetic systems as a tool for horizontal coordinate tie-in have a number of valuable qualities which make them indispensable in conducting many types of marine research and exploration work: high accuracy, continuity of operation, technical simplicity in obtaining a reading of the conditional coordinates. At the same time they have a number of shortcomings restricting the possibilities of their use: low effective range, need for setting up and servicing a chain of shore stations, and ambiguity of the phase reading. How promising are phase radiogeodetic systems and will they not be replaced by other systems and apparatus having positive qualities but which are without some of their shortcomings?

The most probable alternative for phase radiogeodetic systems are satellite navigational and geodetic systems which operate without interruption. Existing satellite navigational systems have a high discreteness of determinations (up to one determination each one or two hours in the low latitudes in the "Transit" system) and a duration of one determination equal to the time of satellite transit over the radiohorizon of the point to be determined (12-18 minutes). In the United States specialists have developed a plan for the continuously operating "Navstar" satellite

navigational system which it is planned will be in operation in 1985. According to preliminary computations, it will provide users (which at first will be the United States Army, Navy and Air Force) with a continuous determination of position with a horizontal and vertical error of 30 m. For the time being no real accuracy evaluations have been published. In the future systems of this class can evidently replace phase radiogeodetic systems. However, this will require that they ensure a guaranteed accuracy in determining position the same as phase radiogeodetic systems and that the cost of the apparatus and its operation be the same as in phase radiogeodetic systems. A period of about 10-20 years after introduction of the "Navstar" system may evidently be required in order to attain these indices and until then the system will be used in regions where the required accuracy and continuity of tie-in cannot be ensured by phase radiogeodetic systems due to the impossibility of further deployment. It can therefore be asserted that in the next 15-20 years phase radiogeodetic systems will not be replaced by satellite systems, at least in the traditional areas of their use.

During recent years communications have appeared in the press concerning the use of tropospheric scattering for increasing the effective range of ultrashort-wave systems to 300 km. The advantages of the ultrashort-wave range are: absence of reflections from the ionosphere and considerably lesser restrictions on the width of the signal spectrum, as a result of which exclusively wide-band systems ensuring an unambiguous determination of position with a still higher accuracy than phase radiogeodetic systems are used in this range. Unfortunately, the effective range of these systems is limited to the distance of direct visibility, not exceeding 70 km over the sea under ordinary conditions (the heights of raising antennas is about 20-30 m). Tropospheric scattering makes possible a considerable increase in the range of propagation of ultrashort waves beyond the horizon, but in this case it is necessary to have a very great increase in transmitter powers. To a considerable degree this limits the possibilities of using such systems. In addition, the conditions for tropospheric propagation are characterized by instability associated with tropospheric turbulence. For these reasons there is no basis for assuming that ultrashort-wave radiogeodetic systems with the use of tropospheric scattering can be an alternative to phase radiogeodetic systems, although in some favorable cases they can be used instead of them.

It therefore follows from everything set forth above that phase radiogeodetic systems operating in the range 1.5-3 MHz will continue to remain an indispensable means for highly precise horizontal coordinate tie-in for the coastal zones of seas and oceans and will be promising for at least the next 15-20 years. This will require their further instrumental improvement and the further development of methods for their use.

CONTENTS Page

[291-5303]
5303/CSO: 1865

ARTICLES ON THEORY AND PREDICTION OF TSUNAMIS

Moscow TEORIYA I OPERATIVNYY PROGNOZ TSUNAMI (The Theory and Operational Prediction of Tsunamis) in Russian 1980 signed to press 1 Nov 79 pp 3-4, 173

[Preface and table of contents from collection of articles edited by V. N. Nekrasova, Izdatel'stvo "Nauka," 800 copies, 179 pages]

[Text] Preface. This collection of articles was prepared by the Commission on Tsunamis of the Interdepartmental Council on Seismology and Seismic Resistant Construction of the Presidium USSR Academy of Sciences in collaboration with the Sakhalin Multidiscipline Scientific Research Institute Far Eastern Scientific Center USSR Academy of Sciences and other organizations. Earlier collections of articles of this type were published by the Interdepartmental Council on Seismology and Seismic Resistant Construction and the Sakhalin Multidiscipline Scientific Research Institute in 1956, 1961, 1968, 1972, 1973, 1977 and 1978 (twice).

Most of the articles in this collection are devoted to improvement in the seismic method for predicting tsunamis, which since the beginning of the 1950's, when the service for warning the population of the Far East about the approach of tsunamis was established, to the present time in essence remains the sole working method for making such predictions. Due to its statistical character it cannot, in principle, ensure a 100% reliability and effectiveness of the service. The universal improvement of this method is evidently of great importance. Appropriate efforts are now being undertaken in the following directions: 1) search for new criteria relating earthquakes to the generation of tsunamis; 2) refinement of the magnitude criterion in relation to generation of tsunamis; 3) automation of processing of seismological data.

As additional criteria relating to the generation of tsunamis, during recent years it has been traditional to study the spectral composition of body waves, earthquake depth and focal mechanism. In this collection of articles A. I. Ivashchenko and A. A. Poplavskiy, R. N. Burymskaya and N. A. Zhbrykunova examine the search for spectral criteria; definite progress is noted here, but it must be noted that the mean absolute level of the amplitude spectrum of a longitudinal wave discriminated by A. I. Ivashchenko

and A. A. Poplavskiy as a criterion for an earthquake generating a tsunami in essence means giving a preference to the magnitude m_p over the ordinary magnitude M in evaluating whether an earthquake leads to the formation of a tsunami. A detailed examination of the possibilities of using the earthquake focal mechanism for increasing the effectiveness of prediction is examined in an article by R. N. Burymskaya and Ye. A. Vorob'yeva; the problem is difficult to solve due to the need for using data for only one station under the present conditions of the service.

The articles of A. I. Ivashchenko and F. D. Zhuk, L. S. Oskorbin and O. N. Solov'yeva refine the peculiarities of computation of magnitude of an earthquake under the conditions of operational work at tsunami stations. The results make it possible to increase the accuracy of computations. A. A. Poplavskiy and I. N. Tikhonov continue a long-term cycle of studies for creating a set of algorithms on the basis of which it would be possible to automate determination of the principal parameters of an earthquake. The article by Ye. A. Vorob'yeva is devoted to a nontraditional method for determining the epicentral distance of an earthquake, since on the records of instruments at tsunami stations in the Far East transverse waves frequently are poorly expressed or are entirely absent. This section was prepared under the direction of A. A. Poplavskiy.

Three published articles describe individual possible components of an observation system for the detection of tsunamis in the open ocean. For example, I. M. Shenderovich and G. N. Mar propose a filter of a fundamentally new type for discriminating tsunamis from the superposing of ocean level oscillations; A. G. Smagin and his colleagues propose a quartz sensor for measuring ocean level; B. V. Levin, B. M. Lisenko and V. Ye. Rokotyan propose that lidars be used for detecting tsunamis at relatively short distances from the shore.

Individual articles are devoted to further theoretical work on problems related to tsunami excitation and propagation. They contain new, original results. S. S. Voyt, A. N. Lebedev and B. I. Sebokin examine the problem of tsunami excitation when there is a horizontal effect on the water layer -- a quite typical case under natural conditions, but virtually not considered in the literature (in contrast to vertical movements of the sea floor). V. F. Ivanov and L. V. Cherkesov undertake a study of the contribution of dispersion and nonlinearity to the transformation of tsunamis in the process of approach of waves to the shore and obtain refined estimates. An article by Ye. N. Pelinovskiy, I. A. Soustova and V. Ye. Fridman examines the phenomenon of diffraction of tsunamis which is difficult to analyze and therefore which has been poorly studied.

The subject matter of two articles is treated for the first time in a collection of articles on the tsunami problem. A note by A. M. Shurygin gives a preliminary statistical analysis of the process of inundation of the coast by tsunami waves in the example of Libya and

the article by V. A. Butkovskiy, N. V. Deryugin and N. A. Simonov describes an automated system for warning the population about tsunamis which has been created on Kamchatka which makes maximum use of the ordinary radio and television system. In the cycle of further studies of the tsunami problem, great attention will undoubtedly be devoted to the problems involved in tsunami regionalization and communication subsystems.

Although within the framework of a collection of articles it is impossible to reflect all the attainments in studies of the tsunami problem in the USSR, it can be hoped that even in this form it will be of considerable interest for specialists interested in development of means and methods for contending with such threatening calamities.

A. A. Poplavskiy and B. N. Sheyn took an active part in preparing the collection of articles.

CONTENTS Page

CONTENTS (Continued) Page

5303
CSO: 1865

UDC 550.34; 551.24+550.312+551.34+621.311.21+625.110

SEISMOGEOLOGY OF THE MONGOLIAN-OKHOTSK LINEAMENT (EASTERN FLANK)

Novosibirsk SEYSMOGEOLOGIYA MONGOLO-OKHOTSKOGO LINEAMENTA (VOSTOCHNYY FLANG) (Seismology of the Mongolian-Okhotsk Lineament (Eastern Flank)) in Russian 1979 signed to press 18 Sep 79 pp 2-4 and table of contents

[Annotation, introduction and table of contents from book by V. V. Nikolayev, R. M. Semenov and V. P. Solonenko, Izdatel'stvo "Nauka," Sibirskoye Otdeleniye, 1,000 copies, number of pages not given]

[Text] Annotation. The geological structure, neotectonics and seismogeology of the Tukuringra-Dzhagdinskaya part of the Mongolian-Okhotsk zone of deep faults are examined for the first time for seismic regionalization purposes. Seismogeological, seismic and geophysical data are used in determining the potential seismicity of specific morphostructures and for carrying out seismic regionalization of a territory earlier considered to be virtually aseismic. The seismogeological conditions of the Zeya Hydroelectric Power Station and the Zeya segment of the route of the Baykal-Amur Railroad are described. The book will be of interest to seismogeologists, seismologists, specialists in the field of neotectonics, and also those engaged in the planning of transportation, hydraulic, industrial and civil structures.

Introduction. A system of ranges, the Yankan, Tukuringra and Dzhagdy, extends latitudinally across the entire upper Amur region. This system is bounded on the north by the Tukuringra-Stanovoye intermontane depression and the Udsko-Zeyskiy downwarp, and on the south by the Verkhne-Amurskaya depression and the Amur-Zeya plain. This mountainous ridge is associated with the Yankanskiy and Tukuringra-Dzhagdinskiy anticlinoria, whose formation is structurally closely related to the Mongolian-Okhotsk marginal suture.

The Tukuringra-Dzhagdinskaya mountainous country is poorly populated. Naturally, information concerning its seismicity was extremely scanty and since seismic catastrophes have not occurred here, it has not attracted the attention of seismologists and seismogeologists. The low level of seismic information was equated to a low level of seismic activity of the territory -- 5 scale units according to the norms given in the SNiP P-A.12-69 (STROITEL'STVO..., 1970), although seismogeologists had assumed earlier

that strong earthquakes can occur here (Gorshkov, 1937; Solonenko, 1950).

In connection with the planning of the Zeya Hydroelectric Power Station the Institute of Physics of the Earth USSR Academy of Sciences during 1964-1968 carried out a study of the seismicity in the seismically dangerous zone of the hydroelectric power station. The period of investigations by the Institute of Physics of the Earth coincided with a period of decreased activity and this zone was deemed to be aseismic.

However, on the basis of reconnaissance seismogeological observations in 1968 the region of the Zeya Hydroelectric Power station was deemed by us to be seismically active; the seismic danger for the Zeya Hydroelectric Power Station was related to specific structures -- the Tukuringra-Dzhagdinskiy anticlinorium and a deep fault (Yuzhno-Tukuringrskiy fault) passing near the dam site. Planning organizations were informed of this on time. But only after a strong (8 scale units) earthquake on 2 November 1973 was it possible to carry out systematic engineering field work in the neighborhood of the hydroelectric power station (data on the seismicity of the Zeya segment of the Baykal-Amur Railroad route were collected incidental to this work).

The seismogeological investigations in 1974-1975 were made primarily in the seismically active zone of the Tukuringra-Dzhagdy Ranges and to a lesser degree to the north and south of it over an area of more than 120,000 km^2. Parallel to this structure, along the Stanovoy Range, there is still another seismically active zone which spatially corresponds to a zone of extensive manifestation of disjunctive tectonics, a complex system of horsts and grabens, high contrast and intensity of neotectonic movements accompanied by Quaternary volcanism. The Stanovoy deep fault with a high potential seismicity can also be traced here.

A segment of the route of the Baykal-Amur Railroad and its branch Tynda-Berkakit is under the influence of the earthquakes of this zone.

The principal purpose of this book is a description of the geostructural, neotectonic and seismotectonic characteristics of the Tukuringra-Dzhagdinskiy mountainous zone in relation to its deep structure and seismicity so that on this basis it would be possible to compile a seismic regionalization map of the general type which in essence would graphically reflect the prediction of intensity of intermediate-maximum earthquakes and the regions of their occurrence. The authors by no means consider the solution of the problem proposed in this study to be above reproach, especially for such a geologically complex region where not a single fundamental problem in the field of structural geology has an unambiguous solution. The age of the folded systems and their boundaries are determined differently on each new map of structural geology. In addition, the geological history evolution of the earth's crust is one of the criteria for determining the seismic potential of specific morphostructures.

The authors express deep appreciation to specialists in various fields at the Geology Institute Yakutsk Affiliate Siberian Department USSR Academy of Sciences (B. M. Koz'min, A. G. Larionov), the Institute of Tectonics and Geophysics Far Eastern Scientific Center USSR Academy of Sciences (F. G. Korchagin, L. A. Mastyulin, F. S. Onukhov, G. F. Ufimtsev) and the Institute of the Earth's Crust (A. D. Sarapulov, A. S. Yendrikhinskiy, V. M. Kochetkov, N. A. Logachev, S. D. Khil'ko, and others), and also specialists in the technical editing laboratory of the Institute of the Earth's Crust, who invested much work in finalizing the manuscript.

CONTENTS

[278-5303]
5303/CSO: 1865

HOLOGRAPHY AND OPTICAL DATA PROCESSING IN GEOLOGY AND GEOPHYSICS

Leningrad GOLOGRAFIYA I OPTICHESKAYA OBRABOTKA INFORMATSII V GEOLOGII I GEOFIZIKE in Russian 1979, pp 2-4, 193-194

[Annotation, table of contents and introduction from book edited by S. B. Gurevich, Order of Lenin Physico-Technical Institute imeni A. F. Ioffe, Leningrad, 500 copies, 195 pages]

[Text] Annotation

Reports read at the All-Union Seminar on Optico-electronic Methods of Processing Geological and Geophysical Data, held in Tomsk in 1978, served as the basis for the present collection. The main theme of the collection is the processing of large masses of geophysical data and the creation of new instruments and devices for the optical processing of geological and geophysical materials. Specific methods and devices are examined along with survey reports on that theme. The materials presented in the articles are of great importance for the development of work envisaged by the national economic plan. They provide the possibility for specialists, geophysicists and geologists to become acquainted with the new possibilities opened up by holography and methods of optical data processing in tasks of searching and prospecting for minerals.

CONTENTS

APPROVED FOR RELEASE: 2007/02/08: CIA-RDP82-00850R000200090015-4

Introduction

The complexity of the problems to be solved in the search for petroleum, gas and solid mineral resources requires a considerable increase of computer capacities and the development of methods and means of effective processing of geological and geophysical data. Computer compleses based on second and third generation electronic computers existing at the present time do not completely meet contemporary requirements, in connection with which a number of important and necessary algorithms for the processing of geological and geophysical data often are not realized in practice. It should be expected that in proportion to the development of work on area systems of observations and seismic holography the requirements for the efficiency and operativeness of data processing will grow still more. In that respect much interest is aroused by the further improvement of digital means of data processing as well as the development of optical and optico-electronic methods which have considerable possibilities with respect to the processing and storage of large flows of data.

At the present time in a number of scientific and production organizations and VUZ's of the country experience has been accumulated in the development and use of optical computer systems, experience that confirms the prospects of development of that direction of automation of the processing of data of exploration geophysics and geology.

The First All-Union seminar on the optico-electronic processing of geological and geophysical data, held in 1978 in Tomsk, summed up definite results of investigations in that area.

The present collection contains reports read at the seminar that were devoted to questions in the development and investigation of optical computing devices and hybrid optico-electronic data processing systems. Some methodical and technological methods of processing, directed toward improvement of the methods and means of processing geological and geophysical materials, are examined.

The publication of the collection, in our view, will undoubtedly have a positive influence on the further conducting of investigations and will permit acquainting specialists with the results achieved in this area.

It is proposed to continue in the future the discussion of optico-electronic methods and means of processing geological and geophysical data and to issue subsequent collections of articles.

Professor S. B. Gurevich and candidates of technical sciences V. P. Ivanchenkov and O. A. Potapov

[291-2174]

2174
CSO: 1863

UDC 550.341

SEISMOTECTONIC DEFORMATION IN THE GARM REGION

Moscow IZVESTIYA AKADEMII NAUK SSSR, FIZIKA ZEMLI in Russian No 10, 1979 pp 24-43

[Article by A. A Lukk and S. L. Yunga, O. Yu. Shmidt Institute of Earth Physics, USSR Academy of Sciences]

Abstract. A study is made of the seismotectonic deformation in the Garm Region of the Tadzhik SSR based on 2250 analyses of the mechanisms for the foci of weak ($M < 4$) surface earthquakes in the period from 1964 to 1976. The tensor for the rate of seismotectonic deformation is presented with accuracy to a constant multiplier as a product of the guiding tensor corresponding to the mean mechanism by the sum of the seismic moments of the earthquakes. Time-stable nuclei of deformation are isolated with linear dimensions 20-30 km. A discussion is held of the general pattern of seismotectonic deformation of the region and qualitative hypotheses are advanced on the causes of this process. A comparison is made of the vertical seismotectonic and tectonic movements. The position of strong earthquakes is examined on the background of seismotectonic deformation.

[Text] 1. Introduction

Currently, based on a number of direct and indirect data it is generally accepted that earthquakes are induced by a shift of the earth's material over a certain weakened surface [1-4]. The model of two orthogonal dipoles without moments is adopted as an adequate representation of the focus of an earthquake both for elastic irradiation, and for the static field of shifts [5-7]. The orientation of the dipoles, i.e., the mechanism of earthquakes, is defined by the position of the fault plane and the direction of the shift vector.

Tectonic and physical analysis of the mechanisms for earthquakes is possible on the path of direct comparison of the orientations of equivalent pairs of forces used in a mathematic description of the radiation from the earthquake

focus, and the really active tectonic stresses. The substantiation of such a comparison is apparently hardly to be implemented without the involvement of a strong hypothesis on the coincidence of the direction of the shift and the direction of action of the maximum tangential stress. Usually the average direction of action of the pairs of forces of "compression" is taken as the direction of the greatest tectonic compression. In precisely the same way the direction of the least tectonic compression ("extension") is found [8]. We note that such a separate finding of the average directions is generally not completely correct, since it does not completely guarantee their perpendicularity.

In the case where the primary data are insufficient for a reliable analysis of individual mechanisms a joint analysis of all the signs of the first arrivals of the P-waves from the earthquakes from one relatively small seismically active volume is used in order to construct a certain average mechanism [9]. Recently methods have been formulated of joint analysis of individual axes of compression and extension. Publications [10,11] have set limitations on the position of the axes of the tectonic stresses in relation to the main axes of the defined mechanism. Based on these limitations and with the additional hypothesis on the constancy of the field of tectonic stresses in the studied volume [11, 12] have suggested a graphic method of finding the directions of the main tectonic stresses. A study of the macroscopically uniform stressed state can be made numerically [13].

An alternative approach is used in relation to the investigation of the mechanisms of earthquakes occurring in the environs of a large regional fault. It is hypothesized that the earthquakes occurring on individual sections of the fault or on its accessory faults of the same course have approximately parallel planes of shifts. The task consists of finding the best orientation of the flat layer that contains these shifts, and of determining the direction of the dominant seismotectonic movement of the opposite sides of the layer. The method for study of such tasks that is reduced to diagonalling of the matrix of the second order compiled from individual mechanisms is suggested in publication [14] and is used in a number of other works [15, 16].

Currently the directions have been revealed of the main tectonic stresses in all the seismically active regions of the world. Horizontal compression dominates in the belts of neotectonic activation, in the young folded zones, as well as in the insular arches and in the zones of Ben'off under them; in the zones of groove-genesis a near-horizontal extension dominates [17]. However, a detailed study of the stressed and deformed states still encounters great difficulties [10].

Here it is appropriate to turn to detailed works on an investigation of the mechanisms for foci of weak earthquakes in the Garm region [18-20]. The Garm region has been studied fairly well in a geological respect and has been described in detail in many works [21, 23-25, and others]. It is a part of the large zone of structural atriculation of Pamir and Tyan'-Shan' [23,24]. The modern mountainous country was actually formed during the

Quaternary time (Pleistocene) [23-25]. The considerations are advanced that the entire zone of articulation is under conditions of intensive near-horizontal tectonic compression in the near-meridional direction [23,24]. This can serve as the cause for the intensive process of mountain formation as a result of deformation of the ancient eopleistocene surface. A study of the parameters of over 1,000 mechanisms of earthquakes made it possible to note that in different parts of the Garm region the orientation of compression axes varied [19-22]. These same publications undertook an attempt to isolate the regions of depression and elevation according to the sign of shift of the suspended sides of the shifts in the foci of earthquakes in relation to the diurnal surface, but within the framework of the employed technique the stability of the results was not high. A simple increase in the statistics does not permit a significant improvement in the obtained results due to the great diversity of the individual analyses of the mechanisms. The evident need arose for the enlistment of new methods for studying the set of mechanisms of earthquake foci.

According to the extant ideas, the seismotectonic deformation of macroscopic volumes of mountain massifs is governed by slippings over the different-oriented weakened zones in the earthquake foci [26-30]. A quantitative study of the link between seismicity and the tectonic process was possible thanks to the appearance of methods for determining the seismic moment of an earthquake from observational data [31]. Brune [32] linked the contributions of earthquakes to the rate of tectonic slip with respect to regional faults with the sum of the seismic moments of these earthquakes. Analysis of the seismotectonic deformation of the region results in a generalization of Brune's formula for the case where the earthquakes occur over chaotically arranged faults [13, 27, 28]. Recently, computations have been made of the seismotectonic deformation of certain seismically-active regions [13, 28, 29]. This work covers a further development of this direction, whereupon special attention is given to development of new method approaches to studying the set of earthquake mechanisms.

2. Technique for Studing Seismotectonic Deformations

Deformation of seismically active volumes of rocks on the macroscopic level of examination is described with the help of the tensor for rate of tectonic deformation $\langle e_{ij} \rangle$ [13]

$$\langle e_{ij} \rangle = \lim_{t/T \to 0} \lim_{l/L \to 0} \frac{1}{VT} \int_S \frac{1}{2} (u_i n_j + u_j n_i)\, ds. \qquad (1)$$

Here u_i ($i=1,2,3$)--vector of movement of a certain point x_i in the Cartesian system of coordinates $0X_1X_2X_3$ in the time T, n_i--unit vector of external perpendicular to the surface S of volume $V \sim L^3$. The intervals l and t correspond to the dimensions of the spatial-temporal environs of the earthquake focus in which significant changes occur in the local deformations, movements and other parameters.

The limit transitions in formula (1) should be understood in that sense that for computation of $\langle e_{ij} \rangle$ with fixed values of l and t by means of an increase in L and T the representative spatial-temporal region is selected. Such a region contains a sufficient number of inclusions in the form of faults in the earthquake foci, so that the average value for the rate of tectonic deformation does not depend on the fluctuations in the field of movements on the surface of the volume.

We will explain the geometric meaning of the tensor component $\langle e_{ij} \rangle$. We will examine as the V area a cube with length of the edge L that is mentally isolated from the rock massif such that the edges of the cube are directed along the axes OX_1, OX_2 and OX_3. Then in accordance with the definition (1) the rate of tectonic deformation can be written in the following form:

$$\langle e_{ij} \rangle = \frac{1}{2}\left(\frac{\Delta V_i}{\Delta X_j} + \frac{\Delta V_j}{\Delta X_i}\right), \qquad (2)$$

where

$$\frac{\Delta V_i}{\Delta X_j} = \frac{1}{L}[(V_i)_{x_j=L} - (V_i)_{x_j=0}]$$

and $(V_i)_{X_j=L}$--average rate of movement of the edge of the cube perpendicular to the OX_j axis and intersecting this axis at the point $X_j=L$.

Formula (2) determines the components of the tensor for rate of deformation $\langle e_{11} \rangle$, $\langle e_{22} \rangle$, $\langle e_{33} \rangle$ through the rates of relative elongation of the material segments that have an explicit geometric meaning and are parallel in the given time interval T to the coordinate axes. The sum of the diagonal components of the tensor $\langle e_{ij} \rangle$ determines the average rate of relative change in the volume. The components of the rate of deformation $\langle e_{ij} \rangle$, $i \neq j$, determine the average rates of change of the right angles that are formed by the material segments parallel to the coordinate axes OX_i and OX_j.

By knowing the tensor for the rate of deformation $\langle e_{ij} \rangle$ one can determine the rate of deformation $\langle e_l \rangle$ in an arbitrary direction assigned by the unit vector l

$$\langle e_l \rangle = \langle e_{ij} \rangle l_i l_j. \qquad (3)$$

In the case that interests us, when within the volume V there are fault surfaces s^α, $\alpha=1,2,3\ldots, N$, the integral in definition (1) naturally is divided into two parts corresponding to the rate of continuous deformation $\langle e_{ij}^r \rangle$ and the rate of seismotectonic deformation $\langle e_{ij}^q \rangle$ [13]:

$$\langle e_{ij} \rangle = \langle e_{ij}^r \rangle + \langle e_{ij}^q \rangle. \qquad (4)$$

Here

$$\langle e_{ij}' \rangle = \frac{1}{VT} \int_{V'} \varepsilon_{ij}\, dV, \qquad (5)$$

$$\langle e_{ij}^{a} \rangle = \frac{1}{VT} \sum_{\alpha=1}^{N} \int_{s^{\alpha}} \frac{1}{2} (a_i^{\alpha} n_j^{\alpha} + a_j^{\alpha} n_i^{\alpha})\, ds. \qquad (6)$$

In formulas (5) and (6) it is considered that a representative spatial-temporal region is selected. In formula (5) integration is carried out with respect to the region V' from which all surfaces of faults are excluded s^{α}, ε_{ij}--local deformation of a certain point in region V' for the time T. Each integral in formula (6) is taken for some one side of the rupture, the external perpendicular to this side of the fault is designated by n_i^{α}, and jump in the movement on the fault by a_i^{α}.

We will examine in more detail the method questions of analyzing from experimental data the rate of seismotectonic deformation (6). Further for the term "seismotectonic deformation" we will adopt the abbreviation STD. Each of the terms in sum (6), being multiplied by the shear modulus μ is a tensor of the seismic moment M_{ij}^{α} [3,27]

$$\langle e_{ij}^{a} \rangle = \frac{1}{\mu VT} \sum_{\alpha} M_{ij}^{\alpha}. \qquad (7)$$

The components of the tensor for the seismic moment M_{ij}^{α} can be computed according to the mechanism and the magnitude of the earthquake. In fact, assume that we know the orientations of the main axes of the equivalent spot source, so that the axis of compression is characterized by a unit axial vector p^{α}, the axis of extension by an analogous vector t^{α}, and we also know the summary intensity of the source assigned by the amount of the seismic moment M_0^{α} [31]

$$M_0^{\alpha} = \mu a^{\alpha} S^{\alpha}, \qquad (8)$$

where a^{α}--average amount of jump in the vector of movement on the fault, S^{α}--area of fault plane. One can evaluate the amount M_0^{α} from the magnitude of the earthquake by using the correlation link between these amounts.

Taking into consideration that the axes p^{α} and t^{α} are bisectors of right a angles formed by nodal planes with perpendiculars n^{α} and a^{α} we obtain

$$\langle e_{ij}^{a} \rangle = \frac{1}{\mu VT} \sum_{\alpha} M_0^{\alpha} \frac{1}{2} (t_i^{\alpha} t_j^{\alpha} - p_i^{\alpha} p_j^{\alpha}). \qquad (9)$$

There is the possibility of considering in a unified manner the mechanisms for earthquakes by asssuming similarity of the seismotectonic deformation in different energy ranges [13, 28]. This results in a modified expression for the tensor of STD rate

$$\langle e_{ij}^{0} \rangle = -\frac{1}{\mu VT} \sum_{\alpha} M_0^{\alpha} M_{ij}^{\alpha}, \qquad (10)$$

where M_{ij} designates the next tensor corresponding to the average mechanism [13]

$$M_{ij} = \frac{1}{N} \sum_{\alpha=1}^{N} \frac{1}{2} (t_i^{\alpha} t_j^{\alpha} - p_i^{\alpha} p_j^{\alpha}). \qquad (11)$$

This definition generalizes the previously known method of constructing the average mechanism for the set of all signs of the first arrivals of the P-waves [9]. The guiding tensor corresponding to the average mechanism of the set of earthquakes reflects the mechanism for deformation of the region, i.e. spatial directivity of the STD.

The symmetric tensor of the second rank M_{ij} can be characterized by three natural values M_1, M_2, M_3 ($M_1 \geq M_2 \geq M_3$) and the position of the corresponding main axes T, B, P. The shift movements on the fault planes do not lead to a change in the volume and in correspondence to this

$$M_1 + M_2 + M_3 = 0. \qquad (12)$$

To evaluate the correspondence of the average mechanism for the set of individual mechanisms it is expedient to use the intensity $\varkappa$ of the tensor M_{ij}

The degree of correspondence of the individual mechanism of the earthquake to the average mechanism will be evaluated with the help of the coefficient k^{α}:

$$\varkappa = (2M_{ij}M_{ij})^{1/2}. \qquad (13)$$

where $M_{ij}' = \varkappa^{-1} M_{ij}$ – matrix with unit intensity. It is easy to be convinced that the intensity of the average mechanism $\varkappa$ is the average arithmetical of all the coefficients k^{α}.

The type of seismotectonic deformation is expressed through the Lode-Nadai coefficient μ_m:

$$k^{\alpha}=M_{ij}^{-1}(t_i^{\alpha}t_j^{\alpha}-p_i^{\alpha}p_j^{\alpha}), \qquad (14)$$

In the limit case where the uniform scattering of the axes $\{t^{\alpha}\}$ around the T axis is much less (much greater) than the uniform scattering of the axes $\{p^{\alpha}\}$ around the P axis, the Lode-Nadai coefficient $\mu_m = -1$ ($\mu_m = +1$) and the process of deformation of the type of uniaxial extension (compression) occurs. With such deformation along a certain fixed direction the deformation occurs that is maximum in magnitude, and in any direction perpendicular to the first the deformation is two times lower in absolute magnitude and has the opposite sign. In another extreme case, in which the distribution of axes $\{t^{\alpha}\}$ in relation to the main axes of the average mechanism (T, B, P) is exactly the same as the distribution of the axes $\{p^{\alpha}\}$ in relation to the (P, B, T) axes, the Lode-Nadai coefficient $\mu_m=0$ and the process of deformation of the pure shift type is realized. With values of the Lode-Nadai coefficient $0< |\mu_m| < 1$ the sign of the coefficient μ_m permits a qualitative comparison of the distribution of axes $\{t^{\alpha}\}$ and $\{p^{\alpha}\}$ a around T and P respectively, and observance of the dominance of the deformation in the direction of one of the axes.

One can give a geometric presentation of the average mechanism in the form of a Koshi surface, which on condition (12) looks like an elliptical cone described by equation

$$\mu_M = \frac{3M_3}{M_1-M_3}. \qquad (15)$$

This surface can be called the nodal surface in that sense that, as follows from expressions (3), (10) and (11) the deformation of any rectilinear segment lying on surface (12) equals 0. The position and shape of the cone are completely determined by the position of the axes T and P and the Lode-Nadai coefficient μ_m.

Study of the STD of the Garm region begins with the selection of a representative spatial-temporal region stipulated in the examination of expression (1). For this purpose an elementary cell was selected that is a parallelepiped with side of the square base 11 km and height 15 km. These dimensions are determined not only by the detailedness of the study, but also in the first place by the representativeness of the number of averaged mechanisms of earthquakes that occur in the limits of such a cell in the examined time interval with its slip movement over the entire studied region. To evaluate the temporal stability of the determination of the average mechanism with a fixed position of the cell of averaging the entire period of observations was divided into two time intervals that did not overlap. The cell was moved over the entire region with a shift by half of the side of the base with respect to latitude and longitude. The analysis included 435 such overlapping cells of averaging and 2,250 determinations of the mechanisms of the foci for the period from 1964 to 1976. The period of

time from 1970 to 1972 was covered by an insignificant number of analyses for technical reasons, and due to this the two comparable periods were selected by a natural method: 1964-1969 and 1973-1976. The number of analyses of the mechanisms for earthquake foci in these periods was 1,330 and 830 respectively.

For each elementary volume of averaging a computation was made of the matrix of average mechanism (11) and the natural values of each matrix, the orientation of the main axes of the average mechanism, its intensity $\varkappa$ and the Lode-Nadai coefficient μ_m were determined. This completed the initial stage of the study.

At the next stage of study the classification of cells was made according to signs characterizing their deformation. Such a classification must possess, on the one hand, the greatest homogeneity of signs within the group, and on the other hand, the most explicit differences possible between the groups. The classification is linked to the study of the discrimination properties of the signs, whose results are given somewhat later. The solution to this task makes it possible to group the elementary cells into uniform regions, for which the STD is again computed.

The specific computations demonstrate that, on the one hand, the STD changes in the transition from one uniform region to another occur gradually and there is no opportunity to indicate the strictly fixed boundaries of the regions; on the other hand, these changes are not so smooth that it was possible in general to abandon the ideas of certain transitional zones separating the neighboring regions. These peculiarities of the seismotectonic deformation state of isolated regions need to be reflected by the special concept "STD nucleus." Precisely the STD nuclei are described most correctly by the parameters of seismotectonic deformation that are specific for each region. The isolation of STD nuclei makes it possible to pass to the most important stage of the study from the geophysical viewpoint--understanding and explanation of the observed STD pattern in the framework of the extant tectonic concepts.

3. Stability of Parameters of Average Mechanism and Evaluation of the Accuracy of Their Determination

We will show the stability of the parameters of the average mechanism for an individual cell of averaging and for two sets of 8 and 17 overlapping cells that represent certain regions with uniform nature of deformation. The number of analyses of mechanisms of earthquakes in the entire period of observations in each of these three samplings is respectively 68, 196 and 315. On figure 1, a-c distributions are given of the deviations in the axes p, t and b of individual mechanisms of earthquakes from the corresponding axes P, T and B of the average mechanisms for these three samplings. The distributions were constructed according to density of the number of intersections of the axes p, t and b with the surface of the unit sphere of the average mechanism in the limits of the solid angles, multiples of $\pi/3$, around the corresponding axes P, T and B minus each

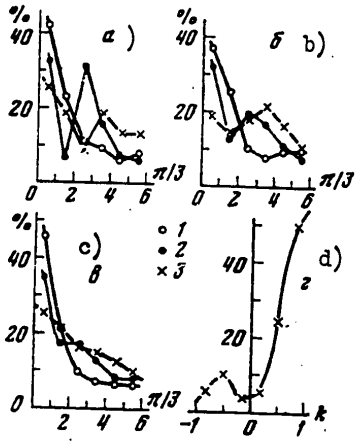

Figure 1. Distributions of Deviations of Individual Axes p,t and b from the Corresponding Axes of Average Mechanisms for Three Samplings and Distribution of Measure of Correspondence for One Sampling

Key:
1. p
2. t
3. b
a. sampling of 63 earthquakes for one cell of averaging
b. sampling of 196 earthquakes for 8 cells
c. sampling of 315 earthquakes for 17 cells
d. distribution of amount k for 315 mechanisms of foci from 17 cells

previous solid angle. On figure 1, a-c the lower magnitude of dispersion of the axes p as compared to the two other axes is distinctly visible, whereupon the sharpness of the distributions depends little on the volume of the samplings. The axes t and b are significantly scattered around the axes T and B of the average mechanisms, and in addition, double-peaked distributions are observed for them. Due to the proximity of the magnitudes of the corresponding main deformations that is evident in the examined case this double-peaked nature can be explained by the mutual reorientation of the T and B axes, which in turn reduces even more the stability of the analysis of the T and B axes.

Thus, the orientation of the P axis of the average mechanism can be considered the more stable and informative parameter as compared to the orientation of the T and B axes for the purposes of zoning according to the deformation state. Figure 1, d presents the distribution of the k amounts defined by formula (14) for the largest of the three samplings examined above for the earthquake mechanisms. It follows from this figure that

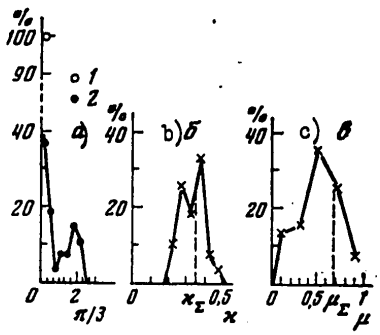

Figure 2. Distributions of Parameters P, T, $\varkappa$ and μ_m of Average Mechanisms for Individual Cells in Relation to Corresponding Parameters of Average Mechanism for Entire Set of 25 Cells at Petr I Range

Key:
1. axis P
2. axis T
a. distribution of deviations of axes P and T
b. distribution of $\varkappa$
c. distribution of μ_m

80% of the individual mechanisms have $k > 0$, i.e., correspond to the average mechanism. The amount $\varkappa$, determined by formula (13) and computed according to the given distribution of k values equals 0.4. The sharpness of the distribution in fig 1,d can serve as an additional evaluation of the stability of the determination of the average mechanism.

Figure 2, a gives the distribution of deviations in the axes P and T of the average mechanisms of 25 cells comprising the sum of cells of the 2 previous samplings, from the corresponding axes of the average mechanism for the entire set of mechanisms of earthquakes of this summary sampling. The very high groupability of the P axes follows from this figure: in limits of the solid angle $\pi/9$ all 100% of the P axes are included. The distribution for the T axes is significantly wider, and in addition, has two maximums. The distribution for the B axes here is not given due to its evident proximity to the distribution of the T axes. Thus, one can strengthen the conclusion drawn above on the increased stability and information content ofthe P axes as compared to the T and B axes.

Figure 2, b presents an analogous distribution of the parameter $\varkappa$ and indicates the value $\varkappa_\Sigma$ for the average mechanism of the collective sampling. The value $\varkappa_\Sigma$ was close in magnitude to the value $\varkappa$, corresponding to the

maximum distribution. The distribution itself is fairly sharp and its width does not exceed ± 43% of the average value of distribution. This amount is ±0.15 units $\varkappa$ and can serve as the lowest evaluation of the significant differences between the values $\varkappa$, obtained from fairly large samplings. The certain double-peaked distribution noted in figure 2, b can testify to the unification in one area of cells with two different average values of $\varkappa$--0.28 and 0.38, but these differences lie on the verge of accuracy of determination of $\varkappa$. The observed range of variations in the $\varkappa$ values is not great, and as a result the magnitude of $\varkappa$ has a low information content for the purposes of zoning the STD. One can only introduce a certain threshold value $\varkappa$=0.30, considering here that the increase in homogeneity of the deformed state must be characterized by an increase in the values $\varkappa$, while the reduction in STD homogeneity--a decrease.

Figure 2, c presents the distribution of Lode-Nadai coefficient for the same 25 cells. Due to the aforementioned dominance of stability of the P axis over the other two axes of the average mechanism, the result of the absence of negative values of μ_m in the cited distribution is evident. Nevertheless, the distribution is fairly broad, and its maximum does not correspond to the value μ_m=0.68 obtained for the entire set of earthquake mechanisms. All of this is testimony to the unstable determination of this parameter of the average mechanism. Nevertheless, taking into consideration the known importance of the parameter μ_m for evaluating the type of deformed state, it is useful to use it in three gradations provided by the dividing potentialities of the method: positive, negative and values of μ_m close to zero. The dividing zero range of the parameter μ_m is adopted in the interval of values from -0.2 to +0.2. We note that despite the fact that on the whole for the region the magnitude of the parameter μ_m = 0.6, in limits of the studied region regions with $\mu_m \approx 0$ and $\mu_m < 0$ are also isolated.

We will now evaluate the accuracy of an analysis of the main parameters of the average mechanism of P, T, $\varkappa$ and μ_m examined above. For this we took 10 equally accurate samplings consisting of 100 mechanisms of earthquakes for different overlapping time intervals in different parts of the Petr I range located in the central part of the region. In the limits of each such sampling the position of the axes p, t and b varied by random numbers by 5°, 10°, 15° and 20°, and for each of these 4 values of variations the average mechanism was determined again. The thus evaluated amounts of dispersion of the P, T, $\varkappa$ and μ_m parameters of the average mechanism for four levels of variations of the initial data are given in table 1. Here the average arithmetical maximum deviations from the 10 series are given for the P and T axes in degrees, and for $\varkappa$ and μ_m --in percentages. As follows from table 1, the thus evaluated accuracy of determining the parameters of the average mechanism is fairly high, which makes it possible to consider the differences between the average mechanisms of 10° for the axes P, 15° for the T axes, 30% for $\varkappa$ and 60% for μ_m to be unconditionally significant.

4. Plan for Zoning STD

The plan for zoning the STD obtained as a result of uniting the cells with similar signs is presented in figure 3. The shading marks the regions of positive determination of the average mechanism. The type of shading indicates the type of STD: proximity to the uniaxial compression (extension) or shift. The unshaded places on the plan mark the sections where in the framework of the technique for averaging mechanisms the average mechanism was not successfully and confidently constructed for a number of reasons: shortcoming of the statistics, sharp time differences in determining the average mechanisms both for individual cells of averaging, and for the entire section as a whole.

Table 1. Variations in Parameters P, T, $\varkappa$ and μ_m of Tensor of Average Mechanism with Variation of Position of Main Axes p and t of Individual Mechanisms by Random Numbers

$\Delta(p, t)$	ΔP, (1)	ΔT, (1)	$\Delta\varkappa$, %	$\Delta\mu_M$, %
5°	0,4	1,4	1,9	4,2
10°	1,1	3,3	2,0	12,7
15°	1,7	4,2	4,3	16,0
20°	2,6	4,8	9,0	21,1

Key:
1. degrees

On the given plan six uniform regions are isolated whose STD is characterized by average mechanisms indicated in the center of each region. The parameters of the average mechanisms are given in table 2. We recall that according to expression (10) the tensor of the average mechanism with accuracy to the scalar multiplier reflects the type of STD tensor. Therefore, the examined plan for zoning reflects the STD of the region standardized for this scalar multiplier--"intensity of STD." We will return to the examination of the STD intensity somewhat later. It follows from figure 3 that the regions with dominance of the near-horizontal compression comprise a greater part of the region, only in the areas of I and III is the STD close to the shear (μ_m=0) and the uniaxial near-horizontal extension (μ_m = -0.25) respectively. At the same time it is necessary to note the considerable range of variations in the azimuth of the axis P and the coefficient μ_m in regions with a dominance of the near-horizontal compression. Thus, the greatest values of the coefficient μ_m=0.7 are reached in the V region (Petr I range) with azimuth of the P axis equal to 135°. At the same time in the IV region the value of the coefficient μ_m drops to 0.3 with the turn of the P axis to 125°, while in the regions II and VI the reverse turn of the azimuth of the P axis to 166° is observed with magnitude of μ_m=0.50. The unshaded sections of the examined plan can be viewed as certain "contact zones" between the stable regions with varying deformed state.

Table 2. Parameters of Tensor of Average Mechanism for Different Sections of Garm Region

	N	P		T		x	μ_M	$\langle \varepsilon_{ij} \rangle$					
		Az°	α°	Az°	α°			ε_{11}	ε_{12}	ε_{13}	ε_{22}	ε_{23}	ε_{33}
1	2	3	4	5	6	7	8	9	10	11	12	13	14
I	41	147	90	237	2	0,60	0	--0,21	--0,13	--0,01	--0,09	0,01	0,30
II	116	166	86	74	63	0,40	0,55	--0,20	--0,09	0,03	0,11	--0,03	0,09
III	279	168	59	78	68	0,25	—0,25	--0,07	--0,04	0,04	0,11	0	--0,04
IV	288	125	70	251	32	0,30	0,30	--0,02	--0,09	0,02	--0,06	0,09	0,08
V	511	135	83	226	81	0,35	0,70	--0,03	--0,16	0,02	--0,04	0,03	0,07
VI	71	165	84	245	32	0,25	0,50	--0,12	--0,05	--0,03	0,04	0,02	0,08
Σ	2250	144	80	239	62	0,25	0,60	--0,06	--0,10	0,02	0,01	0,04	0,05
III_1^A	73	162	13	265	87	0,20	—0,40	--0,03	--0,01	0,01	0,11	0,01	--0,08
III_2^A	28	156	90	66	12	0,40	0	--0,15	--0,08	0,02	--0,03	--0,03	0,18
IV^A	69	128	~90				~0						
V^A	315	134	84	225	83	0,40	0,85	--0,05	--0,18	0,02	--0,05	0,03	0,10
V^B	196	135	79	227	81	0,30	0,35	--0,02	--0,13	0,01	--0,01	0,03	0,03
VII	44	139	77	234	72	0,30	—0,45	--0,02	--0,13	--0,02	0,05	0,06	--0,03
VIII	99	148	90	239	85	0,25	—0,30	--0,04	--0,12	0	0,07	0,02	--0,03
	29	152	19	247	88	0,30	—0,65	--0,05	--0,08	0,01	0,14	0,01	--0,09
	13	158	76	47	35	0,20	0,60	--0,09	--0,06	0,05	0,03	0	0,06
	29	143	81	233	90	0,40	—0,35	--0,03	--0,19	0,01	0,08	0,01	--0,05
	19	134	88	222	49	0,25	—0,45	--0,01	--0,07	--0,08	--0,01	0,04	0,02
1	26	153	90	243	90	0,35	0	--0,10	--0,15	0,02	0,10	0,02	0
2	109	135	~80				>0						

Note. Indices 1 and 2 in the designations of the section (Roman numerals) indicate the periods of observation 1964-1969 and 1973-1976 respectively.

It is important to compare the discussed plan with the plan for zoning the Garm region according to the dominant orientation of the p axes in the foci of individual earthquakes obtained in publication [22]. On figure 3 this plan is shown by a dotted line. One can note the good correspondence of both plans in the northern section and in the extreme southeastern region. In the central part of the region a significant discrepancy is noted among the compared plans.

5. Certain Peculiarities of the STD

We will return to an examination of the sections on the STD zoning plan represented in figure 3 by white spots, as well as note the individual peculiarities of the STD in the limits of the regions isolated above. Identification of these sections is indicated in figure 4, while the main STD parameters are given in table 2. Table 2 also reflects the significant differences in the average mechanisms during the two nonoverlapping periods (1964-1969 and 1973-1976).

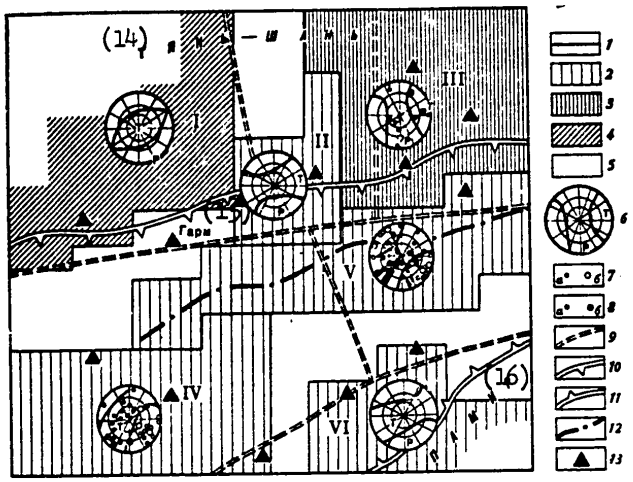

Figure 3. STD Zoning Plan

Key:

1. contours of isolated uniform regions with different STD
2. dominance of near-horizontal compression ($\mu_m \geq 0.3$)
3. dominance of near-horizontal extension ($\mu_m \leq -0.25$)
4. region of shift STD (in mechanical sense)
5. region of unsure STD determination
6. average mechanisms in straight equi-interval azimuth projection; P and T indicate the points of emergence of the corresponding axes of the average mechanism
7. points of emergence of p axes of relatively strong earthquakes; a--$4.0 \leq M < 5$; b--$M \geq 5$
8. the same for axes t
9. plan of zoning from [22]
10. Gissaro-Kokshaal'skiy fault
11. Darvaz-Karakul'skiy fault
12. axis of Petr I range
13. seismic stations
14. Tyan'-Shan'
15. Garm
16. Pamir

The dotted line in the limits of region III isolates the section III^A where in the period of time from 1973 to 1976 sharp changes were noted in the type of STD as compared to the entire III region. Here at this time the shear deformation ($\mu_m = 0$) begins to dominate with near-horizontal position of the P axis and near-vertical position of the T axis during turn of the azimuth of the P axis by 12°.

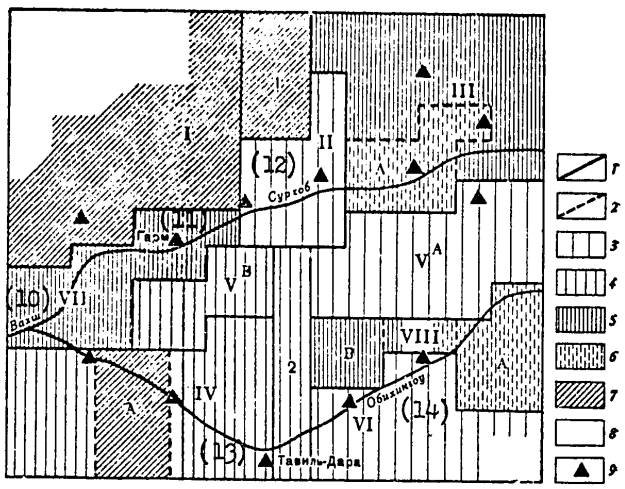

Figure 4. Expanded Variant of STD Zoning Plan

Key:

1. contours of regions with STD stable in time
2. contours of regions with unstable determinations of average mechanisms
3. regions of sharpest dominance of near-horizontal compression ($\mu_m \geq 0.5$)
4. regions of dominance of near-horizontal compression ($0.3 \leq \mu_m < 0.5$)
5. regions of dominance of near-horizontal extension ($\mu_m < -0.25$)
6. regions with considerable changes in STD in time
7. regions of shift STD
8. aseismic sections
9. seismic stations
10. Vakhsh
11. Garm
12. Surkhov
13. Tavil'-Dara
14. Obikhingou

The dotted line in the limits of region IV isolate the section IV^A whose deformed state is close to the shift, but due to the great dispersion of th the initial data precisely here the determination of the average mechanism is unstable and its parameters are not given in complete volume.

It was appropriate to separate region V into two regions V^A and V^B since they differ sharply in the magnitude of the coefficient μ_m (table 2), whereupon these differences are fairly stable even on the level of individual cells of averaging.

In region VII the statistics are insufficient for construction of the average mechanism in individual cells of averaging. Nevertheless, for the entire set of individual mechanisms the STD of this region can be characterized by the dominance of a stable near-horizontal extension in the azimuth 234°.

Region VIII is characterized by a complex deformed state. It consists, to all appearances, of two sections $VIII^A$ and $VIII^B$ in which the near-horizontal extension at azimuth 233°-247° dominated in the first period of observation. The stability of STD in the limits of section $VIII^B$ is higher as compared to section $VIII^A$. For the latter the coefficient μ_m for different periods of observation alters its sign, remaining fairly high with respect to absolute amount.

Section II is a pronounced transitional zone from the deformation by the shear in region I to the dominance of the near-horizontal extension in region III, but the shortage of statistics does not make it possible to judge the stability of the STD in this zone in different periods.

An important feature is found in the near-meridional band 2. It divides the regions with sharply different STD. Thus, the regions IV and V sharply differ in orientation of the P axis. Region IV and section $VIII^B$ sharply differ not only in the orientation of the P axis, but also in the sign of the coefficient μ_m. The regions V^A and V^B significantly differ in the magnitude of the positive coefficient μ_m. It is natural that such drastic differences in the STD on different sides from zone II cannot be realized by a sharp jump, and, apparently, this zone acts as the transitional from one deformed state to another. The deformed state of the zone itself, if only such a description is applicable to the nonisometric narrow plate, can be characterized by a positive coefficient μ_m, with orientation of the near-horizontal compression at the azimuth 135°. One should note that the existence of peculiarities in the nature of the deformation of the material in the earth's crust along this narrow zone has already been previously noted in publications [33-34].

In publications [21,22, 35] for purposes of zoning the Garm region such characteristics were used as the sign of shift of the suspended side in the foci of earthquakes. We note that the near-horizontal position of the p^α axis and the steep position of the t^α axis corresponds to the "positive" movement of the suspended side during overthrust, while the near-horizontal position of the t^α axis and the steep position of the p^α axis corresponds to the "negative" movement of the suspended side with a gently sloping fault, which corresponds to the positive and negative contribution to the STD rate in the vertical direction. The correlation between earthquakes of these two types of movement mainly determines the sign of the vertical component of the tensor for STD rate. Thus, there is the possibility of comparing the approach based on studying the STD of the volume, with the traditional approach to an analysis of the movements of a certain type in the foci of the earthquakes. The latter approach makes it possible also to give a graphic idea about the possibility for mapping the vertical STD component.

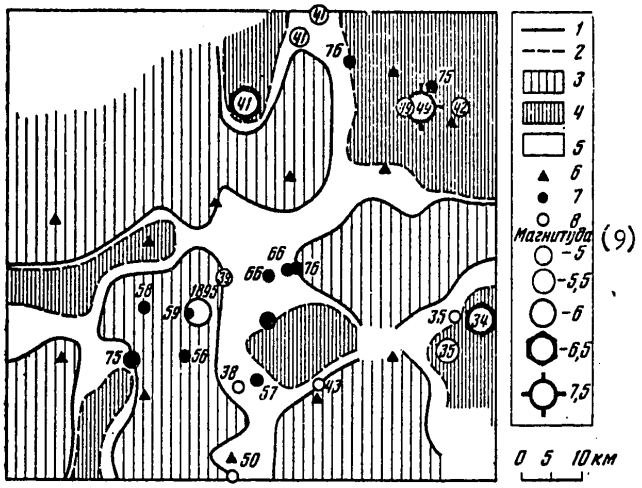

Figure 5. Spatial Distribution of Sign of Vertical STD Component

Key:
1. $\zeta=1.25$
2. $\zeta=0.80$
3. regions of positive values of vertical STD component
4. regions of negative values of vertical STD component
5. regions of approximately zero values of vertical STD component
6. seismic stations
7. earthquakes with M≥5 recorded in instrument period of observations (1955-1976)
8. historical known strong earthquakes with M≥5
9. magnitude

For these purposes in the limits of the same standard slip cells of averaging the ratio ζ is computed of the number of earthquakes with near-horizontal position of the p^{α} axis to the number of earthquakes with near-horizontal position of the t^{α} axis. This near-horizontal nature does not go beyond the limits $\pm 20°$ with the horizon, whereupon the shift movements (in a geological sense) are excluded from the examination. The magnitude of the ζ ratio is not computed if the total number of comparable earthquakes is smaller than six. The mapped magnitude of this ratio is given in figure 5 where the isolines 1.25 and 0.80 are shown dividing respectively the studied territory into regions of significant "positive" and "negative" vertical movements. We note that in the nuclei of the isolated regions of "positive" and "negative" movements the magnitude of the mapped ratio can reach the values 3-6 and 0.3-0.4 respectively. In terms of the STD the elongation of the material of the earth's crust in a vertical direction

corresponds to the "positive" movements, while the shortening of the material--to the "negative." A comparison of the plans in figures 4 and 5 shows the high degree of their correlation, which makes it possible to recommend zoning of the magnitude ξ as an express method for evaluating the deformed state of the studied territory in the absence of computation possibilities on the computer.

6. STD Intensity

As already noted above, in order to obtain a complete idea about the tensor of STD rate it is necessary to multiply the tensor of the average mechanism by the scalar multiplier defined in expression (10)

$$I_\Sigma = \frac{1}{\mu V T} \sum_{\alpha'} M_0^\alpha. \qquad (17)$$

The summing is done according to the number of earthquakes. We note that the intensity of the tensor of STD rate understood in the generally accepted sense in mechanics, equals the product of I_Σ by the intensity of the tensor for the average mechanism $\mathfrak{M}$. We evaluate the amount I_Σ for each of the regions isolated above, having assumed the vertical size of the deformed regions to be equal to 15 km, which corresponds to the thickness of the seismically active layer in the Garm region. The shear modulus μ for the dominant rocks in the upper level of the earth's crust in the Garm region is taken as equal to $\mu = 2.43 \cdot 10^{11}$ dyne/cm^2, according to [34]. For a more reliable long-term evaluation of the amount I_Σ the entire period of instrument observations from 1955 to 1976 is used. In the limits of each of the regions isolated above the number of earthquakes is computed for each energy class K (K=lg E, J) and according to [36], K=4 + 1.8 M, where M--magnitude of earthquake in range K=9-12, and the conversion is made for seismic moments according to the formula

$$\lg M_0 = 0{,}6K + 15{,}7\ldots, \qquad (18)$$

obtained in publication [37] for the range K from 5 to 13 in application to the Garm region. Here M_0 is measured in dyne·cm. The restriction for the upper limit of the earthquakes with K= 12 (M=4.5) in our case was selected from those considerations that the strongest earthquakes on the employed level of description should be viewed as already individual, independent ruptures in the continuity of the medium, since the linear dimensions of the foci of such earthquakes [38] become commensurate with the maximum linear dimensions of the deformed regions and even begin to exceed them. Earthquakes with K< 9 were considered in the summing all the way to K=5 (M≈0.5) according to the graph of recurrence with average incline for the entire region γ_K = -0.45 [36]. The level of the graph of recurrence in the range K=5-9 for each region is defined by the magnitude of activity of the earthquakes with K=9 (M=2.2) obtained on individual graphs constructed for earthquakes with K≥ 9. The parameters of the graphs of recurrence (intensity of the seismic process) A_9^* and γ_K

Table 3. Parameters of Intensity of Seismic A_9*, γ_k and Seismotectonic I_Σ Processes in Different Sections of the Garm Region

(a) Участок	S, км²	$\sum_{K=9}^{14} N_K$	A_9*	$-\gamma_K$	I_Σ
I	$9,5 \cdot 10^2$	77	$0,18 \cdot 10^{-3}$	0,58	$0,55 \cdot 10^{-8}$
II	3,6	64	0,40	0,55	1,34
III	7,0	141	0,44	0,47	1,84
IV	10,1	273	0,56	0,52	2,30
V	9,6	422	0,90	0,50	3,50
VI	4,4	69	0,37	0,51	0,90
VII	4,3	15	0,08	0,52	0,22
VIII	4,9	75	0,37	0,51	1,18
IIIA	2,7	53	0,40	0,49	1,62
IVA	2,3	58	0,52	0,51	1,93
VA	6,5	324	1,04	0,53	3,60
VB	3,1	98	0,61	0,43	3,25
VIIIA	2,6	48	0,37	0,51	1,47
VIIIB	1,3	25	0,41	0,51	1,21
1	2,3	13	0,12	?	0,31
2	2,2	110	0,83	0,36	6,00

Key:
a. Section

for the range K=9-13 are given in table 3. Here the amount A_9* designates the number of earthquakes with K=9 per year in 1 cm^3. Table 3 also indicates the S areas of the regions of deformation and the total number of earthquakes with $K=9-14\left(\sum_{K=9}^{14} N_K\right)$, recorded in limits of these regions in the time from 1955 to 1976. The designations 10^2 for S, 10^{-3} for A_9* and 10^{-8} for I_Σ indicate the order of magnitude in the corresponding columns of table 3. The computed values of the intensity for the seismotectonic process are given in the last column of table 3. We note that on the assumption of the preservation of the law (18) and the linearity of the graph of recurrence towards weaker earthquakes one should increase the computed values by 10% due to the contribution of earthquakes with K=0-4. Every successive five orders of energy make correspondingly 10% contribution each to the magnitude of I_Σ from the previous contribution, and due to the insignificant amount of the subsequent contributions they can be ignored. One should also recall that the accuracy of the conducted evaluation of the STD intensity is determined by the accuracy of the computation of seismic moments, that currently does not exceed half of the order of these magnitudes.

7. Discussion of Results

We will pass to a discussion of the effectiveness of the proposed technique for analyzing the mechanisms for the foci of weak earthquakes and the results of studying the deformed state of the earth's crust in the Garm region.

The work presents a method for determining the average mechanism that is effective with the use of a computer. This method, generalizing the known techniques, makes it possible, in addition, to obtain two new informative parameters (μ_m and $\varkappa$). Enlistment of the components in solid state mechanics promotes the clarification of the physical meaning of the average mechanism as characteristics in the process of deformation of a seismically active volume, as well as its stressed state [13]. The most labor intensive in studying the deformation in the environs of the macroscopic point is the selection of a representative spatial-temporal volume that is equivalent to the implementation of limit transitions indicated in formula (1). This is possible only in the presence in the studied region of a sufficient quantity of acts of shift destruction for different-oriented faults whose dimensions are much smaller than the dimensions of the region. The purely formal use of the expression for the tensor of rate of the seismotectonic deformation given in publication [39] is hardly competent, where 12 shifts for the faults in catastrophic earthquakes are presented as an equivalent macrodeformation of thin spherical layer of the earth's crust in the entire Central Asia. On the other hand it is necessary to note that catastrophic earthquakes in general are not prone to description in terms of seismotectonic deformation and they should be viewed as independent events on its background.

The concept of seismotectonic deformation (STD) is the method of compact physical description of the set of individual ordinary acts of the manifestation of the tectonic process. Such a description makes it possible to pass to a direct comparison of the seismicity with certain geotectonic ideas about the development of the studied region. A reflection of the process of tectonic deformation of the Garm region in the form of a plan of the main fault disorders [40] and total vertical tectonic movements during the Pleistocene [25] is given in figure 6.

The main feature of the seismotectonic deformation of the Garm region is the dominance of the near-horizontal compression in the direction southeast-northwest. In the orientation of the axis of maximum compression deformation in different sections of the region a certain law is observed. In relation to the Pamir section (VI on fig 3) a successive fan-shaped turn of the azimuth of the compression axis is noted along the periphery of the region from 125° in the west (IV on fig 3) to 168° in the north (III in fig 3). Here in the center of the region, in the eastern section of Petr I range (V^A in fig 4) the orientation of the compressions axis at the azimuth 135° is preserved. In the limits of the Pamir section the compression axis is oriented at the azimuth 165°. These peculiarities in the orientation of the compression axis we can attempt to describe by

enlisting the qualitative ideas on the nature of the deformation of the medium by a rigid stamp following from the solution to certain tasks of the theory of elasticity and plasticity, in particular, from the known solution of Hill [41] on the introduction of a stamp into the rigid-plastic half

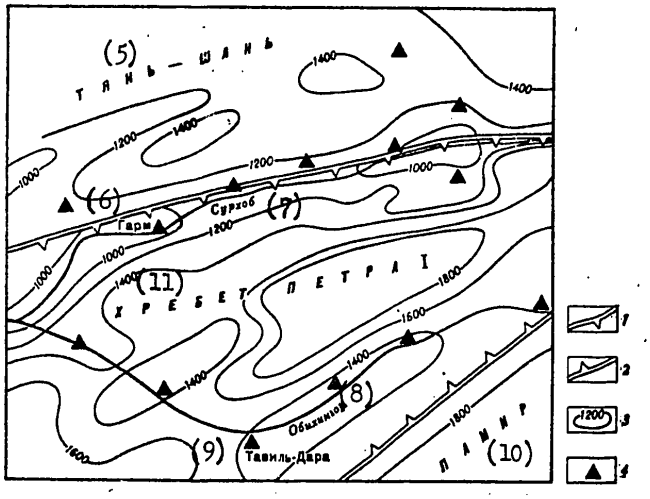

Figure 6. Plan of Region of Work, System of Observations and Vertical Tectonic Movements in the Pleistocene

Key:

1. Gissaro-Kokshaal'skiy edge fault
2. Darvaz-Karakuls'kiy edge fault
3. Isolines of amplitudes of tectonic elevations in 200 m, according to [25]
4. seismic stations
5. Tyan'-Shan'
6. Garm
7. Surkhob
8. Obikhingou
9. Tavil'-Dara
10. Pamir
11. Petr I range

space. In our case as the stamp one can present the northwest projection of the Pamir-Badakhshanshkiy block restricted by the elbow-shaped fold of the Darbaz-Karakul'skiy fault [40]. Figure 6 shows the intermediate section of this fold located just in the limits of the studied region. To the west, roughly on the meridian of Tavil'-Dora the extent of the Darvaz-Karakul'skiy fault is sharply altered to the near-meridional. To the east soon after the emergence from the limits of our region the course

of the fault becomes near-latitudinal [40]. The same course of the Darvaz-Karakul'skiy fault defines the configuration of the frontal edge of the "stamp." In the description of the tectonic movements for the Darvaz-Karakul'skiy fault there exist a number of alternative versions in the geological literature [23, 24, 42-46], nevertheless the possibility of relatively small movements of the Pamir-Badakhshanskiy block to the north along the near-meridional section of the Darvaz-Karakul'skiy fault does not induce any serious objections in anyone. The generally known absence of seismicity within this block [47] can to a certain measure serve as an indication of its increased rigidity. The increased rigidity of the block is confirmed also by the outcrops on the surface of rocks of the Precambrian age in the central part of the block [40]. Movement to the north of such a rigid "stamp" can also be the cause of the observed distribution of axes of maximum compression in the region. In the central section the orientation of the compression axes is perpendicular to the plane of the "stamp" and the axes are turned to both sides the farther from the plane of the "stamp." Enlistment of such solutions to mechanical problems for the purposes of geotectonics has already occurred in seismological studies. The situation closest to our case was examined in publication [45], and since our "stamp" is essentially an angular point of the "stamp" from publication [45] the differences in the interpretations consist only of the scale of examination.

We will dwell in somewhat more detail on one feature of the deformation of the central section in the region. As already noted above, the compression axis at Petr I range is oriented at azimuth 135°, which comprises an angle 45-50° with the course of the eastern section of this structure. At the same time it is known [17] that for the overwhelming majority of linear geological structures the axis of the maximum compression is oriented tranverse to their course. The noncorrespondence of our results to this law, possibly, is explained in light of the aforementioned latest reorientation of the deformation process as the Pamir-Badakhshanskiy block penetrates into the zone of the structural articulation of Pamir and Tyan'-Shan'.

It is important to compare the vertical component of the tensor for STD rate with the vertical tectonic movements in the Pleistocene [25] given in figure 6. The deformation of the 15-kilometer seismically active layer of the earth's crust in a vertical direction we can attempt to present in the form of a movement of free diurnal surface of the layer on the assumption of the immobility of its lower border. After making the second assumption on the constancy of the STD rate for a certain geological time (Pleistocene) we compute the amplitude of the equivalent shift in 1 million years. The main data for these computations are contained in the last columns of tables 2 and 3. Comparison of these computations with the average amplitude of the vertical tectonic movements in the Pleistocene for the previously isolated regions is given in table 4. In such a comparison it is not possible to attribute great importance to the zero of the reading of the tectonic movement amplitudes and the scale of the seismotectonic movements. Of greatest importance is the comparison of

spatial variations in the relative level of these amounts. Therefore the amplitudes of the tectonic elevations given in table 4 are given in relative amounts read off from the level of elevation at 1300 m. For 8 regions a direct correlation is noted between the amounts of relative vertical tectonic movements H^t and the absolute amounts of the seismotectonic movements H^q, and only for four regions I, II, VIII^A and VIII^B these amounts are poorly correlated. The regression equation for the correlated amounts looks like

$$H^t = 10H^q. \qquad (19)$$

Table 4. Amounts of Vertical Seismotectonic Movements H^q, Tectonic Movements H^t and Average Altitudes of Relief H^r in Garm Region

(1) Участки	H^q, м	H^t, м	H^r, м	(1) Участки	H^q, м	H^t, м	H^r, м
I	25	-100	500	V^B	15	200	550
II	18	-100	250	VI	11	150	300
III	-11	-50	200	VII	-1	-100	-200
III^A	-5	-150	-100	VIII^A	-6	150	500
IV	27	250	500	VIII^B	-6	300	600
V^A	55	600	1100	1	0	0	1000

Key:
1. sections

Such a correlation is observed also in a comparison of the seismotectonic movements H^q with the level of the modern relief H^r. The averaged levels of the relief according to the regions are given in table 4, where the altitude at 2000 m is taken as the zero reading. In this case the amounts H^r and H^q are not correlated for the regions III, VIII^A and VIII^B. The regression equation for the correlated amounts looks like

$$H^r = 20H^q. \qquad (20)$$

We note once again that the evaluation of the STD contribution to the vertical tectonic movements is impaired by certain complexities in the structure of the tectonic schemes, the low accuracy of the correlation to one time interval, and the great indefiniteness in extrapolation of the modern rate of STD on the geological time segments.

An important moment is the explanation of that circumstance of whether the regions that differ in deformed state in the limits of the Garm region are blocks in the geological and tectonic sense. Within the framework of the ideas used in this work for the seismotectonic deformation there is no opportunity of giving a clear definition of the boundaries of the isolated regions. Essentially in the work certain "nuclei of deformation" are isolated that are characterized by the fact that in them the process of deformation is the most stable in space and time. Precisely for these

nuclei our description is reliable. According to the geological definition of the concept "block" only one condition is fulfilled here: "section of the earth's crust that is stable or moving with the entire mass..." [48]. The second condition: "...and limited by faults" [48] in our case remains indefinite. But there are certain grounds to assume that further between the concepts "block" and "nucleus of deformation" we will be able to place and approximate equals sign.

The signs for the rate of vertical STD in the isolated nuclei are mainly determined by the type of deformation state, i.e., the Lode-Nadai coefficient μ_m. With negative μ_m and near-horizontal position of the extension axis (region III in fig 3 and regions VII and VIII in fig 4) the material of the earth's crust is squeezed out in a certain cone around this axis, and at the same time the vertical dimension of the deformed volume is reduced. With positive μ_m and horizontal orientation of the axis of the greatest squeezing out of material in the nucleus of deformation the material of the earth's crust is squeezed out simultaneously in all directions outside the compression cone, which, in particular, results in an increase in the vertical size of the deformed volume, i.e., in a growth of mountains. The shift deformation state with $\mu_m=0$ can both lead to a growth of mountains with the near-vertical position of the extension axis (region I in fig 3), and not be accompanied by such in the near-horizontal extension (zone I on fig 4).

In figure 3 on the background of the STD governed by weak earthquakes ($M<4.0$) all the known definitions are given for the mechanisms of the earthquake foci with $M=4.0-5.5$. It follows from such a comparison that the nature of the movements in the foci of relatively strong earthquakes on the whole corresponds to the deformed state evaluated according to the weak earthquakes.

Figure 5 on the background of the vertical component of movements in the foci of weak earthquakes gives the epicenters of all the known strong earthquakes with $M\geq 5$ that occurred in the region during the historical period. One can note such a law that the epicenters of strong earthquakes gravitate towards the outskirts of the nuclei of deformation with negative signs of the vertical STD component and to the transitional zones. It is not excluded that in the transitional zones due to the heterogeneity of the STD field additional elastic deformations appear and stresses that activate the destruction process. One can expect that the study of the laws governing the seismotectonic deformation will be very promising for the purposes of seismic zoning and prediction of the earthquakes. The promising nature of the prediction aspect of the studies follows from the existence of the aforementioned local temporal variations in the STD tensor and from the temporal changes noted in [49, 50] on the conditions of realization of the accumulated stresses.

8. Conclusion

A technique has been developed for studying the mechanisms for the foci of weak earthquakes based on the idea of the seismotetonic deformation. The description of the set of individual mechanisms for the foci with the help of the average mechanism reflects the nature of the seismotectonic deformation of the seismically active volume.

In the studied region nuclei of deformation are isolated with different parameters of the average mechanism. The orientations of the main axes of the average mechanism and the Lode-Nadai coefficient reflect the corresponding characteristics of the tensor for the rate of seismotectonic deformation. The intensity of deformation is evaluated according to the sum of seismic moments of earthquakes and intensity of the average mechanism.

A plan has been suggested for zoning the Garm region for the deformation state that is in satisfactory agreement with the main geological structures and ideas on the vertical tectonic movements in the Quaternary time.

A qualitative model is given that satisfactorily describes the observed deformed state.

We consider it our pleasant duty to thank V. G. Leonova for the possibility of using her definitions of the mechanisms for the foci in the time interval from 1970 to 1976, I. G. Simbireva for the definition of the mechanisms of foci of earthquakes of the earlier period (their work was the basis for this work), and well as I. L. Nersesov for constant interest in the work and fruitful discussions.

BIBLIOGRAPHY

1. Griggs, D.; and Handin, J. "Observations on Fracture and a Hypothesis of Earthquakes," in Griggs, D.; and Handin, J. (Eds) "Rock Deformation Geol. Soc. Amer. Mem., 79, 1960.

2. Sheidegger, A. E. "Physical Aspects of Natural Catastrophes," Elsevier, Amsterdam, 1975.

3. Kostrov, B. V. "Mekhanika ochaga tektonicheskogo zemletryaseniya [Mechanics of Foci of Tectonic Earthquake], Moscow, Nauka, 1975.

4. Myachkin, V. I.; Kostrov, B. V.; Sobolev, G. A.; and Shamina, O. G. "Fundamentals of Physics of Focus and Forerunners of Earthquakes," "Fizika ochaga zemletryaseniya" [Physics of Earthquake Focus], Moscow, Nauka, 1975.

5. Honda, H. "Earthquakes Mechanism and Seismic Waves, J. PHYS. EARTH, 10, No 2, 1962.

6. Vvedenskaya, A. V. "Issledovaniye napryazheniy i razryvov v ochagakh zemletryaseniy s pomoshch'yu teorii dislokatsiy"[Study of Stresses and Faults in Foci of Earthquakes with Help of Theory of Dislocations], Moscow, Nauka, 1969.

7. Khattri, K. N. "Earthquake Focal Mechanism Studies. A Review," REVIEW GEOPHYSICS AND SPACE PHYSICS, Vol 9, No 1, 1973.

8. Scheidegger, A. E. "The Tectonic Stress and Tectonic Motion Direction in Europe and Western Asia as Calculated from Earthquake Fault Plane Solutions," BULL. SEISMOL. SOC. AMER., 54, No 5, 1964.

9. Aki, K. "Earthquakes Generating Stress in Japan for the Years 1961 to 1963 Obtained by Smoothing the First Motion Radiation Patterns," BULL. EARTHQUAKES RES. INST. UNIV. TOKYO., 44, No 2, 1966

10. McKenzie, D. P. "The Relation between Fault Plan Solutions for Earthquakes and the Directions for Earthquakes and the Directions of the Principal Stress," BULL. SEISMOL. SOC. AMER., 59, No 2, 1969.

11. Gushchenko, O. I. "Kinematic Principle of Reconstruction of Directions of Main Stresses (from Geological and Seismological Data)," DOKL. AN SSSR, 225, No 3, 1975.

12. Gushchenko, O. I.; Stepanov, V. V.; and Sim, L. A. "Directions of Action of Megaregional Tectonic Stresses of Seismically Active Regions in Southern Eurasia," DOKL. AN SSSR, 234, No 3, 1977.

13. Nikitin, L. V.; and Yunga, S. L. "Methods of Theoretical Determination of Tectonic Deformations and Stresses in Seismically Active Regions," IZV. AN SSSR. FIZIKA ZEMLI, No 11, 1977.

14. Fara, H. D.; and Sheidegger, A. E. "An Eigenvalue Method for the Statistical Evaluation of Fault Plane Solutions at Earthquakes," BULL. SEISMOL. SOC. AMER., 53, 1963, p 811.

15. Soboleva, O. V. "Determination of the True Fault Plane in the Earthquake Source," COMMUNIC. OBSERV. ROY. BELG. SER. GEOPHYS., No 101, 1971, p 146.

16 Soboleva, O. V. "Method of Unambiguous Determination of Fault Plane in Focus in Example of Gindukushskiy Epicentral Zone," IZV. AN SSSR. FIZIKA ZEMLI, No 1, 1972.

17. Balakina, L. M.; Vvedenskaya, A. V.; Golubeva, N. V.; Misharina, L. A.; and Shirokova, Ye. I. "Pole uprugikh napryazheniy Zemli i mekhanizm ochagov zemletryaseniy" [Field of Elastic Stresses of Earth and Mechanism of Foci of Earthquakes], Moscow, Nauka, 1972.

18. Gotsadze, O. D.; Keylis-Borok, V. I., et al.,"Study of Earthquake Mechanisms," TR. GEOFIZ. IN-TA, No 40 (166), 1957.

19. Neresov, I. L.; and Simbireva, I. G. "Laws Governing the Distribution of Stresses in the Foci of Weak Earthquakes of the Garm Region and Their Link to Seismicity," "Tr. III Vses. simp. po seysm. rezhimu" [Proceedings of Third All-Union Symposium on Seismic Patterns], Pt 1, Novosibirsk, Nauka, 1968.

20. Simbireva, I. G. "Prostranstvenno-vremennyye osobennosti raspredeleniya mekhanizma ochagov slabykh zemletryaseniy Garmskogo i Narynskogo raynov Sredney Azii" [Spatial-Temporal Features of Distribution of Focal Mechanisms of Weak Earthquakes in the Garm and Naryn Regions of Central Asia], Author's abstract of candidate dissertation, Institute of Earth Physics, USSR Academy of Sciences, 1969.

21. Krestnikov, V. N.; and Simbireva, I. G. "Link of Tectonic Structure to Features of Distribution of Dynamic Parameters of Earthquake Foci," "Zemnaya kora seysmoopasnykh zon" [Earth's Crust in Seismically Dangerous Zones], Moscow, Nauka, 1973.

22. Simbireva, I. G.; Lukk, A. A.; and Nersesov, I. L. "Changes in the Dynamic Parameters of Foci of Weak Earthquakes of the Garm Region in Relation to Occurrence of Strong Earthquakes,""Regional'nyye issledovaniya seismicheskogo rezhima" [Regional Studies of Seismic Pattern], Kishinev, Shtiintsa, 1974.

23. Gubin, I. Ye. "Zakonomernosti seismicheskikh proyavleniy na territorii Tadzhikistana" [Laws Governing the Seismic Manifestations on the Territory of Tadzhikistan], Moscow, Izd-vo AN SSSR, 1960.

24. Krestnikov, V. N. "Istoriya razvitiya kolebatel'nykh dvizheniy zemnoy kory Pamira i sopredel'nykh chastey Azii" [History of Development of Oscillating Movements of Earth's Crust in Pamir and Adjacent Parts of Asia], Moscow, Izd-vo AN SSSR, 1962.

25. Chigarev, N. V. "Technique of Constructing Quantitative Plans for Summary Tectonic Movements in Pleistocene (in the Example of Southwest Pamir-Alay)," GEOMORFOLOGIYA, No 3, 1973.

26. Riznichenko, Yu. V. "Seismic Course of Mountain Massifs,""Dinamika zemnoy kory"[Dynamics of Earth's Crust], Moscow, Nauka, 1965.

27. Kostrov, B. V. "Seismic Moment, Energy of Earthquakes and Seismic Course of Mountain Massifs," IZV. AN SSSR. FIZIKA ZEMLI, No 1, 1974

28. Yunga, S. L. "Mechanism of Deformation of Seismically Active Volume of Earth's Crust," IZV. AN SSSR. FIZIKA ZEMLI, No 10, 1979.

29. Riznichenko, Yu. V.; and Dzhibladze, E. A. "Rates of Vertical Movements with Seismic Course of Mountain Massifs," IZV. AN SSSR. FIZIKA ZEMLI, No 1, 1976.

30. Riznichenko, Yu. V. "Calculation of Rates of Deformation with Seismic Course of Mountain Massifs," IZV. AN SSSR, FIZIKA ZEMLI, No 11, 1977.

31. Ari, K. "Generation and Propagation of G-Waves from the Niigata Earthquakes at June 16, 1964. Pt 2. Estimation at Earthquakes Moment, Released Energy and Stress Strain Drop from G-Waves Spectrum," BULL. EARTHQUAKES RES. INST. TOKYO UNIV. 44, No 1, 1966.

32. Brune, I. N. "Seismiv Moment, Seismicity and Rate of Slip along Major Fault Zones," J. GEOPHYS. RES., 73, No 2, 1968.

33. Lukk, A. A. "Spatial-Temporal Sequence of Weak Earthquakes of Garm Region," IZV. AN SSSR. FIZIKA ZEMLI, No 2, 1978.

34. Lukk, A. A.; and Nersesov, I. L. "Nature of Temporal Variations in Rates of Elastic Waves in Earth's Crust of Garm Region," IZV. AN SSSR, FIZIKA ZEMLI, No 6, 1978.

35. Vermisheva, L. Yu.; and Gagnus, A. A. "Use of Typification of Shifts in Foci of Earthquakes to Solve Seismotectonic Tasks," IZV. AN SSSR. FIZIKA ZEMLI, No 3, 1977.

36. Riznichenko, Yu. V., ed. "Methods of Detailed Study of Seismicity," TR. IFZ AN SSSR, No 9 (176), 1960.

37. Vostrikov, G. A. "Determination of Seismic Moment of Local Earthquakes according to Characteristics of Code," IZV. AN SSSR. FIZIKA ZEMLI, No 11, 1975.

38. Riznichenko, Yu. V. "Dimensions of Focus of Crust Earthquake and Seismic Moment," "Issledovaniya po fizike zemletryazeniy"[Studies on Physics of Earthquakes], Moscow, Nauka, 1976.

39. Wang-Ping Chen; and Molnar, P. "Seismic Moments of Major Earthquakes and the Average Rate of Slip in Central Asia," J. GEOPHYS. RES., 32, No 20, 1977.

40. Markovskiy, A. P., ed."Geologicheskaya karta Sredney Azii i prilegayushchikh territoriy. M 1:1,500,000, sostavlena vo VSEGEI"[Geological Map of Central Asia and Adjacent Territories. Scale 1:1,500,000 Compiled in All-Union Scientific Geological Institute], 1964.

41. Hill, R. "The Mathematical Theory of Plasticity," Oxford Univ. Press, London, 1950.

42. Zakharov, S. A. "Razvitiye tektonicheskikh prestavleniy v Tadzhikistane i gopoteza zonnogo tektogeneza"[Development of Tectonic Ideas in Tadzhikistan and Hypothesis on Zonal Tectogenesis],Dushanbe, Donish, 1970.

43. Nikonov, A. A. "Analysis of Tectonic Movements for Gindukush-Darvaz-Karakul'skiy Zone of Faults in Late Pleiocene and Quaternary Period," BYUL. MOIP. OTD. GEOL.,Leningrad, No 2, 1975.

44. Trifonov, V. G. "Late-Quaternary Fault Disorders in West and Central Asia from Data of Decoding Aerial Photographs and Ground Observations," IZV. VUZOV, GEOLOGIYA I RAZVEDKA, No 11, 1976.

45. Molnar, P.; and Tapponier, P. "Cenozoic Tectonics of Asia: Effects at a Continental Collision," SCIENCE, 189, 1975, p 419.

46. Bel'skiy, V. A. "Seismotectonic characteristics of Zone of Articulation of North Pamir and Eastern Edge of Tadzhik Depression," "Voprosy seismicheskogo rayonirovaniya territorii Tadzhikistana" [Questions of Seismic Zoning of Territory of Tadzhikistan], Dushanbe, Donish, 1976.

47. "Atlas zemletryaseniy v SSSR" [Atlas of Earthquakes in the USSR], Moscow, Izd-vo AN SSSR, 1962.

48. "Geologicheskiy slovar'"[Geological Dictionary], Moscow, Nedra, 1973.

49. Nersesov, I. L.; et al. "Possibilities of Predicting Earthquakes in Example of Garm Region of Tadzhik SSR,""Predvestniki zemletryaseniy" [Forerunners of Earthquakes], Moscow, VINITI, Dep No 5498-73, 1978.

50. Lukk, A. A.; Leonova, V. G. "Seismic Fracturing of Earth's Crust of Garm Region according to Statistics of Focal Mechanisms of Weak Earthquakes," IZV. AN SSSR. FIZIKA ZEMLI, No 8, 1978.

[8144/0883 A-9035]

9035
CSO: 8144/0883A

PHYSICS OF THE ATMOSPHERE

POSSIBILITY OF STIMULATION OF TURBULENCE IN THE POLAR MAGNETOSPHERE: FIRST RESULTS OF 'MINI-I'

Apatity ISSLEDOVANIYA PROTSESSOV V AVRORAL'NOY IONOSFERE METODAMI AKTIVNOGO VOZDEYSTVIYA in Russian 1978 pp 106-118

[Article by O. A. Molchanov, M. M. Mogilevskiy, O. A. Mal'tseva, V. A. Krechetov]

[Text] Recently a great deal of attention has been given to the mechanisms of acceleration of electrons along the auroral lines of force of the earth's magnetic field causing bright arcs of the aurora polaris and intensive kilometer emission in the frequency band of 100 to 400 kilohertz leaving the earth for interplanetary space [1]. The accelerated electron fluxes and the less energetic return fluxes also cause various types of polar VLF-emissions [2, 3], in particular the auroral VLF-effervescing. This acceleration can occur as a result of the appearance of regions of anomalous systems in the electrostatic turbulence of the type of the ion-sound or ion-cyclotron waves and (or) the dual layers at altitudes of 3000 to 15000 km [4].

Obviously, there are some threshold values of the longitudinal currents above which the auroral tube of force at the indicated altitudes can move discontinuously from the condition of weak turbulence (absence of double layers) to the state of strong turbulence, as a result of which the above-mentioned geophysical phenomena begin. If we propose that in the magnetically disturbed time the states near the threshold retained for quite a long time are possible, then the effect of a powerful VLF-transmitter on the magnetospheric plasma of the auroral tubes of force can serve as impetus to the discontinuous transition. This includes the idea of stimulation of the auroral processes by the emission of a ground-based VLF-emitter. The mechanism of this effect is the cyclotron heating of plasma electrons which was analyzed in great detail in connection with the analogous problem in the laboratory systems of the cyclotron type [5-7]. A characteristic feature of the heating is the occurrence of turbulence on the electron potential oscillations in the region where the wave frequency is close to $\omega_{He}\cos\psi$ (ω_{He} is the electron cyclotron frequency, ϕ is the angle between the wave vector of the initial hiss wave and the direction of the external magnetic field).

Turbulence is also possible on the low-frequency electrostatic waves of the ion sound type or ion cyclotron oscillations into which the hiss waves can decay or which can be generated as a result of the nonlinear hydrodynamic scattering of the hisses [8]. Finally, the increase in anomalous resistance of the auroral tube of force can occur as a result of the appearance of fluxes of erupted electrons as a result of pitch-angle diffusion of the captured electrons on the hiss waves. All of these factors -- heating, pitch-angle diffusion, additional turbulence -- can have a noticeable effect on the quasiequilibrium state of the tube of force. We shall not present a further discussion of the details of the mechanisms of cyclotron heating by VLF-waves in the polar magnetosphere. We shall only demonstrate the experimental proofs of the theoretical possibility of such heating at altitudes of 5000 to 15000 km and some theoretical estimates connected with the experimental data. Let us emphasize that we are talking about the theoretical possibility inasmuch as the experiments were performed only with subauroral VLF-transmitter (L~4).

The experiment with respect to the injection of the VLF-waves into the subauroral magnetosphere was started in the Soviet Union in 1975 within the framework of the "Araks" project [9]. Later they were continued [10]. The experiments with the Siple subauroral VLF-transmitters (Antarctica, L=4.1) and TELF (Alaska, L=4.0) were also performed by American and Australian researchers [11, 12]. The frequency of the emitter $\omega<05\omega_{He\ min}$ was selected during the experiments so that the VLF-wave was recorded with respect to a closed beam trajectory to the magnetically conjugate region, being only slightly absorbed in the equatorial plane of the magnetosphere. The authors of these papers recorded the induced (trigger) emission near the initial frequency, but, in spite of the special conditions, they were unable to detect the stimulation of the fluxes of erupted electrons (using photometry or x-radiation in tanks) or the effects connected with the development of noticeable turbulence along the path of propagation.

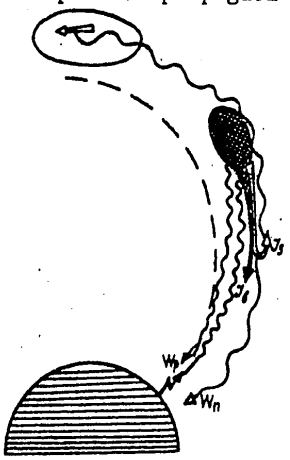

Figure 1. MINI-1 experimental set up

In this article some results will be presented with respect to the effect of the VLF-emitter on the subauroral magnetosphere and ionosphere obtained in the summer and fall of 1977 within the framework of the "MINI-1" program. The schematic of the experiment appears in Fig 1. In contrast to the experiments described in references [11, 12], we have selected a high frequency of the VLF-wave $\omega>\omega_{He\ min}$ and we have been oriented on the fact that in some quite narrow region where $\omega\leq\omega_{He}\cos\psi$ (crosshatched in Fig 1), the initial wave will be strongly absorbed, transmitting its energy to the resonance electrons and the turbulence. Here, effects can occur which are connected with the eruption of electron fluxes in the ionosphere I_B by reemission of W_n, mirror-reflected electrons with large initial pitch angles in the equatorial plane where, as is known, the radiation intensity is maximal. Finally, the backscattering of the initial hiss waves from the turbulent region W_p can occur. In order to estimate the expected effect we calculated the trajectory characteristics of the VLF-waves for $M_0=4$, various models of the electron concentration and the distribution functions of the high-energy electrons. Fig 2 shows the values of the L-parameter of the trajectory, the angle ψ of the double group delay 2tg and the relative proportion of the energy absorbed by the plasma for f=25.0 kilohertz and various magnetic disturbance conditions (different Kp-indexes) depending on the current magnetic latitude of the trajectory ($\theta=60°$ -- the initial latitude, $\theta=0°$ -- latitude of the geomagnetic equator). Let us explain the meaning of the last value($(\partial W_E/\partial t)\ (NT)^{-1}$). The process of the absorption of the wave energy and the corresponding increase in energy of the electrons or turbulent degrees of freedom can be described by the following equation

$$\frac{\partial NT_e}{\partial t}+\delta\nu^*\Delta(NT_e)=\langle\tilde{j}\tilde{E}\rangle=-\frac{dW_E}{\partial t}. \qquad (1)$$

Equation (1) is written by analogy with the equation of the energy balance in a colliding plasma. Here W_E is the energy density of the heating wave, NT^e is the effective thermal energy of the plasma electrons, and the term $\delta\nu^*\Delta(NT^e)$ describes the energy transmission to the turbulence with turbulent "frequency of the collisions" ν^* and the coefficient δ. If the initial level of the turbulence is low, then the value of $((-dW_E/\partial t)(NT)^{-1}=P)$ has the meaning of the inverse type of building up the turbulence. If we propose that the established level of turbulence is such that $\Delta NT^e/NT^e\sim10^{-2}-10^{-3}$ (and this is characteristic for weak turbulence), it is possible to estimate ν^* proportional to the square of the turbulent field amplitude [3].

$$\nu^*\approx 10^2-10^3P\delta^{-1}. \qquad (2)$$

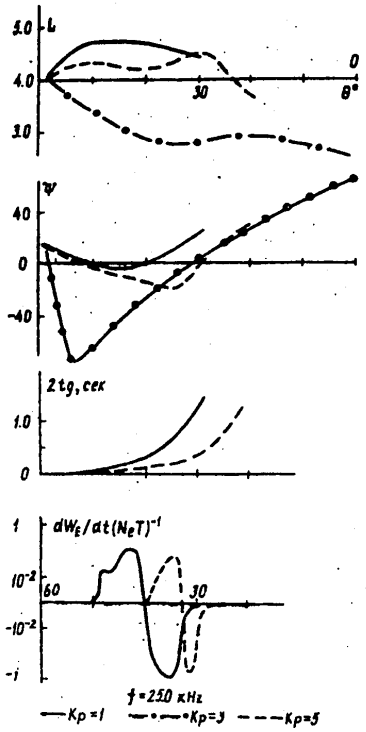

Figure 2. Beam trajectory parameters as a function of latitude

Obviously, the turbulence develops in the region of minimum value of P, whereas in the regions of the maximum, energy transferred to the wave from the plasma and a buildup of its amplitude take place. It is easy to find the explicit form

$$P = \langle JE \rangle / NT_e = \gamma \tilde{E}^2 \mu \mu_g \cos \alpha (NT)^{-1}, \qquad (3)$$

where γ is the increment (the decrement) of the system wave with an amplitude of $\tilde{E}$; μ, μ_t are the phase and group indexes of refraction and α is the angle between the group phase wave velocities. The calculations, part of which are illustrated in Fig 2 indicate that the length of the turbulent region is 1000 to 3000 km, and its position is shifted toward the beginning of the trajectory with respect to the point where $\omega = \omega_{He} \cos \psi$. This means that the wave energy absorption takes place not on the cold, but on the low-energy electron component with characteristic energies of ~0.1 to 5.0 kev. Fig 3 shows the results of the trajectory calculations for several frequencies, L=4.0; Kp=1 and the standard model of the electron concentration with base level at the altitude of 1000 km, $N_{e0}=1.5 \cdot 10^4$ cm^{-3}. The circles indicate the minimum values of P, and the x's, the region of disappearance of the wave ($E/\tilde{E}<10^{-3}$). Let us note that the frequency variation from 37.0 to 12.5 kilohertz increases the altitudes of the turbulent regions from ~8000 km to 15000 km. Finally, let us also note that by the graphs in Fig 2 the values of the group delays are ~0.5 to 1.0 sec. All of these factors determined the choice of the operating conditions during the experiment.

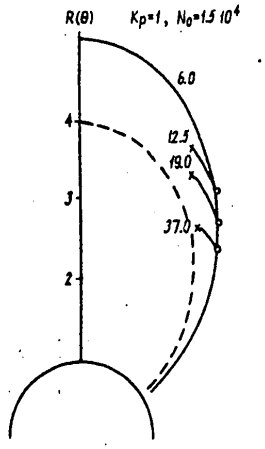

Figure 3. Regions of absorption of the VLF-waves as a function of frequency

The observations were performed for periods of 6-14 June and 5-20 September 1977 night and morning at a distance of 450 km from the VLF-transmitter. For observation of the backscattering, the pulses of 0.25 and 0.5 were used with a repetition period of 4 seconds. In part of the sessions, pulses of duration 2 seconds, 16 seconds and 180 seconds were used; in this case the repetition period was 4.32 and 360 seconds respectively and sometimes the pulses were modulated by 8 and 20 hertz frequencies. Finally, for short sendings the repetition period sometimes decreased to 2 (0.5 hertz) and 1 second (1 hertz). In all of the sessions the VLF-emitter operated on frequencies in the range of 19-29 kilohertz.

The effectiveness of the backscattering turned out to be not too high; therefore a special procedure was used to convert the time sequence in the narrow band near the initial frequencies (Δf=30 hertz) to the spectral band with subsequent accumulation of the spectra. In each session lasting 30 minutes we had 450 sendings. In spite of this, in only two sessions were we able to isolate the echo. One of them (8 June, several hours after the substorm) is illustrated in Fig 4a (the mode 0.25/3.75 sec) and 4b (0.5/3.5 sec). The flash near τ=0 corresponds to the initial pulse. The stable flash near the reflection time of τ~0.8 seconds corresponds to the reflected pulse after 128, 256 and 512 accumulations of the signal series (Fig 4a). The lowest curve (IV) corresponds to the second half of the session, whereas curve I corresponds to the result of averaging for the first 8 minutes, curve II, for the first 18 minutes, and III, for the entire session.

Fig 4b also shows the flash near τ~0.7 to 0.8 sec (the time is reckoned from the end of the pulse) except there is an illusion of the second flash, possibly from the second boundary of the region. However, the most interesting characteristic of the given session is regular decrease in the delay with the session time of ~0.1 sec for 20 minutes. This corresponds to the approach to the earth of the boundary of the turbulent region with a velocity of ~1 km/sec which is close to the thermal velocity of the ions or the ion sound at the altitudes of the magnetosphere. Let us note that the experimentally observed delays in the scattered signal are close to calculated (see Fig 2).

As has already been mentioned, it is quite complicated to discover the effects of the electron eruptions into the ionosphere from the turbulent region using photometry or x-radiation on balloons. In particular, the second procedure obviously is ineffective as a result of the fact that the low-energy electrons erupt (E<1 kev). Therefore, we have tried to discover the effect of the eruption by observation of emission on the modulation frequency of the VLF-transmitter. Initially, we related this emission to the excitation of the ionosphere currents in the E-layer (see the article [14] for more details). However, the oscillations of the ionospheric current are theoretically forced inasmuch as the modulation time $\Omega << V_{em}$ at altitudes of the ionosphere. In addition, in a number of sessions sometimes the radiation did not stop after completion of the modification for several minutes. For illustration of this Fig 5 shows samples of the recordings for 20 September 1977.

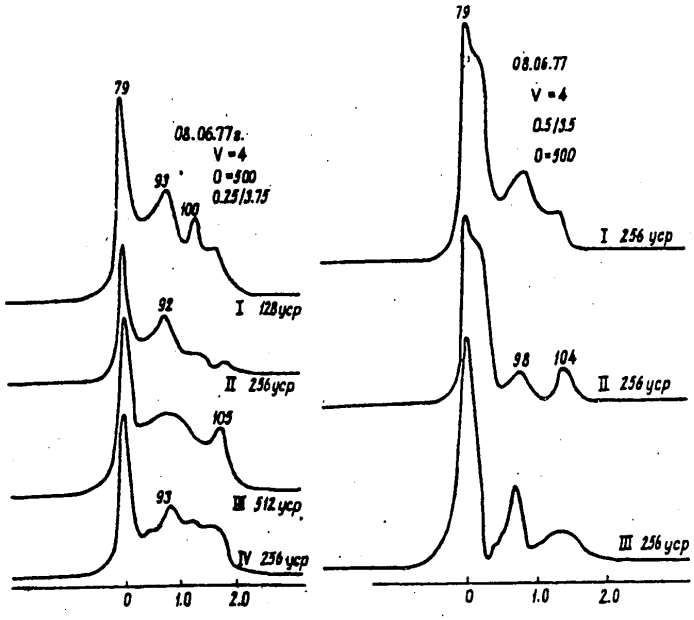

Figure 4. Reflected VLF-signals observed in two different sessions

Here the session lasted 120 minutes, the minute and second marks were noted automatically at the bottom of the recording. On the lower track, the control signal was recorded on the frequency of the VLF-transmitter, and on the upper track, the detected signal of the KPK-receiver, tuned to the modulation frequency 8. The first 30 minutes of the observations were performed at an altitude Ω=8 hertz; the work was done by 16/16 sec sendings. The intensity of the radiation builds up slowly for the first 10 minutes, and generally coincides with the modification regime for the next 20 minutes, but it does not stop for ~2 minutes after the end of the modification effect, for beginning with 30 and 90 minutes, ω=20 hertz and the 180/180 sec modes were changed (the KPK receiver was tuned to Ω=20 hertz at 34 minutes). The aftereffect was noted on every 3-minute launch as is obvious in Fig 5b. However, the picture of the process was quite visible for 30 minutes of the session (see Fig 5c) when for the same Ω=20 hertz sendings of 2.2 seconds began. Obviously this is no accident, for the period T_n=4 sec is close to the bounce period of the low-energy electrons (~0.5 kev) for L=4. For better understanding of Fig 5c it is necessary to explain that during the first minute of this part of the session the more frequent

*Short-period oscillation.

sendings -- 1/1 sec -- were suppressed (and the radiation was low), and beginning with 93 minutes the speed of the pen recorder was increased by 5 times. Just as before good synchronousness of the radiation in the initial sendings during the session is obvious, but the radiation does not cease after completion of the session for 2.5 minutes. From our point of view this effect can be explained by the fact that the emission during the session and especially after it is connected with the excitation of ionospheric currents by the electrons falling out of the magnetosphere, inasmuch as the relaxation of the electron distribution in the collision-free magnetosphere occurs much more slowly than in the ionosphere. The relaxation time is on the order of the "congealing" time of the turbulence or the lifetime of the low-energy electrons which is ~10^2 to 10^3 sec, which corresponds to our results. Let us note that the excitation of the radiation in the KPK range by the modulated sendings of the VLF-transmitter as a result of eruption of the magnetospheric electrons was investigated theoretically in reference [5]. Finally, the flashes of intensity of the glow of the night sky according to the photometer with characteristic times of ~3.5 sec under the effect of the Soviet subauroral transmitter were reported in reference [9], the authors of which also explain these results by eruption of electrons from the magnetosphere.

It was stated above that we hoped to detect heating and variation of the distribution with respect to velocities of the electrons captured in the magnetosphere (unerupted) by their reemission in the equatorial plane. In one of the preceding papers mention has already been made of the modification of the VLF natural noise in the 2-3 kilohertz range under the effect of the VLF-transmitter on the magnetosphere [6]. In the given experiment, as it appears to us, it was possible in several cases (four sessions) to detect variation of the VLF noise on the filter channels of the standard VLF receiver at 0.7 kilohertz (one session) and 1.0 kilohertz (three sessions). The effect was observed only for the magnetically disturbed time against a background of increased VLF noise level. Fig 6 illustrates the session of 12 September which began at 0500 hours local time. The lines under the recording indicate the times of the 3-minute sendings on a frequency of 19 kilohertz. A slow recording is presented for the 0.7 and 1.0 kilohertz channels. In spite of the fact that there is no detailed comparison of the VLF flashes during the sendings, their correlation on the 0.7 kilohertz channel obviously is unquestioned. Theoretically it is complicated to calculate the reemission intensity, but it is quite simple to estimate the expected spectrum inasmuch as from the trajectory calculations we know the position of the turbulent region and the resonance energy of the electrons in it E_r. From the condition of cyclotron resonance and conservation of the energy of the electrons during drift to the equator we obtain the equation

$$\frac{z^2\mu_0^2(z)}{(1-p\varkappa z)^2}=\frac{\mu^2\cos^2\varphi\cos^2\psi}{(1-\varkappa)^2p^2\left(1-\frac{\sin^2 I}{p}\right)\cos^2\psi_0}, \qquad (4)$$

where $z=f_0/f$, f_0 is the frequency reemitted on the equator, ψ is the angle of the wave normal of the initial wave with the magnetic field, I, x, μ

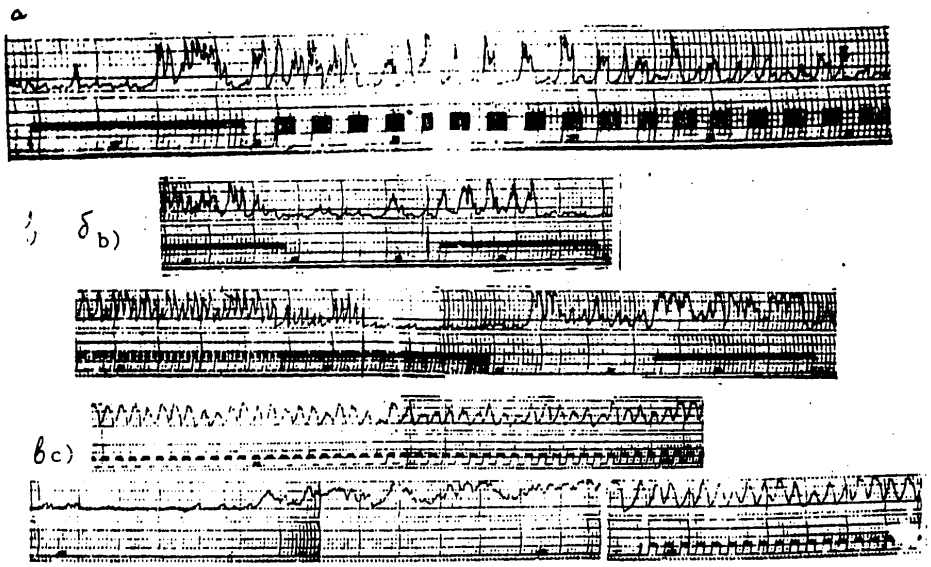

Figure 5. Sample recordings of the KPK signals for 20 September 1977 (upper track -- the KPK signal; lower track -- the control signal of the VLF-transmitter).

are the pitch angles of the resonance electrons, the normalized frequency of the initial wave and the index of refraction in the turbulent region, $x=\omega/\omega_{He}$, $P=\omega_{He}/\omega_{Ho}$ is the mirror ratio. The equation (4) is easily solved numerically. The results of the calculations for different models and different pitch angles are shown in Fig .7. It is obvious that the reemitted frequencies for f=15-30 kilohertz lie in the range of 0.5 to 2.5 kilohertz, which in general corresponds to the experimental results.

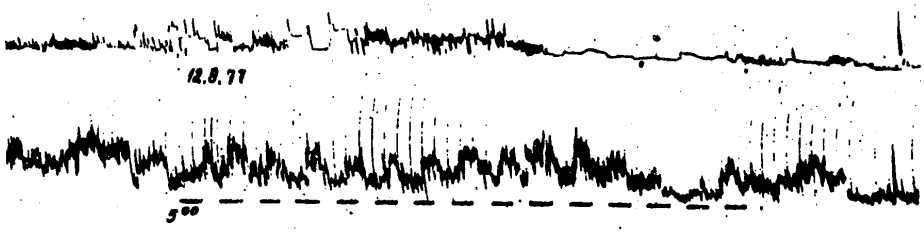

Figure 6. Intensity of the VLF-noise emission over the 0.7 and 1.0 kilohertz channels during the first operating period of the transmitter

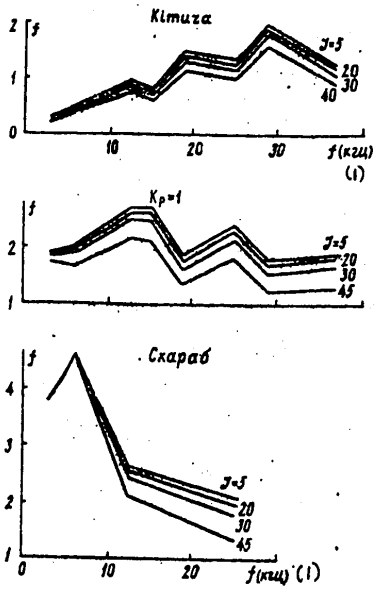

Figure 7. Reemitted frequency f_0 as a function of the initial frequency f.

Key:
1. kilohertz

Thus, in this article we have tried to demonstrate the possibility of noticeable turbulization and heating of the plasma at altitudes of 8000 to 15000 km. Obviously the intensity of the effect does not change sharply on transferring the VLF-emitter to the auroral zone; nevertheless the stimulating effect of it in this case can increase significantly for the reasons discussed at the beginning of the article.

The authors are grateful to V. I. Karpman for discussion of the results and also to A. A. Shchekotov and Yu. M. Markeyeva for their assistance.

BIBLIOGRAPHY

1. Shawhan, S. D., "Magnetospheric Plasma Waves," REPT. ROYAL: INST. OF TECHNOLOGY, Stockholm, Sweden, No 44, 1977, p 100.

2. Gurnett, D. A., Frank, L. A., "VLF Hiss and Related Plasma Observations in the Polar Magnetosphere," J. GEOPHYS. RES., No 77, 1972, p 172.

3. James, H. G., "VLF-Sensors," J. GEOPHYS. RES., No 81, 1976, p 501.

4. Frederiks, R. W., Scarf, F. L., Russel, C. T., "Field-Aligned Currents, Plasma Waves and Anomalous Resistivity in the Disturbed Polar Cusp," J. GEOPHYS. RES. No 78, 1973, pp 2133-2141.

5. Brambilla, M. "Cell-Consistent Field from Electron Cyclotron Resonance in a High-Frequency Plasma Accelerator," PLASMA PHYS., No 10, 1968, p 358.

6. Kuckes, A. F., "Resonant Absorption of Electromagnetic Waves in a Non-uniformly Magnetized Plasma," PLASMA PHYS., No 10, 1968, p 367.

7. Timofeyev, A. V., "Theory of Cyclotron Heating in Long Adiabatic Traps," FIZIKA PLAZMY [Plasma Physics], No 1, 1975, p 88.

8. Trahtengers, V. U., "Nonlinear Hydrodynamic VLF-Wave Scattering in the Earth's Magnetosphere," PLANET SPACE SCI., No21, 1973, p 359.

9. Zhulin, I. A., "Artificially Stimulated Electron Eruption from the Earth's Magnetosphere," DAN SSSR, SER. FIZIKA [Reports of the USSR Academy of Sciences, Physics Series], No 230, 1976, p 1073.

10. Molchanov, O. A., "Nonlinear Effect of Powerful VLF-Waves on a Magneto-spheric-Ionospheric Plasma," IZV. VUZOV, SER. RADIOFIZIKA [News of the Institutions of Higher Learning, Radio Physics Series], No 20, 1977 p 1763.

11. Helliwell, R. A., Katsufrakis, J. P., "VLF-Wave Injection into the Magnetosphere from Siple Station," J. GEOPHYS. RES., No 79, 1974, pp 2551-2518.

12. Dowden, R. L., Rycroft, M. J., "Wave Injection Experiments and Wave-Particle Interaction," SPACE RES., No 16, 1976, p 613.

13. Tsytovich, V. N., TEORIYA TURBULENTOY PLASMY [TURBULENT PLASMA THEORY], Moscow, Atomizdat, 1971, p 422.

14. Molchanov, O. A.; Shchekotov,A. Yu., "Excitation of Ionospheric Current Oscillations," see the current collection.

15. Bell, T. F., "VLF-Wave Generation Through Particle Precipitation Induced by VLF-Transmitters," J. GEOPHYS. RES., No 81, 1976, p 3316.

16. Mogilevskiy, M. M.; Molchanov, O. A.; Markeyeva, Yu. M., ISSLEDOVANIYA IONOSFERY I MAGNITOSFERY METODAMI AKTIVNOGO VOZDEYSTVIYA [Studies of the Ionosphere and Magnetosphere by Active Modification Methods], Apatity, Izd. Kol'skogo Filiala AN SSSR, 1977 p 25.

[8144/1072-10845]

10845
CSO: 8144/1072

IONOSPHERIC EFFECTS IN A GEOPHYSICAL EXPERIMENT WITH A POWERFUL MHD-GENERATOR

Apatity ISSLEDOVANIYA PROTSESSOV V AVRORAL'NOY IONOSFERE METODAMI AKTIVNOGO VOZDEYSTVIYA in Russian 1978 pp 3-13

[Article by Ye. P. Velikhov, O. M. Raspopov, Yu. M. Volkov, A. V. Zotov, Yu. A. Dreyzin, Yu. L. Sverdlov, Yu. F. Zarnitskiy, E. V. Sukhorukova, N. V. Shul'gina]

[Text] A solid-fuel pulse MHD-generator was started up for the first times on the Kola Peninsula in 1976. The current from this generator was sent through a cable laid on the isthmus of the Sredniy Peninsula to the bays on both sides of the isthmus (see Fig 1). The characteristic shape of the current pulses is presented in Fig 2. The use of the MHD-generator combined with an enormous circuit formed by the current closed basically through the sea, made it possible to create an electromagnetic field pulse which could be directly recorded (without accumulation) over the entire territory of the Kola Peninsula and in the northern part of Karelia. The purpose of the experiments was to obtain information about the abyssal geoelectric structure of the earth's crust in the vicinity of the Kola Peninsula [1]. Along with this goal it was of interest to consider the possibility of studying the interaction of an artificial magnetic field pulse with the polar ionosphere and the earth's magnetosphere. The structure of the magnetic field created by the MHD-generator current reduces to the following in its general features.

The magnetic flux $\Phi \approx 10^6 \gamma\text{-km}^2$ intersects the surface of the earth from bottom to top over the territory of the Rybachiy and Sredniy Peninsula and the strip of coastline adjacent to them ~10-15 km wide (see Fig 1). AS a result of the high integral conductivity of the Barents Sea, the magnetic lines of force cannot penetrate great distances from the shore. Therefore, in the opposite direction this flux intersects the earth's surface and the territory of the Kola Peninsula and Scandinavia. The main part of the magnetic flux is concentrated at distances of approximately 20-30 km from the Kola-Sredniy Isthmus. However, a noticeable part of the flux $1\text{-}2 \cdot 10^5 \gamma\text{-km}^2$ intersects the earth's surface at distances of ~100-200 km from the isthmus. By these data it is possible to estimate the magnitude of the magnetic field in the lower layers of the ionosphere at an altitude of ~100 km:

$$H_{100\ км} \sim 2 - 3\ \gamma.$$

As a result of the diffusion nature of the propagation of the magnetic field in the earth's crust, the duration of the pulse front of the magnetic field at the altitude of the ionosphere is greater than the duration of the current pulse front, and its magnitude is approximately 1 to 1.5 sec.

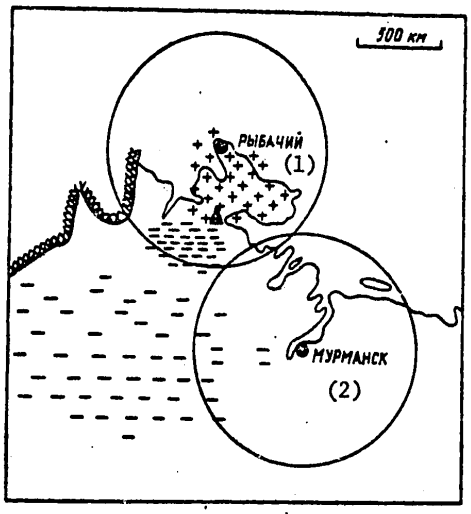

Figure 1. Mutual arrangement of the MHD-generator and the zones of effect of the ionosondes located in Murmansk and on the Rybachiy Peninsula. The x's and the dotted lines on the figure schematically indicate the regions of intersection of the lines of force with the earth's surface.

Key:
1. Rybachiy
2. Murmansk

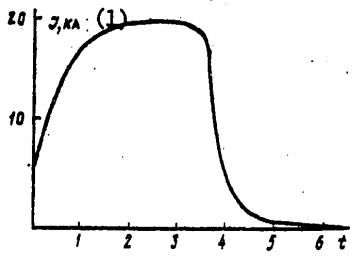

Figure 2. Shape of the current and voltage pulses during operation of the MHD-generator, start 10 October 1977

Key:
1. I, kiloamps

The variable magnetic field causes induction currents in the ionosphere which can change the initial magnetic field, especially at great distances. In order to solve the problem of the role of the distortions, it is necessary to estimate the characteristic time τ of penetration of the magnetic flux concentrated between the earth and the ionosphere through the ionosphere:

$$\tau = \frac{4\pi}{c^2} \frac{h_н (\Sigma_1^2 + \Sigma_\Lambda^2)}{(1)\Sigma_1}.$$

Key: 1. i

Here h_1 is the distance between the E-layer of the ionosphere and the conducting (shielding the magnetic field) horizons in the earth's crust, Σ_1 and Σ_Λ are the integral Pedersen and Hall conductivities of the ionosphere with respect to altitude. Taking $\Sigma_1 \sim 3$ siemens, $\Sigma_\Lambda \approx 3\text{-}5$ siemens (1 siemen $= 9 \cdot 10^{11}$ units) and $h_n = 1.5 \cdot 10^7$ cm as the standard values, we obtain $\tau \sim 1\text{-}2$ sec, which is commensurate with the front duration. Thus, it is possible to expect that at least on the pulse front the magnetic field can be significantly shielded by the ionosphere and, consequently, the role of the ionosphere in the formation of the shield at differences of $\gtrsim$ 200-300 km from the source will be completely noticeable. The above-presented estimates describe only the average situation and can, depending on the state of the ionosphere, vary within quite broad limits.

Along with shielding of the magnetic field by the ionosphere the propagation of artificial magnetic pulsations -- magnetosonic waves -- the source of which is the ground current circuit, in the magnetosphere and the ionospheric waveguide and also the generation of an Alfven wave are of interest. The theoretical investigation of these effects was performed in references [2,3]. The reflection of the Alfven wave at the magnetically conjugate point with low interference level offers the possibility of observing the Alfven echo several minutes after switching on the MHD-generator.

The estimation of the induction electric field induced in the ionosphere on the pulse fronts gives values of $E_{ind} \sim 0.5$ millivolts/meter. This field is small by comparison with the background values of the electric field $E_0 \sim 20\text{-}40$ mv/m characteristic for the polar ionosphere. The variation of the electron temperature occurring as a result of disturbance of the field E_0 by the induction field is $\Delta T \sim 1$ to 10°K and is hardly available for observation. However, as a result of the spatial nonuniformity of the induction electric field it can lead to the occurrence of longitudinal currents directed along the lines of force of the earth's magnetic field. As is demonstrated in [4], the presence of the ionospheric-magnetospheric coupling through the longitudinal currents, in turn, can intensify the initially weak ionospheric disturbance and cause a set of phenomena typical of the auroral substorm.

The arguments presented above and also the 5 October 1976 recording of a radioaurora occurring over the Rybachiy Peninsula at the time of starting the MHD-generator demonstrated the expedience of supplementing the research program with observations of possible manifestations of ionospheric and magnetospheric effects accompanying the current pulse.

The goal of the 1977 experiments included the study of the nature of propagation of artificial magnetic pulsations in the ionospheric waveguide, the recording of the Alfven echo and also the study of the nonlinear effects of the field pulse on the polar ionosphere. For this purpose a set of methods was used including the magneto-variation measurements, vertical sounding of the ionosphere, shortwave dispersion on isotropic nonuniformities, measurement of the VLF and x-radiation.

The given paper is devoted to a description of the effect of the occurrence of a sporadic E-layer during the periods of operation of the MHD-generator detected during the experiments of 4 and 10 October 1977. The observation of this effect was made using two ionosondes located in Murmansk and on Rybachiy Peninsula.

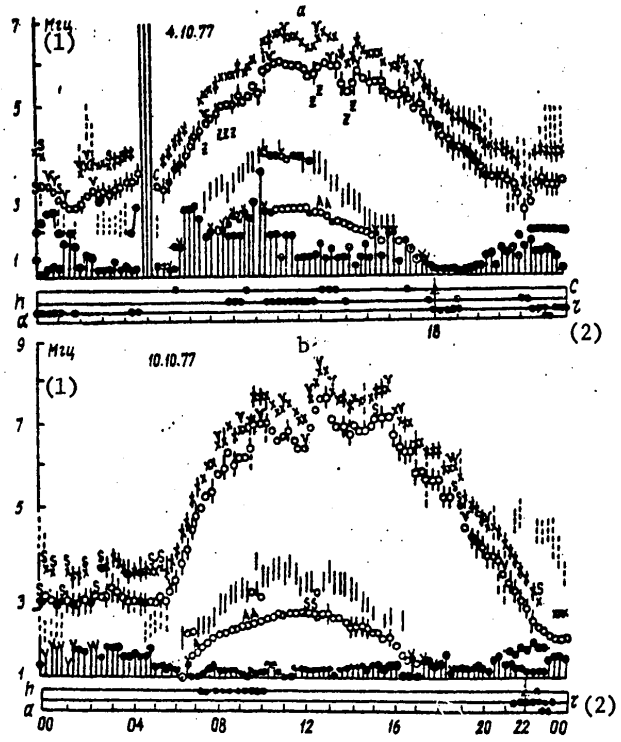

Figure 3. f-graphs of the ionospheric data.
a -- for 4 October 1977, b -- for 10 October 1977.

Key:
1. megahertz
2. hours

The ionosonde in Murmansk (AIS type) gave ionograms every 30 seconds; the ionosonde located on the Rybachiy Peninsula (MIS-5) gave ionograms every

second. This operating mode was realized 5 minutes before the time to switch on the MHD-generator and it was maintained for 3-5 minutes after switching it off. The location and the range of the ionosondes are shown in Fig 1. Fig 3 shows the f-graphs for 4 October (a) and 10 October (b) 1977 which indicates the general ionospheric situation on these days.

Let us present a brief characteristic of the state of the ionosphere and the ionospheric effects recorded by the ionosondes on switching on the MHD-generator. During the first half of the day on 4 October 1977, the disturbance ended which began earlier (Fig 3a). By approximately 11 LT the disturbance ended and a quiet state was observed, absorption near 1.5 megahertz; sporadic c and h layers were observed in the E-region. In the F-region, reflections from the Z-component were observed. At the time of switching on the MHD-generator (18.00 LT) the absorption is small ~1.3 megahertz; the frequencies of the regular E-layer at that time dropped below this frequency, and it could not be observed. The sporadic type r layer, very weak, diffuse and nonshielding, was observed. At the time of inclusion, the frequencies of the regular E-layer decreased to 1.1 to 1.2 megahertz and could not be observed on the ionosonde, for the absorption was equal to 1.2 megahertz. A weak sporadic layer with delay at the limiting reflection frequency was visible in the E region. The limiting frequency was equal to 2 megahertz, which corresponds to an ionization density of $\sim 0.5 \cdot 10^5$ el.cm^{-3}. On the ionogram (Fig 4a) obtained 30 seconds after switching on the MHD-generator ($18^h00^m30^s$ LT) by the ionosonde in Murmansk, stratification of the sporadic layer was visible which was realized before it was switched on. An additional layer was formed which gave reflections on frequencies of 0.3 to 0.5 megahertz higher than the basic sporadic layer. The altitude of the stratification formed was ~140 km; then it was increased to 145 km and again diminished before disappearance of the stratification. The additional layer existed for 2 minutes. The data from the ionosonde on the Rybachiy Peninsula permit more detailed tracing of the time characteristics of the additional stratification. The stratification appeared 8 seconds after switching on the MHD-generator; the duration of its existence was 2 minutes. The additional layer gave reflection on frequencies exceeding the frequency of the basic layer by 0.3-0.4 megahertz. The stratification and altitude changed: initially the additional layer was observed at altitudes of the basic layer (120-125 km); then it could be seen at high altitudes, 150-160 km, and at the end of its existence, the additional layer again dropped, merging with the basic sporadic layer.

Fig 5 shows the graphs of the frequencies and altitudes of reflections from the E-region obtained by the ionosondes in Murmansk and on the Rybachiy Peninsula on 4 October 1977 at the time of switching on the MHD-generator. The circles denote the basic sporadic layer existing at that time. The black dots denote the additional layer.

On 10 October 1977, the ionosphere was quiet; the critical frequencies of the F-region (see Fig 3b) increased by 1 megahertz by comparison with the normal level. By comparison with 4 October 1977, the conditions of

illumination in the ionosphere changed noticeably; the diurnal behavior was expressed more sharply, and a smaller number of stratifications in the E-region were observed (of the sporadic types c and h). At the time of starting the MHD-generator (22^h00^m LT) absorption of 1.2 megahertz, a sporadic E-layer of the r type with shielding frequency of 1.7 megahertz was observed. At the time of switching on the MHD-generator the regular E layer had a criticial frequency of less than 1 megahertz and was not visible on the ionogram. A sporadic layer of the type r with shielding frequencies of 1.7 megahertz was observed in the E region which corresponds to electron concentration of ~$0.4 \cdot 10^5$ el.cm^{-3}, the MHD-generator was switched on at $22^h00^m30^s$ LT closest with respect to the time of the ionogram ($22^h00^m30^s$ LT) just as at the time of inclusion on 4 October 1977, indicated layering in the sporadic layer (see Fig 4b). The additional layer had frequencies 0.4-0.5 megahertz higher than the basic frequency, and it was observed at altitudes greater than the basic sporadic layer. After 2 minutes the additional layer ceased to exist, merging with the basic sporadic layer.

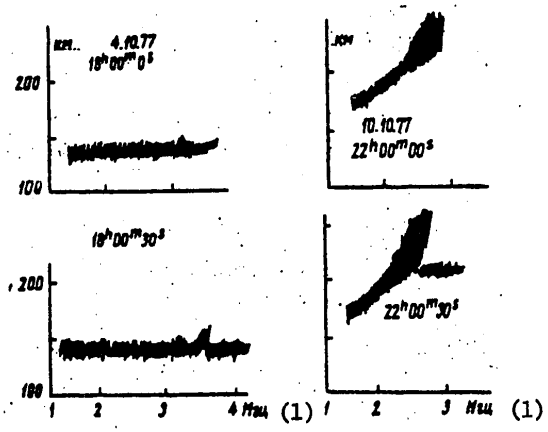

Figure 4. Stratification in the sporadic E layer manifested on the screen of the ionosonde after inclusion of the MHD-generator

Key:
1. megahertz

It must be noted that the stratification observed on the ionogram after switching on the MHD-generator is a local phenomenon; the ionosonde at Rybachiy and the ionosonde at the Murmansk see it from the side. Therefore the altitude and frequency measurements of the additional stratification are somewhat high.

Fig 6 shows the graph of the E-region for 10 October 1977 at the time of switching on the MHD-generator, the Murmansk ionosonde. Simultaneous observations of new ionosondes on 4 October 1977, in Murmansk and Rybachiy, and also observations on 10 October 1977, make it possible to draw the following conclusions:

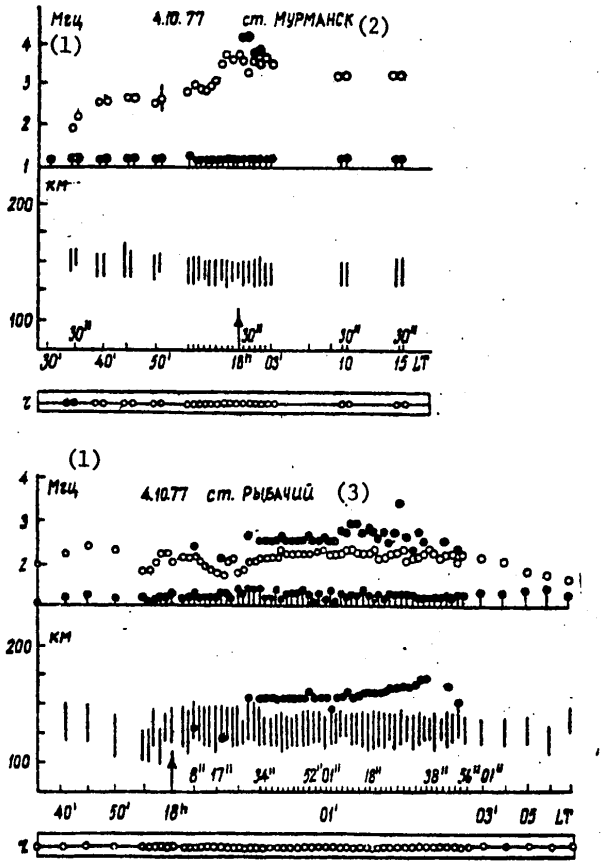

Figure 5. Graphs of the frequencies and altitudes of the reflections from the E-region on 4 October 1977.
The circles indicate the frequencies of the basic sporadic layer; the dots indicate the frequencies of the additional sporadic layer; the vertical lines indicate the altitude of the basic layer E; the points indicate the altitude of the additional layer E.

Key:
1. megahertz
2. Murmansk station
3. Rybachiy station

1. On 4 and 10 October 1977, the MHD-generator was switched on under similar ionospheric conditions in the lower ionosphere. The absorption was minimal, which made it possible to observe the reflection on frequencies 1.2-1.3 megahertz above the lower limit of the equipment and to trace from the weak stratifications. The primary ionization in the E-region determined by the sporadic layers corresponds to an electron concentration of $0.5.10^5$ el.cm^{-3}.

2. After switching on the MHD-generator, stratification appeared inside the existing sporadic layer in the form of a denser additional layer, the limiting frequencies of which exceeded by 0.3-0.5 megahertz the limiting frequencies of the basic layer.

3. On 4 October at the beginning of the observations the altitude of the additional layer observed in Murmansk was 10-15 km above the altitude of the additional layer above the Rybachiy Peninsula. This agrees with the concept of localness of the stratification formed. During its two-minute existence, the layer rose upward and then it dropped again before disappearing.

4. The stratification appears 30 seconds after switching on the MHD-generator although the data are in need of refinement. The duration of the existence of this stratification of 2 minutes is more certainly determined by the available data.

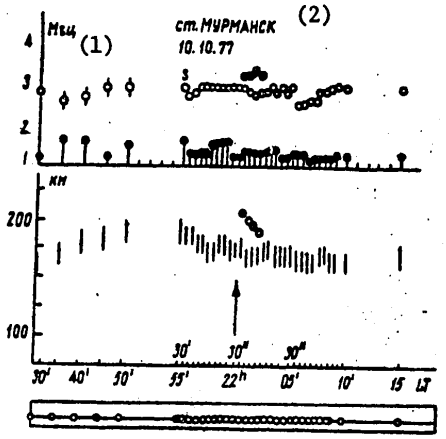

Figure 6. Graphs of the frequencies and altitudes of the reflections from the E-region on 10 October 1977. The notation is the same as in Fig 5.

Key:
1. megahertz
2. Murmansk station

During the observations on 10 October, the additional layer in Murmansk was formed at an altitude of 200 km, and then it dropped until it merged with the basic layer.

Thus, the results of the Khibiny-IM experiment indicate that the active effect of the field of the ground current pulse (created by the powerful MHD-generator) on the polar ionosphere is capable of leading to a noticeable change in its state. Inasmuch as the existing experimental data is insufficient to construct a physical picture of the observed ionospheric effects, the studies in the indicated area will be continued in the near future to accumulate further experimental data.

BIBLIOGRAPHY

1. Velikhov, Ye. P.; Volkov, Yu. M.; D'yakonov, B. P. "Use of Pulse MHD-Generators for Geophysical Studies and Earthquake Forecasting," TRUDY UI MEZHDUNARODNOY KONFERENTSII PO MGD-GENERATORAM [Works of the Sixth International Conference on MHD-Generators], preprint IAE-2532, 1975, Vol V, pp 211-218.

2. Sato, T.; Holzer, T. E. "Quiet Auroral Arcs and Electrodynamic Coupling Between the Ionosphere and the Magnetosphere," J. GEOPHYS. RES., No 78, 1973, p 7314.

3. Lyatskaya, A. M.; Lyatskiy, V. B.; Mal'tsev, Yu. P. "Possibility of Artificial Generation of Geomagnetic Pulsations," GEOMAGNETIZM I AERONOMIYA [Geomagnetism and Aeronomy], Vol 16, No 2, 1976, p 331.

4. Zhulin, I. A.; Mishin, Ye. V.; Mishin, V. M.; Chmyrev, V. M. "Possibility of Artificial Localization of a Substorm," GEOMAGNETIZM I AERONOMIYA, Vol 18, No 3, 1978, p 551.

[8144/1072-10845]

10845
CSO: 8144/1072

POLARIZATION OF ARTIFICIAL VLF EMISSIONS IN THE AURORAL ZONE

Apatity ISSLEDOVANIYA PROTSESSOV V AVRORAL'NOY IONOSFERE METODAMI AKTIVNOGO VOZDEYSTVIYA in Russian 1978 pp 14-19

[Article by I. N. Kapustin, O. M. Raspopov, A. A. Arykov, A. N. Vasil'yev, N. V. Galakhova, I. K. Korneva, V. F. Larin, V. S. Smirnov]

[Text] The measurements of the polarization of artificial VLF emissions is of interest from the point of view of the solution of the problem of the generation of them by the region of the ionosphere heated by a powerful shortwave transmitter. The results of an experiment performed at middle latitudes are described in reference [1]. The VLF signal had predominantly linear polarization tracing the direction of the currents induced by the ionospheric winds. The magnitude of the nonlinear current responsible for generation of the artificial VLF radiation is determined by two factors: the side electric field and the conductivity of the ionosphere which depends on the electron concentration. If in middle latitude both the electric field and the electron concentrations vary within comparatively small limits, then the concentration in the auroral ionosphere varies by several orders depending on the level of the geophysical disturbance, and it is possible to expect more varied effect for measurements of the fine structure of the artificial VLF-signals. Therefore in our experiment equipment was used which permits measurement of the polarization characteristics of the signal not only in the case of linear polarization as was done in [1], but also elliptic.

The reception of the artificial VLF emissions was realized on two mutually perpendicular frames oriented in the north-south and the west-east direction with an area of 62.5 m^2 and a number of turns equal to 40 each. The receiver is made in the form of two channels with respect to a superheterodyne circuit with common heterodyne. The sensitivity is no worse than 10^{-8} volts/m. The band of the terminal intermediate frequency amplifier in the given experiment was 0.03 hertz.

The polarization of the artificial VLF signals was characterized by two parameters: the ellipticity coefficient K (the ratio of the minor axis of the polarization ellipsed to the major axis) and the angle of inclination of the major axis of the ellipse α. In order to measure these parameters

the signal of each channel was summed with the other 90° out of phase. The sum of the signals of these additional channels gives the major halfaxis of the polarization ellipse, and the difference, the minor halfaxis. In order to determine the slope angle of the major axis of the polarization ellipse α, information was used about the phase shift between the frame signals measured by the phase detector. The value of K equal to zero corresponds to linear polarization of the wave. The positive values of K correspond to rotation of the vector $\vec{H}$ clockwise; the negative values, counterclockwise. The values of α were reckoned from the direction to the geographic north. For convenience of comparison with the electrojet azimuth, the values of α were increased by 180°, which, of course, has no theoretical importance.

For monitoring the position of the auroral electrojet, the data were used from tricomponent magnetovariation stations located in Apatity, Loparskaya and Lovozera (50-80 km from the center of the zone of effect of the heating transmitter). The recordings of the riometer on a frequency of 32 megahertz located in the Apatity and directed toward the North Star were also used (that is, its radiation pattern also encompassed the zone of the heating transmitter). The general diagram of the experiment is shown in Fig 1.

During the course of the processing it was discovered that the values of K and α experienced fluctuations caused obviously by variations of the electron concentration. Therefore K and α were averaged by the sliding mean method with a time of ~4 minutes. Examples of this processing are presented in Figures 2-4.

In contrast to the middle latitude the polarization of the signal differs sharply from linear. The vector $\vec{H}$ can have both righthand and lefthand rotation. The orientation of the major axis of the polarization ellipse also expresses significant variations. In Fig 2 for comparison the dotted line is used to indicate the azimuth of the electrojet during the observation period. The orientation of the polarization ellipse of the VLF signal depends not only on the azimuth of the electrojet, but it also experiences the effect of additional factors. According to the results of reference [1], in the middle latitude experiment in only 10% of the cases was polarization of the signal differing from linear observed. In our experiment, on the other hand, the linearly polarized signal was observed quite rarely. The disturbed region of the ionosphere emits both ordinary and extraordinary VLF waves. One of the normal waves (ordinary) is a nonpropagated wave. The linear nature of the polarization of the artificial VLF-signals in [1] is explained by the fact that the source of the emission is located quite closely to the boundary of the ionosphere (at a distance of less than the wave length in the medium). Under the conditions of a disturbed ionosphere this proposition possibly is not always satisfied. However, then the VLF wave at the reception station must have elliptic polarization with right-handed rotation. However, in the experiment signals were also observed with lefthanded rotation of the vector $\vec{H}$. Accordingly, let us note that the size of the region of generation is on the order of the wave length, and the interference effects will be felt in the nature of the polarization.

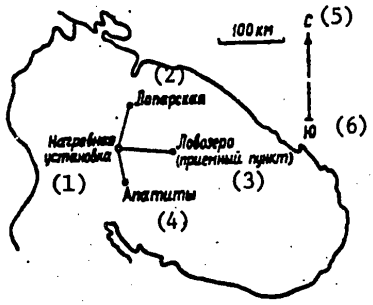

Figure 1. General diagram of the experiment

Key:
1. Heating unit
2. Loparskaya
3. Lovozera (receiving station)
4. Apatity
5. north
6. south

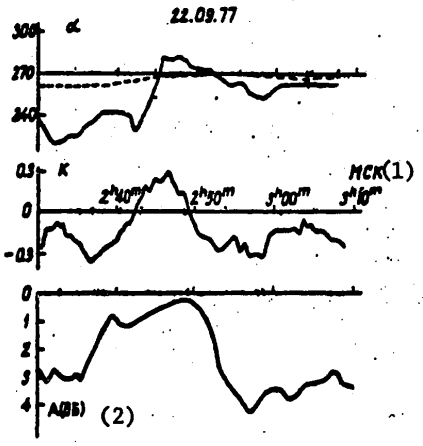

Figure 2. Variation of the parameters of the polarization ellipse of artificial VLF-emission and riometric absorption on a frequency of 32 megahertz.
The dotted line indicates the azimuth of the electrojet.
Moscow time.

Key:
1. Moscow time
2. A(decibels)

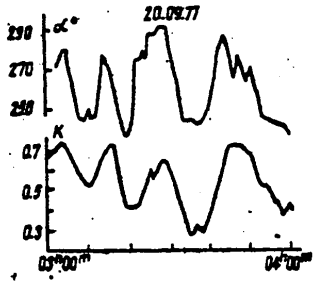

Figure 3. Positive correlation between the parameters of the polarization ellipse of artificial VLF emission. Moscow time.

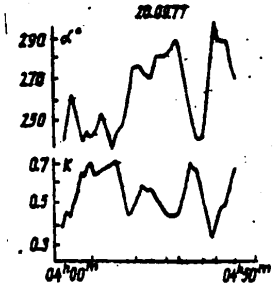

Figure 4. Negative correlation between the parameters of the polarization ellipse of artificial VLF emission. Moscow time.

During the performance of the experiment, unfortunately, there were no means of exact diagnosis of the lower ionosphere. Some information about the state of the D-region can be obtained from the recordings of the riometer located in Apatity. In Fig 2 the lower curve indicates the riometric absorption during the observations of 22 September. There is a satisfactory correlation with the variation of the polarization parameters of the VLF-signal, which provides a basis for relating its variation to the electron concentration profile in the lower ionosphere. During the observations, the results of which are demonstrated in Fig 3, 4, the riometric absorption varied slightly within the limits of 0.5 to 1.2 decibels. The absence of a correlation can be explained by the too wide radiation pattern of the riometer, on the one hand, and by the fact that it gives only integral absorption in the ionosphere, on the other hand. Let us note that the riometer in Loparskaya operating on a frequency of 32 megahertz and aimed at the North Star indicated significant variations of the absorption at this time (to 3.6 decibels).

Noticeable correlation with the electrojet parameters was not detected, which is explained by two factors. First, the variations of the magnetic

field measured at the magnetovariation stations are determined by the maximum electrojet located at altitudes of 100-120 km, that is, appreciably above the region of generation of the artificial VLF waves. Secondly, the polarization effects are finer by comparison with those which were studied up to now, and it is necessary to know the fine structure of the electrojet, that is, the current density in the zone of effect of the heating transmitter. Such information can be obtained during simultaneous operation of several magnetovariation stations.

The presence of both positive and negative correlations between the parameters of the polarization ellipse of the artificial VLF-signal K and α (Figures 3, 4) indicates that these characteristics can actually provide information about the signal generation mode of the disturbed region of the ionosphere. In reference [2] estimates were made of the effect of the electron concentration profile on the polarization of the artificial VLF-signal. The numerical calculations indicate significant variation of the orientation of the nonlinear current with variation of the electron concentration profile, but the interpretation of all of the results obtained in the experiment is possible only when solving the complete problem of radiation by the heated region of the ionosphere and stimulation by the VLF-wave of the earth-ionosphere waveguide.

BIBLIOGRAPHY

1. Getmantsev, G. G.; Budilin, A. V.; Ivanov, V. A.; Kotik, D. S. Mityakov, N. A.; Rapoport, V. O.; Sazonov, Yu. A.; Arykov, A. A. "Measuring the Polarization of Combination Frequency Signals," ISSLEDOVANIYE IONOSFERY METODAMI AKTIVNOGO VOZDEYSTVIYA [Study of the Ionosphere by Active Modification Methods], Apatity, izd. Kol'skogo filiala AN SSSR, 1977, pp 32-34.

2. Vasil'yev, A. N.; Larin, V. F.; Smirnov, V. S. "Stimulation of Nonlinear Currents in the Auroral Electrojet by Powerful Shortwave Emission," see the present collection.

[8144/1072-10845]

10845
CSO: 8144/1072

RESULTS OF OBSERVATIONS CARRIED OUT DURING VERTICAL SOUNDING OF THE REGION OF THE HIGH-LATITUDE IONOSPHERE DISTURBED BY POWERFUL RADIOEMISSION

Apatity ISSLEDOVANIYA PROTSESSOV V AVRORAL'NOY IONOSFERE METODAMI AKTIVNOGO VOZDEYSTVIYA in Russian 1978 pp 43-50

[Article by I. N. Bardeyev, I. N. Kapustin, A. D. Kravtsov, O. M. Raspopov, A. M. Royzen, A. A. Ul'yanchenko]

[Text] The vertical sounding of the region of the ionosphere emitted by high-power radio waves made it possible to establish the fact of artificial modification of the ionosphere for the first time in 1970 [1].

The experiments in Boulder marked the beginning of the rapidly developing studies of the ionosphere artificially disturbed by ground radio means. Almost simultaneously with the experiments in Boulder, analogous studies were made in Gor'kiy [2, 3, 4].

During the course of the experiments the artificial disturbance of the ionosphere was manifested in the form of various effects observed on the ionograms. In Boulder in 1970 an artificially F-spread was detected. In the same year of 1970, the idea of the development of nonuniformities extended along the field was stated [5]. In 1974 this idea received experimental confirmation [6].

Under the prolonged effect of a powerful radio wave, along with the basic echo traits on the ionograms, accompanying traces appeared which were connected with the side reflections. The side reflections arose as a result of distortion of the lines of equal concentration [1, 2, 7].

Significant absorption of the O-mode during vertical sounding of the modified ionosphere has come to be called WBA (wideband attenuation). The WBA was observed in Boulder and also in Gor'kiy. The attenuation exceeded 10 decibels and depended on the polarization of the disturbing wave [8, 9].

The cause of the appearance of WBA remains unknown. Some consider that the diagnostic waves are diffracted or scattered by quickly-developing

ionospheric nonuniformities; others give preference to the absorption effects connected with the generation of parametric instabilities.

During sounding of the ionosphere by test waves, anomalous absorption of these waves was detected at an altitude of 110 km [9]. The absorption reached 6 decibels under the effect of the X-mode of the disturbing wave on a frequency of 3.15 megahertz.

The results of the experiments performed in Gor'kiy were to a great extent analogous to those which were obtained in Boulder. However, new effects were noted which were discussed in [4]. In [4] the most important cause of anomalous attenuation of the test waves during O-mode irradiation of the ionosphere is considered to be the transformation of the incident wave of ordinary polarization to the Z-mode with subsequent absorption of it. All of the enumerated results were obtained in middle latitudes. The modification of the high-latitude ionosphere, the structure of which differs from middle-latitude and the geomagnetic field is oriented differently, was of interest.

In 1976 the Polar Geophysics Institute performed the first experiments with respect to the effect of powerful shortwave radio waves on the high-latitude ionosphere [10]. The emitting test stand was located in the vicinity of Monchegorsk (ϕ_m=63°). The equivalent power P.G≈10 megawatts. The study was made on a frequency of 3.3 megahertz. More detailed information about the installation appears in [11]. During the experiment vertical sounding was performed by an ionosonde installed 70 km from the source of powerful emission. Although the equivalent power of the disturbing device is comparatively low, and the ionosonde could record only the effects connected with dispersion of the signals and the appearance of side reflections, nevertheless it was possible to detect some changes occurring in the ionosphere.

Along with the already-known phenomena such as the F-spread and additional traces on the ionograms, modification of the E_s layer was observed which was manifested in an increase in the limiting frequencies, that is, the development of effectively scattering nonuniformities of a smaller scale.

In this paper new results are presented from the observations performed in February 1978 which are also a continuation of the above-indicated papers [12].

The vertical sounding was realized by an ionosonde installed under the zone disturbed by the powerful emission. The second ionosonde located in Loparskaya (70 km to the north) was used as the control in this series of experiments. For analysis of the geophysical situation, the data were used from the magnetovariation observatory in Loparskaya, the magnetovariation station in Lovozera operating in the KPK mode and also the riometric data (the 32 megahertz riometer).

The modifying transmitter was switched on at 01^h15^m; then until 04^h45^m, 30-minute intervals of operation were alternated with 30-minute pauses.

At 04^h45^m the transmitter was finally switched off (Moscow time). The MIS-5 ionosonde operated in the 1-minute mode; the SP-3 ionosonde in Loparskaya operated in the 15-minute mode. Measures were taken to equalize the "potentials" of the ionosondes. During the course of the experiment, significant attenuation of the signals reflected from the F-region was detected during vertical probing of the ionosphere. The attenuation came 10-15 minutes (sometimes sooner) after the beginning of irradiation of the ionosphere by the powerful radio wave. It must be noted that during the experimental period -- from 5 to 25 February 1978 -- it was possible to select only a limited number of 30-minute intervals suitable for analysis. This is connected with the fact that the disturbed periods drop out of the processing as a result of the complete absorption of the ionosonde signals in the ionosphere or shielding of the F-layer by the E_s layer. On the other hand, the high-latitude ionosphere is characterized by low critical frequencies which turned out frequently to be below the frequency of the modifying radiation. Accordingly, it was possible to take 13 observation intervals for processing. In seven of them the effect of the anomalous attenuation was certainly observed. The attenuation of the signals was manifested in partial or complete dropping of the traces on the ionograms. Initially the reflections disappeared in the high-frequency range.

The limited number of data did not allow for certain discovery of the relation of the anomalous attenuation of the signals to the geophysical situation. However, the attenuation was more noticeable in the preliminary and the recovery phases of the substorm. As an example, let us consider the characteristic case observed between 04^h and 05^h on 10 February 1978 3 hours after completion of significant disturbance.

According to the data from the magnetometer installed in Loparskaya, during this period the magnetic field was quiet. On the 32 megahertz riometer, the diagram included the disturbed zone, and variations in absorption did not occur by comparison with the quiet level.

In the figure there is a series of ionograms taken during the indicated period. The ionograms (Figures a, b, c) pertain to the ionosonde located under the disturbing zone (Fig g, h, i), to the control. In the first ionogram made at 04^h14^m, 1 minute before switching on the powerful transmitter, it is possible to observe reflection from the F-layer: both components are visible; the critical frequencies are easily defined. On a frequency of about 100 km the E-sporadic and multiple reflections from it are visible.

The second ionogram was made the next minute when the powerful transmitter was switched on. Here some decrease in the traces in the high-frequency part of the ionogram is noticeable. For the same minute there is an ionogram made in Loparskaya. The reflections from the F-region in practice do not differ on the two ionograms. The reflections from the E_s are different; the differences are not connected with instrument peculiarities. On the subsequent ionograms it is possible to see that at 04^h25^m (Fig c)

dropping of the traces of the O-component of the reflections is observed, and at 04^h30^m (Fig d) the reflections from the disturbed F-region are absent in general. The variations occurring in E_s are the more natural nature. On the ionogram made at the same time in Loparskaya there are no significant changes. At 04^h45^m the transmitter modifying the ionosphere was switched off; 4 minutes after the reflections from the F-region which were of a diffuse nature (Fig f) newly appeared.

Let us again return to the ionogram made at 04^h30^m. On this ionogram, by comparison with the others, significant intensification of the noise is observed almost with respect to the entire field of the ionogram. On the ionogram made at 04^h40^m, on frequencies of 1.4-2 megahertz quite dense reflections were obvious at all altitudes above 100 km. At 04^h44^m (Fig e), consolidation of the reflections forming into "inclined trails" at altitudes of 110-300 km was observed. At 04^h45^m at the minute when the modifying transmitter was switched on, the inclined trails began to decay, and the interference dropped sharply.

On the ionogram made at 04^h50^m, the inclined trails are hardly to be guessed. The case of such development of the events in the high-latitude ionosphere with heating of it was noted by us only on 10 February 1978. Thus, the vertical sounding of the region of the ionosphere disturbed by powerful linearly polarized shortwave radiation reveals the anomalous attenuation of the linearly polarized signals reflected from the F-region under defined geophysical conditions in the entire spectrum of the observed radio reflection frequencies.

The interpretation of this result, similarly to how this was done in [4], encounters difficulties. In [4] the absorption coefficient of the test waves increases with an increase in frequency, and on a frequency of 5.5 megahertz reaches a total of only K=2. In addition, in Monchegorsk, in contrast to the experiments in Gor'kiy and Boulder, both waves -- test and disturbing -- had linear polarization.

The explanation of the anomalous absorption given in [9] also encounters difficulties. In [9] the absorption came immediately with the beginning of the effect of the powerful radiation and it was connected with absorption in the D-region. The case observed in Monchegorsk cannot be explained by active heating and subsequent absorption in the D-region at least because the time of development of the attenuation is very large. Such time delays could be expected for absorption in the D-region caused by stimulated eruption of the energy particles.

The most probable cause of anomalous attenuation appears to be element of effective scattered inhomogeneities of a small scale (<100 meters) which are sharply elongated along the geomagnetic field [13, 14, 15] in both directions, dropping sufficiently deeply downward.

The appearance of diffuse reflections visible on the ionograms (Fig e) can be connected with the same nonuniformities, the formation of reflections

in the inclined trails and a large set of "reflecting" altitudes takes place near the gyrofrequency of the electrons. At the gyrofrequency the delay of the signals is large, and it decreases on going away from the gyrofrequency. This can be used to explain the inclination of the radio reflection trails. In the series of experiments performed in Monchegorsk, the goal was stated of developing the technique and the procedure for diagnosing a region of high-latitude ionosphere disturbed by powerful radio emission. The results obtained in this series indicate that the artificially generated nonuniformities in the high-latitude ionosphere have a number of peculiarities: quite low stimulation threshold; large delay in time of development and a number of others requiring more detailed checking. The explanation of these peculiarities will be of great interest in future research.

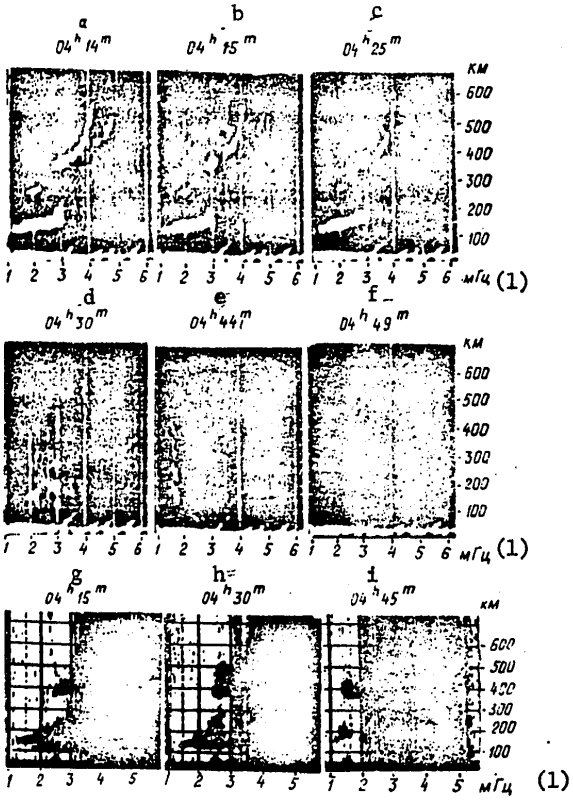

Ionosonde data obtained on 10 February 1978. The series of ionograms, a, b, c, d, e, f illustrates the development of the effect of attenuation of the echoes. The ionograms g, h, i were obtained in Loparskaya.

Key:

1. megahertz

BIBLIOGRAPHY

1. Utlaut, W. F. "Radiowave Modification of the Ionosphere (an Ionospheric Modification Using Very High Power, High Frequency Transmission), J. GEOPHYS. RES., No 75, 1970, p 6402.

2. Mityakov, N. A.; Rapoport, V. O.; Trakhtengerts, V. Yu. "Experimental Studies of Nonlinear Effects in the F-Layer of the Ionosphere," IZV. VUZOV, RADIOFIZIKA [News of the Institutions of Higher Learning, Radiophysics], Vol 19, No 1, 1976, pp 33-42.

3. Getmantsev, G. G.; Komrakov, G. P.; Korotkov, Yu. S., et al. "Some Results of Studying Nonlinear Phenomena in the F-Layer of the Ionosphere," PIS'MA V ZHETF [Letters to the Journal of Experimental and Theoretical Physics], No 18, 1973, p 621.

4. Belikovich, V. V.; Benediktov, Ye. A.; Getmantsev, G. G.; et al. "New Methods of Studying Nonlinear Phenomena in the Ionosphere," IZV. VUZOV. RADIOFIZIKA, Vol 18, No 4, 1975, pp 516-526.

5. Georges, T. M. "Amplification of Ionospheric Heating and Triggering of Spread-F by Natural Irregularities," J. GEOPHYS. RES., No 75, 1970, pp 6436-6438.

6. Allen, E. M.; Thome, G. D.; Rao, P. B.; St. Germain, R. L. "The Angular Distribution of Spread-F Returns from an Artificially Modified Ionosphere," J. GEOPHYS. RES., No 79, 1974, p 3161.

7. Utlaut, W. F.; Violette, V. J. "Further Ionosonde Observations of Ionospheric Modification by a High-Powered HF Transmitter," J. GEOPHYS. RES., No 77, 1972, pp 6804-6818.

8. Carroll, J. C.; Violette, E. J.; Utlaut, W. F. "The Platteville High Power Facility," RADIO SCI., Vol 9, No 11, 1974, pp 889-894.

9. Utlaut, W. F.; Violette, E. J. "A Summary of Vertical Incidence Radio Observations of Ionospheric Modification," RADIO SCI., Vol 9, No 11, 1974, pp 895-903.

10. ISSLEDOVANIYE IONOSFERY I MAGNITOSFERY METODAMI AKTIVNOGO VOZDEYSTVIYA [Study of the Ionosphere and Magnetosphere by Active Modification Techniques], Collection of articles, Apatity, izd. Kol'skogo filiala AN SSSR, 1977, 90 pp.

11. Kapustin, I. N.; Pertsovskiy, R. A.; Ul'yanchenko, A. A. "Device for Modification of the Polar Ionosphere by Powerful Shortwave Emission," ISSLEDOVANIYE IONOSFERY I MAGNITOSFERY METODAMI AKTIVNOGO VOZDEYSTVIYA, Apatity, izd. Kol'skogo filiala AN SSSR, 1977, pp 3-6.

12. Royzen, A. M. "Effects Observed During Vertical Sounding of the Auroral Ionosphere Disturbed by Powerful Shortwave Emission," ISSLEDOVANIYE IONOSFERY I MAGNITOSFERY METODAMI AKTIVNOGO VOZDEYSTVIYA, Apatity, izd. Kol'skogo filiala AN SSSR, 1977, pp 62-69.

13. Grach, S. M.; Karashtin, A. N.; Mityakov, N. A.; Rapoport, V. O.; Trakhtengerts, V. Yu. TEPLOVAYA PARAMETRICHESKAYA NEUSTOYCHIVOST' V NEODNORODNOY PLAZME. CHAST' I. LINEYNAYA TEORIYA [Thermal Parametric Instability in a Nonuniform Plasma. Part I. Linear Theory], Preprint NIRFI Institute, No 114, 1978, 30 pp.

14. Grach, S. M.; Karashtin, A. N.; Mityakov, N. A.; Rapoport, V. O.; Trakhtengerts, V. Yu. TEPLOVAYA PARAMETRICHESKAYA NEUSTOYCHIVOST' V NEODNORODNOY PLAZME. CHAST' II. NELINEYNAYA TEORIYA [Thermal Parametric Instability in a Nonuniform Plasma. Part II. Nonlinear Theory], Preprint NIRFI Institute, No 115, 1978, 47 pp.

15. Gurevich, A. V.; Shvartsburg, A. Ye. NELINEYNAYA TEORIYA RASPROSTRANENIYA RADIOVOLN V IONOSFERE [Nonlinear Theory of Radiowave Propagation in the Ionosphere], Moscow, Nauka, 1973, 271 pp.

[8144/1072-10845]

10845
CSO: 8144/1072

'ARAKS' EXPERIMENT. DOPPLER RADAR MEASUREMENTS OF THE EFFECTS OF INJECTION OF AN ARTIFICIAL ELECTRON BEAM INTO THE NORTHERN HEMISPHERE IONOSPHERE

Apatity ISSLEDOVANIYA PROTSESSOV V AVRORAL'NOY IONOSFERE METODAMI AKTIVNOGO VOZDEYSTVIYA in Russian 1978 pp 57-76

[Article by M. V. Uspenskiy, Ye. Ye. Timofeyev, Yu. L. Sverdlov]

[Text] During the Soviet-French "Araks" experiments on 25 January and 15 February 1975, the E-region of the northern hemisphere, where intrusion of an artificial beam was expected, was monitored by a spatially separated radiophysical radar complex of the Polar Geophysics Institute. The complex was located in the Kostromskaya and the Vologodskaya regions approximately 500 km south of the expected intrusion of the particles so that at an altitude of 110 km the conditions of the orthogonal approach of the radio beams to the magnetic line of force were satisfied.

The problem of radio observations included two sections. The first was the measurement of the parameters of the artificial electron beam after magnetospheric transportation, that is, the beam dimensions, the places of its intrusion, and the transportation time. The second section was devoted to measuring the conditions of the occurrence of the dispersion itself. It was expected that the scattering from the dissipation zone of the beam in the ionosphere permits simulation of the radio aurora under controlled conditions.

Equipment. Unmodulated monochromatic radiation transmitters were installed in the village of Nikolo-Shanga near Shar'ya in the Kostromskaya Oblast. The transmitter was operated on frequencies of 23.2 and 44.96 megahertz. The signals were received from Sloboda near Gryazovets in the Vologodskaya Oblast. The distance between Shar'ya and Gryazovets is 300 km. The possibility of penetration of the interfering direct signals of the transmitters to the inputs of the receivers has been eliminated at such a distance. In addition to the two monochromatic signals in Gryazovets, the scattered pulse signal of the radar was received from Chukhlomy in the Kostromskaya Oblast on a frequency of 43.8 megahertz. The wide-band 43.8 megahertz receiver was used simultaneously as a radiometer.

Both in the transmission and in the reception, stationary antennas were used which were oriented to the zone of expected intrusion of the particles. The aspect conditions of the observation and direction of the antennas are illustrated in Fig 1. In the first experiment the signal appeared for an aspect angle of -0.5° (the northernmost part of the trail). Then the observation conditions gradually became worse so that the latter part of the trajectory was at an aspect angle of -3°. On the second launch the trail moved from west to east; the observations were made for positive aspect angles not exceeding the limits of 0.5°. All of the calculations of the aspect angles were made for an altitude of 110 km. For an altitude of 100 km the isolines were shifted by 1.3° to the south on the average.

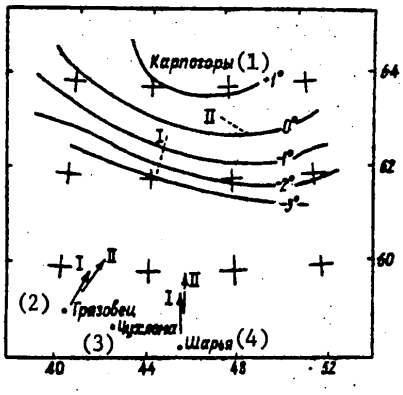

Figure 1. Map of the aspect angles of the signal observations on the first and second launches.
The arrows indicate the directions of the main maxima of the antennas.

Key:
1. Karpogory
2. Gryazovets
3. Chukhloma
4. Shar'ya

The received signals were recorded on a pen recorder and two tape recorders. The pulse signal was photographed on an amplitude indicator and range-time brightness indicator. The energy potentials of the channels $\Pi=P_t G_t G_r \cdot P_r^{-1}$ for 44.96 megahertz~224 decibels; for 23.2 megahertz and for 43.8 megahertz, ~222 decibels. Here P_t is the radiation power, $G_{t,r}$ are the amplifications of the antenna for transmission and reception; P_r is the power of the actual noise at the input of the receiver for a 1 kilohertz band -- for continuous radiation channels -- and 250 kilohertz -- for the 43.8 megahertz pulse channel.

On reproduction of the tape recording, depending on the processing conditions, the signals were filtered and copied. Filters were used with pass bands of 30 and 200 hertz for copying and also 3 and 20 hertz for sonographic processing. The radiometer used a receiver with a pass band of 250 kilohertz,

the postdetector filter of 5 hertz and the frequency compensation circuit for the constant component. The sensitivity of the radiometer was $(2-3)\cdot10^{-23}$ watt-m^{-2} $hertz^{-1}$.

General Observation Characteristic. In Table 1 the data are summed up from observations on both launches. The basic peculiarities of the signals and the provisional form are illustrated in Fig 2. On the launch to the north on 26 January 1975 the signal is detected after 127 seconds of flight time and undoubtedly is a consequency of the first electron injection pulse with a pitch angle of ~70°.

Table 1. Observation of the "Araks" Experiment on 26 January and on 15 February 1975

Operation of the observation channels	Frequency of the observation channels: 44.96 megahertz	23.2 megahertz	43.8 megahertz	43.8 megahertz radiometer
Launched to the north 26 January 1975	+	data on the spectrum missing	+1)	+2)
Launched to the east 15 February 1975	+	+4)	+	+3)

Notes. 1 -- industrial interference with feed network frequency;
2 -- possibly short weak signals occur; 3 -- emission absent;
4 -- spectrum with interference

Low frequency fading is noted in the signal with a period of the total operating cycle of the electron gun of ~13 sec. The maximum signal is observed at 125-142 seconds, after which its intensity decreases monotonically. The switching of the operating conditions of the injector from 27 to 15 kev is clearly not detected in the signal. The increase in the signal intensity at 287 seconds attracts attention. After 330-340 seconds the signal becomes weak, and in the 1 kilohertz reception band it is almost not detected. The short increase in intensity is observed in the last section of the injector at 386 seconds, but there is no complete certainty that this signal is connected with the operation of the gun. The ionospheric situation during the launch period to the north is quiet; during the entire night the natural H_E-scattering was not observed.

For the launch to the east on 15 February 1975, the scattering level was noticeably lower. The unmodulated radiation channels reveal a signal at ~148 seconds, approximately 4 seconds after the beginning of operation of the neutron beam. The signal amplitude is extremely low, the signal is detected only on the sonograms. In the pulse channel the signal appears at 260-262 seconds when the observability of the signals becomes worse in the unmodulated radiation channels. After 260 seconds, the pulse signal is observed almost to the end of operation of the injector. The signal has the form of a series of pulses beginning after injection with minimum pitch

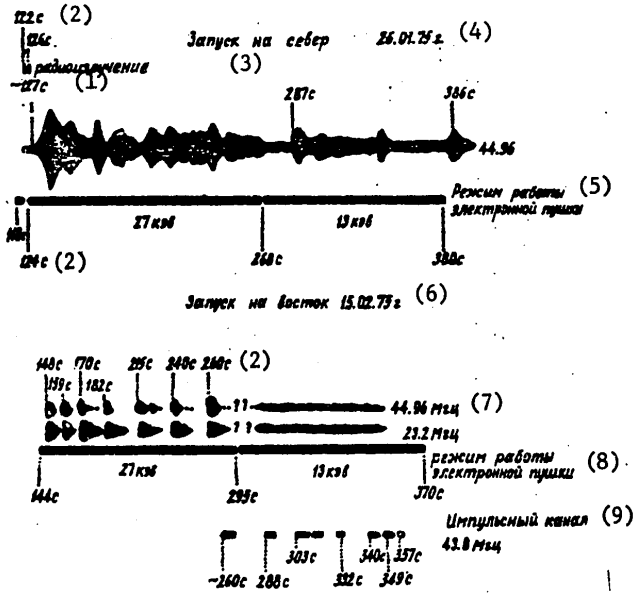

Figure 2. Basic peculiarities of signals in provisional form. The time is indicated from the time of launching the rocket.

Key:

1. Radio wave length emission
2. sec
3. Launch to the north
4. 26 January 1975
5. Operating conditions of the electron gun
6. Launch to the east 15 February 1975
7. megahertz
8. Operating conditions of the electron gun
9. Pulse channel

angles. The variation of the frequency energy by ~295 seconds is not detected in the signal. The ionospheric situation during the launch to the east is moderately disturbed. The launch was made in the phase of reproduction of the substorm of moderate intensity. The natural HF-scattering was observed an hour before and an hour after launch.

Dispersion Spectrum. When launching to the north from 127 to 265 seconds, two frequency components of the signal are clearly present in the spectrum: unshifted (or, more precisely, slightly shifted) and shifted with respect to frequency (see Fig 3). For the second component of the spectrum the frequency shift is positive, 55-70 hertz. Such a shift corresponds to the phase velocity of the nonuniformities along the direction $\bar{q}=\bar{k}_2-\bar{k}_1$; $v_\phi=f_D(\lambda/2)(\sin(\theta/2))^{-1}=194-247$ m/sec. Here $\bar{K}_{1,2}$ are the wave vectors of the incident and scattered signals, f_D is the Doppler frequency shift, θ is the scattering angle. The slightly shifted component has frequency shifts from

-5 to +15 hertz. The velocities of the nonuniformities corresponding to this are from -17 to +53 m/sec. After the transition to the 15 kev injection mode, the shifted component of the spectrum with positive Doppler shift is not observed on the sonogram. Here the unshifted component predominates, and at certain points in time, weak scattering is detected with a negative Doppler shift. The magnitude of the shift is 30-40 hertz, the velocities of the nonuniformities are 105-141 m/sec in the direction of going away from the radar. In the lower part of Fig 3, the ratio of the amplitudes of the shifted and the unshifted components of the spectrum is shown. The shifted component is detected by the solid line; the scale along the y-axis is linear.

The spectra line of the shifted component is broader than for the unshifted component. The shifted component is similar to the natural H_E-scattering, Fig 4. This scattering from the zone of the expected intrusion of the particles L=3.7, was recorded at approximately 30% of the observation time in practice during all of the disturbed periods. With respect to the nature of the diurnal variation and the relation to the magnetic disturbance and spectral characteristics, this scattering corresponds most closely to the auroral nonuniformities of a drift-gradient nature. The unshifted component has a relatively narrow spectrum. With respect to nature of the signal and its behavior in time the unshifted component is similar to the scattering (reflection) on the long-lived ionized meteor trail in the last stage of evolution of the trail, see Fig 5. The long-lived meteor which was used in the example was observed on 26 January 1975 at 0233 UT, that is, 14 minutes before launch. For comparison, a fragment of the spectrogram of the meteor signal ~30 seconds after the appearance of a reflection from the head part of this meteor was used.

The filtration and detailed measurement of the signal-noise ratio of the shifted component of the signal demonstrated that the spectral width at the maximum amplitude at 135-142 seconds$\lesssim$30 hertz. In addition to the two discussed spectral components it is possible that from the beginning of the signal to approximately 160 seconds there is a third component present in the spectrum, a broader spectral line which overlaps both signals. This explains the closure of the structure of the components during the initial operating period of the injector.

Fading and Delay of the Signals. The signal was copied several times in different modes to analyze the fading. The long-period commutation of the gun current (periods of 1.28 seconds -- modulated pulse -- frequency 25 hertz; 2.56 seconds -- unmodulated pulse) in the scattered signal was not reliably detected. The signal modulation with a frequency of 25 hertz was not detected. The total operating period of the programming unit of the gun observed in the signal of 12.8 seconds constitutes an exception.

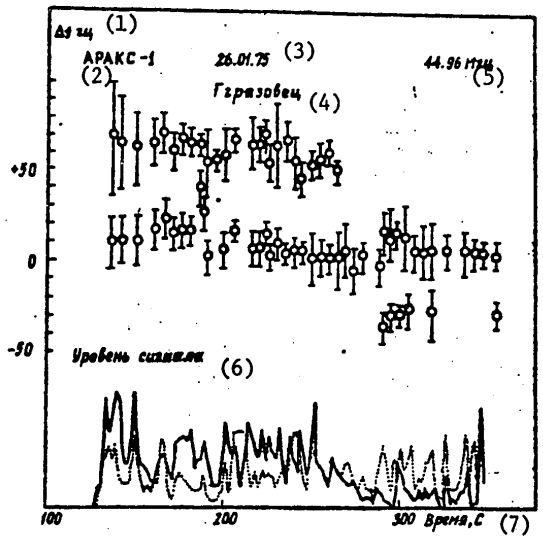

Figure 3. Behavior of two spectral components of the signal during the first launch.
In the upper part, the signal spectrum; in the lower part, the amplitude ratio of the spectral components. On the right along the vertical the corresponding magnitude of the projection of the velocity of the nonuniformities on the direction of observation.

Key:
1. Δf, hertz
2. ARAKS-1
3. 26 January 1975
4. Gryazovets
5. megahertz
6. Signal level
7. Time, sec

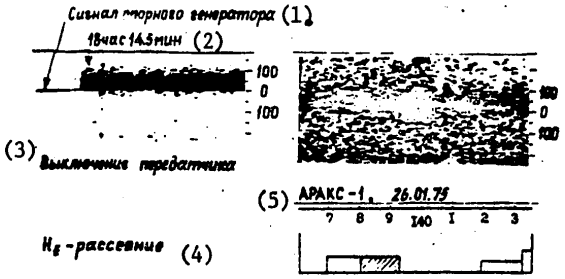

Figure 4. Sonogram of the H_E-dispersion observed on 23 January 1975 and the signal at the beginning of the first launch. Along the horizontal, the flight time in seconds, at the bottom, the operating diagram of the injector on board the rocket.

Key: 1 -- Reference generator signal; 2 -- $18^h14.5^m$; 3 -- transmitter switched off; 4 -- H_E-dispersion; 5 -- ARAKS-1, 26 January 1975

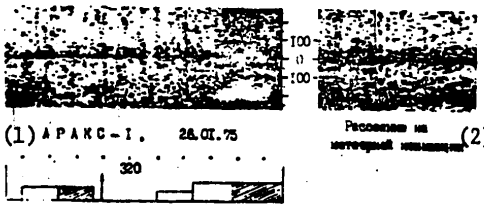

Figure 5. Sonogram of the first launch signal, slightly shifted component. The flight time in seconds is plotted along the horizontal, the operating diagram of the injector is at the bottom. The arrow indicates the time the plasmogenerator was switched off. On the right is the spectrum of the meteor ionization 30 seconds after the formation of the trail.

Key:
1. ARAKS-1, 26 January 1975
2. Dispersion on meteor ionization

In the case of component by component filtration of the signals and copying (30 hertz filter) it is possible to increase the signal/noise ratio by approximately an order. It has been discovered that the shifted component is observed to 347-350 seconds of the light although after 270 seconds its intensity is low; the unshifted component appears simultaneously with the entire signal and drops near 350 seconds. The dropping of the signal at 350 seconds obviously is connected with the increasing shielding of the beam by the atmosphere with a reduction in altitude of the rocket to 125 km. All of the remaining operating period of the electron gun is observed satisfactorily in the scattered signal. The signal drops only in the 284-287 second interval after the first very short 15 kev pulse and in the 323-327 second interval when the scattering intensity becomes low.

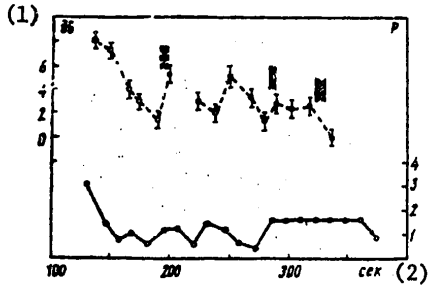

Figure 6. Correspondence between the intensity of the slightly shifted scattering component, the upper curve, relative intensity, decibels, and the total injection energy along the rocket axis; on the left along the vertical in relative units.

Key: 1 -- decibels; 2 -- seconds

The unshifted component of the signal demonstrates good correspondence between the scattering intensity and total injection energy along the axis of the rocket $P=IE\cdot\Delta t$, Fig 6. Here I is the gun current, E is the energy, Δt is the actual pulse duration. It is considered that the modulated pulse has a duty cycle of 0.5. The scattering intensity was measured at the maximum fadings of the signal with 13 sec period; therefore the course of the signal is somewhat delayed with respect to the dependence of the total energy on time. The values of the total energy calculated by the telemetric data were provisionally reduced to the beginning of the modulated pulse, that is, the very beginning of injection along the rocket axis. The total duration of the normal pulse is 3.84 sec.

The first, largest of the peaks in the signal follows the long injection pulse of 27 kev. As a result of breakdown in the gun, the pulses are foreshortened in the other cycles. The scattered signal drops proportionately tothe decrease. The signal again increases after an increase in the total energy in the sixth cycle (195-198 seconds) and in the ninth cycle (233-237 sec). With the transition to the injection mode of 15 kev and elimination of the breakdowns, the signal stabilizes, but the proportionality is violated. This can be connected with a change in altitude of dissipation of the beam in the ionosphere. The deep minimum of the signal shown in Fig 6 by the vertical dotted lines follows one of the minimum P in the fifth cycle (182-186 sec). Only the modulated pulse was injected here. In the 12th cycle (271-274 sec) after breakdowns of the gun during the first 17 kev pulse and very low P the dispersion disappears entirely for some time. This period is isolated by the solid vertical lines. After the load P in the 8th cycle (220-224 sec) when a short unmodulated pulse was injected (in contrast to the fifth cycle), no deep fading is observed.

The delays in the occurrence of the scattering in the case of joint processing of the sonogram (20 hertz filter) and component by component recording are illustrated in Fig 7. The time of appearance of the signal with respect to the beginning of injection along the axis of the rocket changed. The fiducial intervald do not take into account the systematic errors as a result of the width of the spectrum and different observability of the shifted and unshifted components. It is obvious that the unshifted component most frequently leads the shifted one by 0.5 to 1.0 sec. The delay is basically 2.5 to 4.5 sec.

The growth time constant of the scattered field measured indirectly by the signal oscillograms for the middle part of the trajectory when the injection with a pitch angle of 70° could not erode the minima at 12.8 seconds modulation is $\tau_c \sim 2.5$ sec for the shifted component and $\tau_H \sim 1.5$ sec for the unshifted component. Inasmuch as the radio systems do not have significant sensitivity reserves, we consider that the total delay of the received signal with respect to the beginning of the modulated pulse $T=T_1+T_2$, where T_1 is the transportation time of the beam along the magnetic line of force from the southern hemisphere to the northern hemisphere (0.6 sec for 27 kev and 0.8 sec for 15 kev [1]), $T_2=k\cdot\tau_{c,H}$. For K=1 the relative level

where the sgianl is detected is -4 decibels to the established value. For this K the total delay for an energy of E=27 kev will be 3.1 and 2.1 sec, and for E=15 kev, 3.3 and 2.3 sec for the shifted and unshifted components f the signal, respectively. For very weak signals delay can still increase more approximately for the duration of the modulated pulse (1.28 sec). This is connected with the fact that the current of the unmodulated pulse was twice as great as for the modulated pulse. Though the unmodulated pulse is detected at the limit, the modulated pulse can turn out to be below the detection threshold.

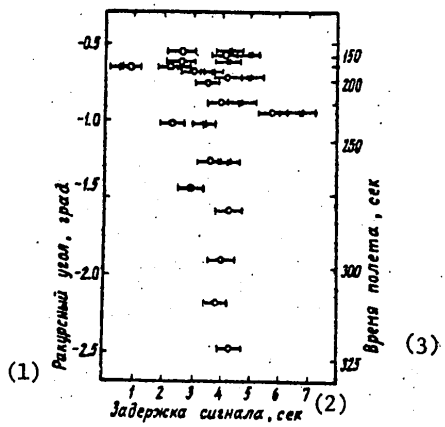

Figure 7. Delays in the occurrence of dispersion.
o - for unshifted; x - for shifted component measured by the first launch sonogram.

Key:
1. Aspect angle, degrees
2. Signal delay, sec
3. Flight time, sec

In the 43.8 megahertz pulse channel, the launch to the east, the signal level was very weak. In contrast to the launch to the north the electrons were injected at an angle of 30° to the rocket axis. The rocket axis had a significant angle to the magnetic line of force. In the process of rotation of the rocket around the longitudinal axis the pitch angle varied continuously, and at certain times it passed through zero values. The scattering delay with respect to the injection pulses at an angle 30° to the rocket axis differs insignificantly from that which was observed in the first launch, Fig 8.

Aspect Sensitivity. As a result of the small sizes of the dispersion region we shall consider that the intensity of the signal is proportional to the fourth power of the distance, R^{-4}. Let us ignore the changes in the generation conditions of the nonuniformities along the trajectory of the particle trace. Then by the known values of the aspect angle, the scattering

indexes can be constructed for both components of the spectrum, Fig 9. The data for the shifted components are normalized to the signal maximum at the beginning of the flight. The scattering intensity as a function of the aspect angle is ~12 db/deg. The data for the unshifted component are constructed in the actual amplitude ratio between the two components. For normalization of the function it is necessary to raise the points along the y-axis by 4 decibels. The unshifted component almost does not decrease in intensity with an increase in the aspect angle. Considering the laws presented in Fig 6 which were discussed above, we shall consider that within the limits of 3° this component has no aspect dependence. For analogous reasons the slope of the curve for the shifted component becomes somewhat lower. Let us note that the measured steepness of the index for the nonuniformity responsible for the shifted component of the spectrum coincides satisfactorily with the data of [2] 10 decibels/deg for the nonuniformities of natural origin.

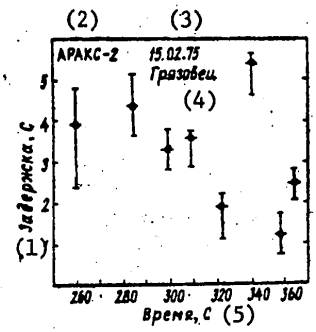

Figure 8. Along the vertical, the dispersion delays with respect to the injection pulses at an angle of 30° to the rocket axis, 25 February 1975

Key:
1. Delay, °C; 2. ARAKS-2; 3. 15 February 1975; 4. Gryazovets; 5. time, sec

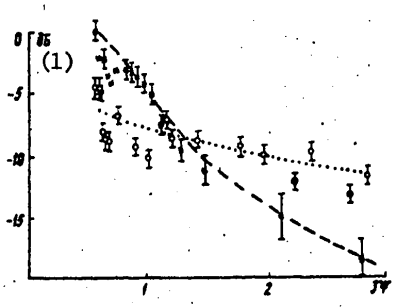

Figure 9. Scattering signal amplitude as a function of the magnitude of the aspect angle.
* -- shifted component; o — unshifted component. Along the vertical is the relative signal intensity with respect to its maximum value, decibels.

Key: 1. decibels

Concentration in the Beam Intrusion Zone. Let us assume that all of the electrons reach the ionosphere of the northern hemisphere. As the lower bound of the transverse dimension of the zone occupied by the secondary electrons in the region of the maximum altitude dissipation of the beam, let us take the value of $2r_b \sim 200$ m [3]. The upper limit is taken as 1.2 km. The speed of the trails through the ionosphere $U \sim 300$ msec^{-1} at the beginning and ~600 msec^{-1} at the end of the launch to the north. Then the time during which the electrons will hit the circle of radius r_b, $\Delta t = 2r_b/U$. The rate of ion formation in the ionosphere trail of the beam will be

$$q = \frac{N_K}{\pi r_b^2 \Delta h}, \qquad (1)$$

where N=I/e is the electron flux, K=E (ev)/30 is the number of ion pairs for one electron, Δh is the effective thickness of the energy dissipation layer of the beam amounting to, according to the data of [4], ~10 km, E is the particle energy, I is the injector current. From (1) it follows that the rate of ion formation depends on the gun current, the particle energy and the beam size. Then for a radius of 100 and 600 meters the ion formation rates will be

$q_1 = 8.95 \cdot 10^6 - 2.49 \cdot 10^5$ см$^{-3}$сек$^{-1}$, E=27 кев, I=0.5 амп;
$q_2 = 4.47 \cdot 10^6 - 1.24 \cdot 10^5$ см$^{-3}$сек$^{-1}$, E=27 кев I=0.25амп;
$q_3 = 4.97 \cdot 10^6 - 1.38 \cdot 10^5$ см$^{-3}$сек$^{-1}$, E=15 кев, I=0.5 амп;
$q_4 = 2.48 \cdot 10^6 - 6.91 \cdot 10^4$ см$^{-3}$сек$^{-1}$, E=15 кев, I=0.25амп.

For the electron reproduction and loss budget the equilibrium concentration

$$n = r_b^{-1} \sqrt{\frac{NK}{\pi \Delta h \alpha}}, \qquad (2)$$

where α is the recombination coefficient. The ionization growth is

$$n(t) = \sqrt{\frac{q}{\alpha}} \frac{e^{2\sqrt{q\alpha}\Delta t} - 1}{e^{2\sqrt{q\alpha}\Delta t} + 1}, \qquad (3)$$

from which for the minimum and maximum beam radii, the maximum concentration itself in the trail will be:

$n_1 = 3.75 \cdot 10^6 - 6.26 \cdot 10^5$ см$^{-3}$, E=27 кев, I=0.5А, U=300 м·сек$^{-1}$
$n_2 = 2.27 \cdot 10^6 - 3.78 \cdot 10^5$ см$^{-3}$, E=27 кев, I=0.25А, U=300 м·сек$^{-1}$
$n_3 = 1.52 \cdot 10^6 - 2.53 \cdot 10^5$ см$^{-3}$, E=15 кев, I=0.5А, U=600 м·сек$^{-1}$
$n_4 = 7.91 \cdot 10^5 - 1.32 \cdot 10^5$ см$^{-3}$, E=15 кев, I=0.25А, U=600 м·сек$^{-1}$

Here the electron losses were taken into account by the coefficient of effective recombination which we shall assume to be $\alpha_{eff} \sim 5 \cdot 10^{-7}$ $cm^3 sec^{-1}$ [5]. The proportionality of n_3 and n_4 to the gun current almost indicates that the recombination here insignificantly influences the maximum concentration in the trail.

The shape of the trail in the plane orthogonal to the magnetic line of force will depend strongly on the radius of the trail. For minimum radii the longitudinal and transverse dimensions are distinguished significantly. For example, for r_b=100 m in the initial part of the trajectory the trail dimensions are 200x1350 meters; in the final part of the trajectory 200x2500 m, and for r_b=600 meters these values are 1200x2350 and 1200x3500 meters respectively for the total pulse duration of 3.84 sec.

The decrease in concentration on completion of ion formation

$$n(t) = \frac{1}{1/n_0 + \alpha t}, \qquad (4)$$

where n_0 is an initial concentration. 1, 5, 10 and 20 seconds after departure from the range of effect of the beam the maximum and minimum initial ionizations n_{1-4} decrease to the following values:

t=1 sec, $n(1) = 1.3 \cdot 10^6 - 1.24 \cdot 10^5$ cm^{-3},
t=5 sec, $n(5) = 3.6 \cdot 10^5 - 0.99 \cdot 10^5$ cm^{-3},
t=10 sec $n(10) = 1.9 \cdot 10^5 - 0.79 \cdot 10^5$ cm^{-3}
t=20 sec $n(20) = 0.97 \cdot 10^5 - 0.57 \cdot 10^5$ cm^{-3}.

The residual beam ionization is approximately an order greater than the background even after 10-20 seconds. Thus, the estimate of the decrease in ionization from expression (4) is sufficiently correct.

Unbiased Dispersion Component. The characteristic features of this component of the signal spectrum are to a great extent similar to that known from the radio observations of the long-lived meteoritic ionization. This includes the absence of the aspect dependence of the dispersion, Fig 9. In addition, in our observations the close nature of the fading and the type of signal spectrum was noted. There are also significant differences. The beam forms a comparatively thick trace, the density of which is always below critical. This distinguishes the initial stages of occurrence of the signals cardinally. The gradient with the characteristic dimension r_b is not capable of giving noticeable reflection; as an illustration of the impossibility of noticeable partial reflection on the gradients, let us consider the unrealistic situation of nonuniform structure of the zone of intrusion with characteristic size of the nonuniformities equal to the gyroradius of the electrons ~10 m, E=27 kev. Such nonuniformities must disappear on decay and expansion of the beam in the dissipation zone. If the concentration gradient

$$\frac{\alpha n}{dx} = \frac{n}{a\sqrt{\pi}} \cdot e^{-x^2/a^2}, \qquad (5)$$

then a decrease in the reflection coefficient by comparison with the sharp boundary can be considered by the relation $c=e^{-8\pi^2a^2/\lambda^2}$. Substituting λ=6.7 m, we find $c\sim10^{-76}$. This is an extremely weak gradient reflection.

Inasmuch as the initial concentration is much below the critical, and the gradient reflections are too weak, the only explanation of the observed dispersion can be the fine-scale turbulization of the trail. The low phase velocities and narrow spectrum complicate the application of the mechanisms of plasma turbulization. For analysis of the situation let us use the calculations of the preceding section. The signal becomes maximum approximately 4-6 seconds after the beginning of injection; at that time the initial concentration decreases to the level (1-4) 10^5 cm^{-3}. The volume of the region occupied by the beam changes during the flight process, first, as a result of variation in the velocity of the trail, and, secondly, as a result of breakdowns of the gun and, as a consequence, shortening of the current pulses. Let us assume that the volume occupied by ionization does not depend on the energy, but is determined only by the duration of the current pulse and the velocity of the trail. It is obvious that after normalization by volume (Fig 10) the experimental points of the dispersion cross sections for the beam energies of 15 and 27 kev were divided into two groups with a difference in the cross sections by approximately an order. With a 15 kev beam the dispersion is weak. This agrees with the decrease in the effectiveness of the turbulization of the trail with an increase in altitude.

Shifted Component of the Dispersion. With respect to nature of the spectrum, this component is similar to the ordinary radioaurora (RA) or H_E-dispersion. Let us consider the possibility of the generation of RA as a result of the traditional mechanisms of plasma instability in the E-region [6]. Let us estimate the characteristic values of the fields and currents in the intrusion zone on the basis of the following model problem. The longitudinal current of the intruding electrons leaks orthogonally to the planar ionosphere with interval conductivities Σ_H and Σ_p. Outside the intrusion zone, according to [7], we set $\Sigma_p/\Sigma_H\sim1$ and Σ_p=0.2 mohs. The maximum energy release of the electron flux with E=27-15 kev is near the altitude maximum of the Hall conductivity. Inside the intrusion zone Σ_H/Σ_p=4, which corresponds approximately to the brightness radiant arcs in the natural aurora polaris [7]. Let us consider the presence in the ionosphere of a background westerly electron field E_0=2 mv/m [8]. Let us neglect the beam losses during transportation and the variations of its transverse cross section as a result of dispersion of the velocities in the presence of magnetospheric drift.

Let us consider that the E-region of the northern hemisphere within the boundaries of the intrusion zone of the current density is constant, and it drops sharply to zero on its boundary. With a current diameter of ~200 m and a speed of movement of the beam through the ionosphere of ~300 $msec^{-1}$

in 0.5 seconds the problem can be considered stationary. Let us divide the problem into two parts. 1. Closure of the beam current on a counter longitudinal current and leakage currents through the ionosphere, Fig 11a. 2. Flow around the region of increased conductivity by background ionospheric currents, Fig 11b. The latter part is a special case of the solution of [9] for $\Sigma_W=0$ or the solution of [10] for equality of the ellipse halfaxes.

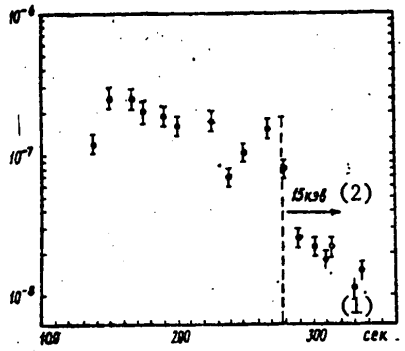

Figure 10. Relative magnitude of the volumetric scattering cross section for the unshifted component. The dotted line indicates the time of change in injection energy.

Key:
1. sec
2. 15 kev

The choice of the circuit in problem 1 is determined by the requirement of minimum resistance. As the estimates show, the closure only as a result of the counter flow along the intrusion tube requires a velocity of the counter transfer of the background plasma at the apex of the line of force which exceeds the speed of sound by an order. The anomalous resistance occurring in this situation would significantly increase the resistance of the leakage circuit [11].

In the adopted model the closure in the ionosphere is realized by radial Pedersen currents. Near the outer boundary of the beam their linear density $i_0=1/2\pi r_b \sim a \cdot km^{-1}$. The required maximum radial field for I=0.5 amps and $r_b=100$ m can be found in terms of the integral Pedersen conductivity $E=i_0/\Sigma_p \sim 4$ mv m^{-1}. Considering the counter longitudinal currents, this field will decrease outside the beam proportionally to r^{-2}. The linear density of the Hall currents in the outer zone will be approximately the same here, for outside the trail $\Sigma_p \sim \Sigma_H$. From the continuity of the normal component of the current at the boundary we find the electric field near the inside edge of the intrusion zone. $E_i=(\Sigma_{po}/\Sigma_{pi})E_0 \sim (10^{-1})E_0$, where the index i refers to the internal parts of the zone, and 0 refers to the outer parts of the zone. The cross section of the counter background current is appreciably greater than the beam cross section; therefore inside the

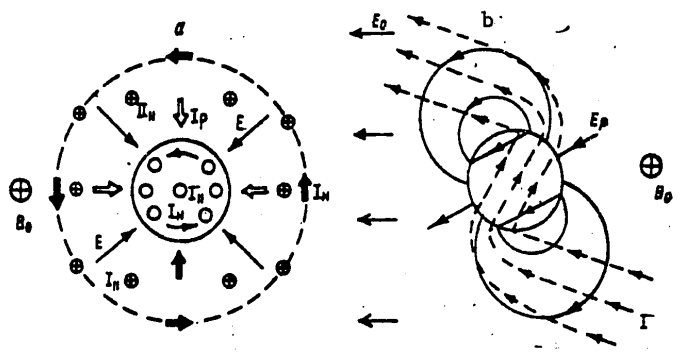

Figure 11. Spatial structure of electric fields and currents in the vicinity of the beam intrusion:
a -- closure circuit of the beam current. Inside circle, beam cross section, r_B=100 meters; b -- flow around the intrusion zone by the background ionospheric currents. Eo -- background field of westerly direction. Ep -- polarization field. The dotted line indicates the current line.

electric field decreases primarily toward the center. Let us assume that the thickness of the current leakage layer through the ionosphere is equal to the thickness of the layer of maximum energy release of the beam of ~10 km. Then the surface density of the currents ~0.8 10^{-11} amps/cm^2. Hence, the relative speed of the charged carriers near the outer boundary of the intrusion zone: $\vec{V}=\vec{V}_i-\vec{V}_e=j/en_0$. For the night subauroral E-region under the conditions of absence of magnetic activity of the first launch let us take n_0~2·10 cm^{-3}. Then we obtain $\vec{V}$~250 m/sec, which is close to the threshold velocity of the excitation of the Fali-Buneman instabilities. Thus, outside the trail near its boundary for r_b≈100 m and I=0.5 amps, nonuniformities of type 1 can be formed [9]. However, this conclusion is very critical to the variation of the model parameters; thus, already for n_0≈5·10^3 cm^{-3} and r_b≈200-300 meters, $U_{ie}<<V_S$. The solution of problem 2 will be the solution of the Laplace equation in the coordinates r, ϕ satisfying the boundary conditions of the continuity of the potential and normal component of the current for $r=r_b$. At infinity the total field must equal the background. For potential polarization we obtain the solution which decreases in the form of the field of the two-dimensional dipole on removal from the region of increased conductivity, Fig 11b. It is easy to obtain an expression for the tangent of the slope angle of the dipole axis with respect to E_0

$$\operatorname{tg}\varphi=\frac{2\Sigma_{Po}(\Sigma_{Hi}-\Sigma_{Ho})}{(\Sigma_{Hi}-\Sigma_{Ho})^2+(\Sigma_{Pi}^2-\Sigma_{Po}^2)}, \qquad (6)$$

where the index "i" refers to the inside part of the trail, and "o", to the outer part of the trail. Since in the given case the conductivities inside

the trail are an order greater than the conductivities outside it, it is convenient to use the approximate expression:

$$\operatorname{tg}\varphi = \frac{\Lambda}{5+19\Lambda} \text{, where } \Lambda = \Sigma_{Hi}/\Sigma_{Pi}.$$

Here $\phi \approx 183°$, and the total field near the outer boundary exceeds by almost 2 times the background field -- E_0 -- that is, it will be ~4 mv/meter.

The superposition of problems 1 and 2 leads to an increase in the electric field in the western sector of the trail to 8 mv/m and attenuation to zero in the eastern sector. The constriction of the sector of generation of the nonuniformities leads to a decrease in width of the signal spectral line to a value proportional to $V_B/2$. The doubling of the field to 8 mv/meter somewhat expands the limits of the model parameters causing type 1 nonuniformities. However, only in a quite narrow range of the parameters $r_b \sim (1-2)\cdot 10^2$ m, $n_0 \sim (1-2)\cdot 10^3$ cm^{-3} is it possible to explain the behavior of the shifted component by the Fali-Buneman mechanism.

The second basic mechanism responsible for the generation of current nonuniformities in the E-region is the drift-gradient instability. Inasmuch as from all sides of the beam the gradient is directed toward the center, the conditions of excitation of the nonuniformities of drift-gradient origin theoretically are satisfied. Here, the maximum increment will coincide with the maximum of the electric field, that is, the best conditions for excitation are found approximately in the western part of the beam. This picture is explained in Fig 12. In addition, here it is considered that on the lower altitude section of the beam an additional contribution to the gradient (in the direction across the magnetic line of force) is made by the vertical gradient component directed toward the pole. Then the resultant gradient will be increased somewhat from the southerly direction and will be decreased from the northerly direction, that is, the best conditions for excitation are shifted to the southwestern sector, and the magnitude of the sector decreases. This coincides qualitatively with the fact that immediately after the occurrence of scattering, the signal spectrum was wider, and after some time it became more narrow; here its Doppler shift decreased slightly.

The horizontal gradient of the concentration near the trail is quite large. The characteristic length where the concentration changes by its amount

$$H = \left(\frac{1}{n_0}\frac{dn}{dr}\right)^{-1} \qquad (7)$$

is close to the radius of the trail r_b. For such high gradients generation of the nonuniformities directly of the scale $L=(\lambda/2)(\sin(\theta/2))^{-1} \sim 3.6$ meters is possible, where λ is the wave length on which the sounding is done, θ is the dispersion angle of the signal in the case of bistatic observations.

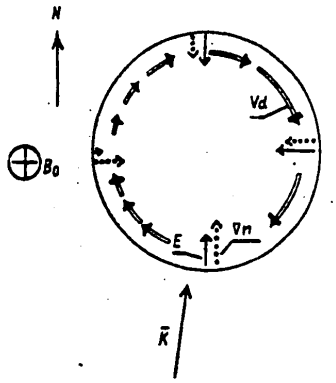

Figure 12. Schematic of the electric fields, the gradient and the drift velocities near the outer edge of the beam. The vector K indicates the direction of observation.

A moderate drift velocity is required here

$$V_{\perp} > \frac{K^2 V_s^2 \nu_e H}{\nu_i \Omega_e} \left(1 + \frac{\nu_e \nu_i}{\Omega_e \Omega_i}\right). \qquad (8)$$

Let us take $\nu_e = 1.6 \cdot 10^4\ sec^{-1}$, $\nu_i = 10^3 \cdot sec^{-1}$, $\Omega_e = 10^7 \cdot sec^{-1}$, $\Omega_i = 1.8 \cdot 10^2 sec^{-1}$, where ν_e and ν_i are the electron and ion collision frequencies, Ω_e and Ω_i are the electron and ion gyrofrequency. For H=100 to 600 meters from (8) we obtain the drift velocities $V_d \sim (60\text{-}350)\ msec^{-1}$. With a decrease in gradient with decay of the trail, generations of small-scale nonuniformities can be promoted by nonlinear mechanisms [6]. Thus, the drift-gradient mechanism of generating nonuniformities makes it possible to explain the basic characteristics of the shifted component of the scattering spectrum.

The observation of the negative Doppler shifts with transition to 15 kev injection agrees qualitatively with turning of the current jets as a result of a change in altitude of intrusion. A quantitative comparison is difficult as a result of measurements of only one projection of the drift velocity vector.

In conclusion, the authors express their appreciation to R. Z. Sagdeyev for his constant interest in the work and his valuable comments, Ye. V. Mishin and Yu. P. Mal'tsev for useful discussion of the materials. The authors express special appreciation to Yu. G. Miroshnikov, P. I. Yakovlev, Yu. P. Lukosyak, T. V. Miroshnikova and G. S. Stepanov for performing the experimental part of the work and processing the materials.

BIBLIOGRAPHY

1. Gendrin, R. "The French-Soviet 'ARAKS' Experiment," SPACE SCIENCE REVIEWS, No 15, 1974, pp 905-931.

2. Chestnut, W. G.; Hoges, J. C.; Leadabrand, R. L. RADAR PROPAGATION IN ARCTIC, AGARD, 1972.

3. Davis, T. N.; Holliman, T. J.; Mead, G. D.; Mead, G. M.; Tricheland, M.C.; Hess, W. N. "Artificial Aurora Experiment: Ground-Based Optical Observations," JGR, No 76, 1971, pp 6082-6092.

4. Izhovkina, N. I. "Secondary Electrons for Propagation of Artificially Injected Electron Beams in the Upper Atmosphere," ISSLEDOVANIYA PO PROBLEMAM SOLNECHNOZEMNOY FIZIKI [Studies of the Problems of Sun-Earth Physics], Moscow, Nauka, 1975, pp 184-191.

5. Watt, T. N.; Newkirk, L. L.; Shellej, E. G. "Joint Radar-Satellite Determination of the Effective Recombination Coefficient in the Auroral E-Region," JGR, No 78, 1973, pp 7471-7479.

6. De la Beaujardiere, O.; Vondrak, R.; Baron, M. "Radar Observations of Electric Fields and Currents Associated with Auroral Arcs," JGR, No 82, 1977, pp 5051-5062.

7. Balsley, B. B.; Farley, D. T. "Radar Observations of Two-Dimensional Turbulence in the Equatorial Electrojet," JGR, No 79, 1974, p 4725.

8. Pudovkin, M. I. "Models of the D-P-I Systems and Electric Fields in the Ionosphere," SUBBURI I VOZMUSHCHENIYA V MAGNITOSFERE [Substorms and Disturbances in the Magnetosphere], Leningrad, Nauka, 1975, pp 3-38.

9. Maltsev, Yu. P.; Leontyev, S. V.; Lyatsky, W. B. "Pi-2 Pulsations as a Result of Evolution of an Alfven Impulse Originating in the Ionosphere During a Brightening of Aurora," PLANET. SPACE SCI., No 22, 1974, p 1519.

10. Asaulenko, L. G.; Pudovkin, M. I. "Current System of Elementary Geomagnetic Disturbance in the Vicinity of Aurora Polaris," GEOMAGNETIZM I AERONOMIYA [Geomagnetism and Aeronomy], Vol 5, No 2, 1965, pp 322-328.

11. Kaplan, S. A.; Tsytovich, V. N. PLAZMENNAYA ASTROFIZIKA [Plasma Astrophysics], Moscow, Nauka, 1972, 440 pp.

[8144/1072-10845]

10845
CSO: 8144/1072

RADAR OBSERVATIONS OF DENSE IONIZATION CREATED BY AN ARTIFICIAL ELECTRON BEAM

Apatity ISSLEDOVANIYA PROTSESSOV V AVRORAL'NOY IONOSFERE METODAMI AKTIVNOGO VOZDEYSTVIYA in Russian 1978 pp 77-88

[Article by I. A. Zhulin, A. V. Kustov, M. V. Uspenskiy, T. V. Miroshnikova]

[Text] Within the framework of the active "Zarnitsa" experiments performed under the direction of Academician R. Z. Sagdeyev, radar observations were made of the ionospheric effects of the decay of the artificial beam. In the "Zarnitsa-2" experiment performed on 11 August 1975 at 23^h40^m Moscow Standard Time, in the part of the trajectory discussed below, the electron beam has the following parameters:

Electric energy	~7 kev;
Beam current	~0.45 amps;
Pitch angles of injection	30-40°;
Injection altitude	95-78 km.

The rocket was launched from the vicinity of Volgograd.

In this paper the results are presented from observations of the special types of reflections of a signal by dense artificial ionization which occurred only after submersion of the rocket below 100 km. A discussion is presented of the diagnostic possibilities of such radar observations. Some results and conditions of performing the "Zarnitsa" experiments are discussed in references [1, 2].

Observations. A two-frequency radar was used with unmodulated monochromatic radiation on frequencies of 23.2 and 44.96 megahertz. Transmitters were located in Troitskoye, the Kalmytskaya ASSR, and the receivers were located in Belyy Il'men', Astrakhanskaya Oblast. The spatial separation of about 310 km excluded the direct penetration of the disturbing signals of the transmitters to the receiving inputs. The radar was located approximately 300 km south of the zone of the expected intrusion of the particles in such a way that at altitudes of 100-110 km the conditions of orthogonality of

the vector were satisfied $\bar{K}=\bar{K}_2-\bar{K}_1$ to the magnetic line of force. Here $\bar{\bar{K}}_{1,2}$ are the wave vectors of the incident and reflected signals. The observations are performed for stationary antennas with a width of the radiation pattern in the azimuthal cross section of about 50° for low frequencies and 30° for high frequencies. This provided for untuned observation of the entire territory of the ionospheric trail of the electron beam. Both of the received signals were recorded by a pen recorder and a tape recorder. The magnetic recording made it possible to perform a further detailed study of the amplitude and spectral characteristics of the signals. The parameters of the radio devices are as follows: radiation power ~750 watts, reception band for the recording of the pen recorder of 1 kilohertz for both channels, amplification of the antennas ~13 and 18 db considering the effect of the earth for low and high frequencies, respectively. In Fig 1 the observed situation is shown provisionally for the time of a prolonged injection pulse (0.6 sec). The wave vector $\bar{K}$ is approximately perpendicular to $\bar{B}$; the observation azimuth, that is, the angle between the velocity vector of the ionospheric trail of the electron beam $\bar{V}_B$ and $\bar{K}$ is ~143°. Thus, the radar observes at an angle of ~53° with respect to the perpendicular to the wide wall of the loop of the secondary ionization flare.

After 300 seconds of flight the rocket dropped below 100 km, the electron gun continued to operate stably to an altitude of 78 km. During this period the signals were observed, the nature of which differed significantly from that which occurred in the remaining part of the trajectory. This paper is devoted to a study of the peculiarities of this type of signal. Primary attention is given to the effects observed after switching off the electron gun.

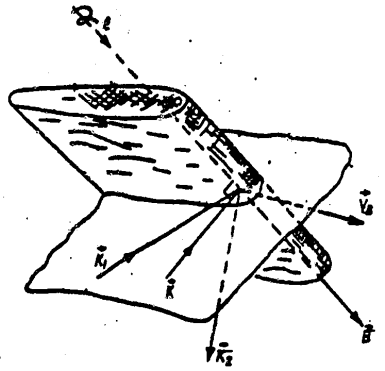

Figure 1. Conditions of observations of radio reflections during a long injection pulse.
$\bar{K}_1$, $\bar{K}_2$ -- vectors of the incident and reflected waves, $\bar{V}_B$ -- beam velocity vector.

Scattering or Reflection? An example of a signal recording is presented in Fig 2. The two types of signals are easily distinguished: the first for operation of the injector, and the second, after it is switched off. In the first mode (with the electron gun operating) the signal has a significant Doppler shift. The magnitude of the shift varies with rotation of the rocket and, as a consequence, variation of the pitch angle of the injection. The width of the signal spectrum is several hertz. The velocity component of motion of the nonuniformities along $\bar{K}$ can be determined from the expression $V_{\bar{K}}=\lambda \cdot F_D/2\sin(\theta/2)$, where F_D is the Doppler shift of the signal, $\theta=116°$ is the dispersion angle (the angle between the vectors $\bar{K}_1$ and $\bar{K}_2$ during the investigated time period). The average magnitude of the shift at high frequency corresponds to a velocity of ~540 m/sec, at low frequency ~460 m/sec; the total variation of the velocity is ~230 and 270 m/sec, respectively. Thus, each of the frequency channels of the radar sees its zone of formation of the signal.

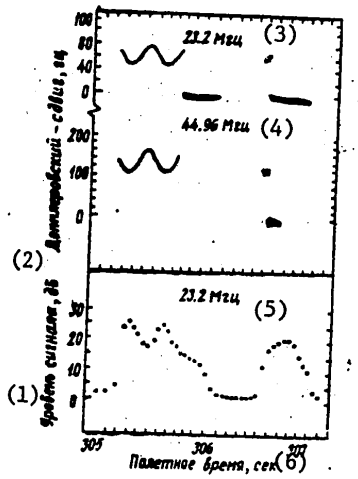

Figure 2. Doppler spectrum and amplitude of the reflected signal for the long and short injection pulse.

Key:

1. Signal level, db
2. Doppler shift, hertz
3. 23.2 megahertz
4. 44.96 megahertz
5. 23.2 megahertz
6. Flight time, sec

After switching off the electron gun the picture changes sharply. The Doppler shift becomes entirely significant with respect to magnitude. The signal decreases its intensity smoothly and disappears after some time. The average lifetime of the signal on low frequency is ~0.4 sec, and on high frequency, ~0.1 sec. This law is illustrated in Fig 3. Inasmuch as the lifetime of the high-frequency signal is commensurate with the time of establishment of the signal in the filter of the spectrum analyzer, the accuracy of measuring the ratio of the echo durations is no better than 30%.

Let us note that at high frequencies this signal is observed not after each injection pulse. This is connected with strong dependence of the amplitude of the first type of signal on the phase of rotation of the rocket. If the completion of injection coincides with minimum amplitude, the "residual" signal is not observed.

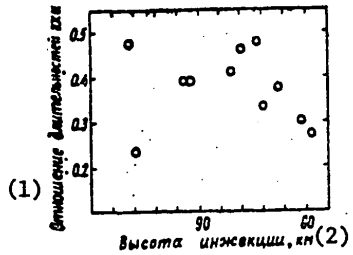

Figure 3. Ratio of the echo times on high and low frequencies

Key:
1. Duration ratio of the echo
2. Injection altitude, km

Let us discuss the second type of signal observed after switching off the electron gun. It also has a spectral line with a width that does not exceed several hertz. It is most probable that such a signal is formed as a result of reflection from dense secondary ionization caused by decay in the ionosphere of the primary electron beam injected from on board the rocket. A confirmation of the proposition of the mirror reflection is the lifetime of the signals and the ratio of their duration at different frequencies. In neglecting the confusion, the variation of the concentration in time from some initial level n_0 is subject to the law

$$n(t) = \frac{1}{1/n_0 + \alpha_{эфф} t}, \quad (1)$$

Key: 1. eff

where α_{eff} is the effective recombination coefficient. The lifetime $T_{1,2}$ of a dense flare with concentration $n>n_{1,2}$

$$T_{1,2} = \frac{1(1)}{\alpha_{эфф}} \cdot \left(\frac{1}{n_{1,2}} - \frac{1}{n_0}\right),$$

Key: 1. eff

hence $$\frac{T_1}{T_2} = \frac{n_2}{n_1} \frac{n_0 - n_1}{n_0 - n_2} \approx \frac{\omega_1^2}{\omega_2^2},$$

where $n_0 >> n_{1,2} \cdot \omega_1 \omega_2$ are the radar frequencies. This corresponds to the measured ratio of the echo durations. The recombination decay to $n_1 = 6.6 \cdot 10^6$ cm^{-3} (which corresponds to the critical frequency of 23.2 megahertz) for the time ~0.4 sec is insured for a recombination coefficient

$\alpha_{eff}=3.6\cdot10^{-7}$ cm^3sec^{-1}. In addition, it is somewhat extraordinary that the lifetime of the signal and, consequently, the recombination coefficient, in practice does not change on submersion of the rocket in the dense atmosphere in the altitude range from 95 to 78 km. This problem requires further study and explanation. The value of α_{eff} obtained from observing ionization decay, just as an average value for the given altitude range, does not contradict the data of other experimental measurements [2] (Fig 10).

It must be noted that the analogous ratio of the echo durations will be observed for scattering on weak nonuniformities decaying as a result of diffusion. Such nonuniformities, for example, could occur as a result of turbulent mixing of the atmosphere [4]. The characteristic scale of the observed nonuniformities here must be $L=(\lambda/2)(\sin(\theta/2))^{-1}$. Inasmuch as the spreading time $T\sim L^2/D$, where D is the diffusion coefficient, here again $(T_1/T_2)\alpha(\omega_2^2/\omega_1^2)$. However, taking the diffusion coefficient of ~10 m^2 sec^{-1}, at low frequency we obtain $T_1\sim5.6$ sec which differs from the observations significantly. Below we shall present another proof confirming the hypothesis of the nature of the reflection on the basis of the direct estimates of the dimensions of the flare and the density of the secondary ionization.

Effective Radius of the Secondary Ionization Flare. Let us take the delay in the occurrence of the reflections with respect to the beginning of the injection pulse of 0.02 sec as the initial value. This delay is established after 305 seconds of flight. The measurement of the delay for high frequency was performed by the observation data of A. Kh. Pyats' and Yu. F. Zarnitskiy from Prudovyy with more precise determination of the time scale of the recorders with respect to the beginning of the radio emission pulses. The accuracy of measuring the delay of 0.02 sec is no better than 50%.

The growth of the secondary ionization in the flare after switching on the injector

$$n(t)=\sqrt{\frac{q}{\alpha_{эфф}}}\cdot\frac{e^{2\sqrt{q\alpha_{эфф}}\,t}-1}{e^{2\sqrt{q\alpha_{эфф}}\,t}+1}, \qquad (1)$$

(1)

Key: 1. eff

where q is the ion formation rate. For a time of $t\leq0.02$ sec the approximation $n(t)=qt$ is suitable. The rate of ion formation can be calculated with some indeterminacy on the part of the longitudinal dimensions of the flare with respect to the known initial beam parameters. Indeed,

$$q=\frac{I\cdot k\cdot t}{e\cdot V}, \qquad (2)$$

where I is the beam current, K=E/30 is the coefficient taking into account the number of secondary electrons created by one primary, E is the energy of the primary electrons; $V=\pi r_b^2 z$ is the volume of the flare, assuming it

equivalent to a cylinder; r_b is the radius of the flare. For such approximate calculations within the limits of the entire flare q=const. From (2), knowing the delay in the occurrence of the signal and the value of n_0, let us determine the radius of the flare

$$r_b = \sqrt{\frac{Ikt}{\pi \cdot l z n_0}} \approx 9.1 \text{ m}. \quad (3)$$

The calculation of r_b by formula (1) decreases the radius of the flare to 8.7 m, which is insignificant for our accuracy. The length of the flare along the magnetic line of force is taken as $z=2 \cdot 10^3$ meters.

The growth of the concentration in the flare will continue for the time interval $\Delta t=2r_e/V_\perp$, where $V_\perp$ is the speed of the beam in the plane perpendicular to the magnetic lines of force. The actual magnitude of Δt for 303-305 seconds of flight is about 0.06 seconds. The maximum concentration which can be reached in that time, considering $\alpha_{eff}=4 \cdot 10^{-7}$ $cm^3 sec^{-1}$ is $4.9 \cdot 10^7$ cm^{-3}. Here and hereafter we shall use the value of α_{eff} calculated by the lifetime of the signal after switching off the beam. The performed estimates of the electron density in the flare also confirm the hypothesis of reflection of the signal by dense ionization.

Shape of the Flare, Concentration in the Loop, Decay of the Flare. On the basis of the discussed laws of the nature of growth and decrease in ionization, neglecting the diffusion and the electrodynamic processes of the drift and turbulization, maps have been constructed of the distribution of the ionization in the transverse cross section of the flare (perpendicular to the magnetic lines of force) for different points in time after the beginning of operation of the electron gun, see Fig 4. It is assumed that the injection is carried out in pulses with duration of 0.06 and 0.6 sec. The pictures for subsequent times denoted, for example, 0.6 to 0.1 sec and 0.6 to 0.4 sec, illustrate the decay of the flare 0.1 and 0.4 sec after switching off the gun. The points were used to plot the isolines of equal electron density every 2 decibels; the reckoning is done with respect to the level of 1.10^7 cm^{-3}. Thus, the level of +6 decibels corresponds to ionization of $4 \cdot 10^7$ cm^{-3}. Inasmuch as the concentration distribution in the transverse cross section of the flare is provisionally taken as rectangular, the variation of the concentration from the long side of the cross section is also sharp. This provisionalness must be taken into account for the interpretation.

For high frequency the critical value of the electron density is close to the +4 decibel level. Thus, here the flare has a relatively short loop. The total length of the flare along the velocity vector beam is ~30 meters; transverse cross section in accordance with the estimate of r_b is 18 m. For low frequency the flare acquires significant loop. Here the critical value of the density is ~-2 decibels; the flare length is ~120 meters; the width is 18 meters. After switching off the gun the length of the flare decreases sharply. After 0.1 seconds, the low-frequency radar sees the

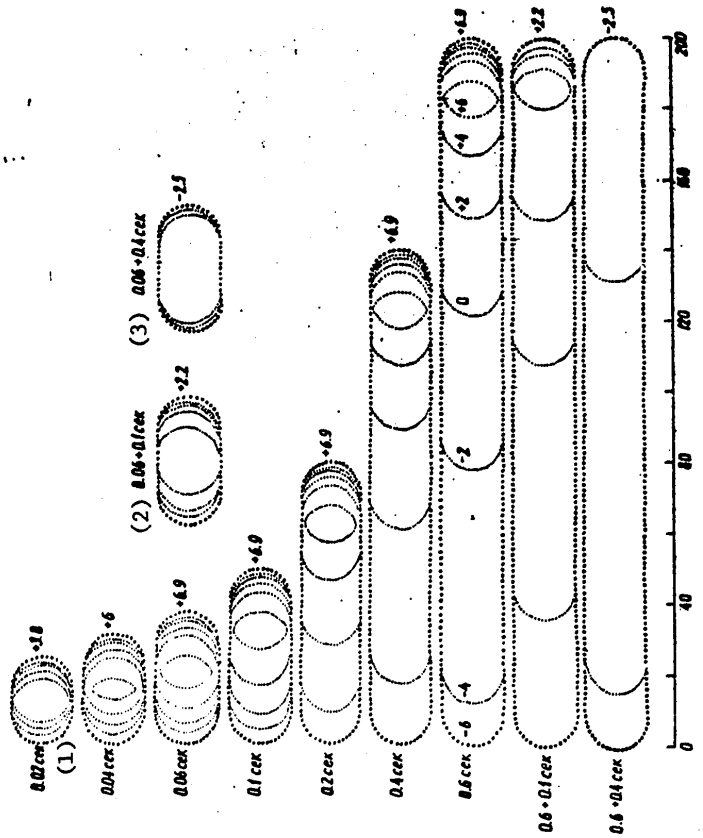

Figure 4. Maps of the ionization distribution in the plane orthogonal to the magnetic line of force for short (third row from the top) and long injection pulses. The zero time coincides with the beginning of operations of the gun. On the right the maximum value of the concentration is indicated; the isolines are drawn every 2 decibels; the reckoning is from the 10^7 cm^{-3} level. At the bottom is the scale of the maps which corresponds to the beam velocity of 300 m/sec.

Key:
1. sec; 2. 0.06 to 0.1 sec; 3. 0.06 to 0.4 sec

localized region near the rear edge of the beam (correspondingly, its position at the time of switching on the gun). For the low-frequency radar the loop is reduced to 90 meters. After 0.4 seconds, the ionization decreases below -4 decibels.

The significant loop of the flare, the length of which varies during the process of operation of the gun and movement of the rocket, determines the azimuthal anisotropy of the reflection which varies in time. It is obvious that the maximum signal will be observed for orientation of the beam normally to the surface of the loop.

In Fig 5 we have calculated the relations for the azimuthal anisotropy of reflection. For the calculations the diffraction effects were not taken into account which are significant for amplitudes near 0 and 180°. Here the transverse dimensions of the region participating in the coherent reflection are significantly greater than the wave length.

Reflection Indexes. In the plane passing through the magnetic line of force, the reflection index for a thin cylinder is

$$\sigma \alpha \left[\frac{\sin(Kz\sin\varphi)}{Kz\sin\varphi}\right]^2, \qquad (4)$$

where K is the wave length, z is the cylinder length, ψ is the aspect angle (the angle between the radial beam and the cylinder axis). Hence, the flare length can be estimated as $z \sim 0.44\lambda^*/\Delta$ $1.5 \cdot 10^3$ meters. Here $\lambda^* = \lambda(\sin(\theta/2))^{-1}$, Δ is the experimentally measured width of the reflection index. These index measurements turned out to be possible with respect to the current variation of the reflection amplitude during the flight time of the rocket through the point of orthogonal reflection (the point of the maximum signal) for 303.7 seconds of flight of the rocket. For low frequency this relation is shown in the lower part of Fig 6. In the upper part of the figure we have the curve for the current values of the aspect angle at the flight altitude of the rocket.

Unfortunately, the estimates of the observed and calculated values of the reflection cross sections differ noticeably. The cross sections were calculated on the basis of the above-discussed estimates of the shape and the dimensions of the flare. Then for the known area of the coherent reflection A the effective cross section $\sigma = 4\pi A^2/\alpha$. The low value of the observed signal could be explained by the roughness of the flare as a result of various plasma instabilities during the injection time. However, the nonfluctuating nature of the 23.2 megahertz signal with picture is the most convenient for interpretation, does not support this hypothesis. It is most probable that the greater part of the noncorrespondence is due to the equipment effects with significant buildup of the signal amplitude. Actually, the recorder was designed for reception and recording of relatively weak signals observed for high injection altitude.

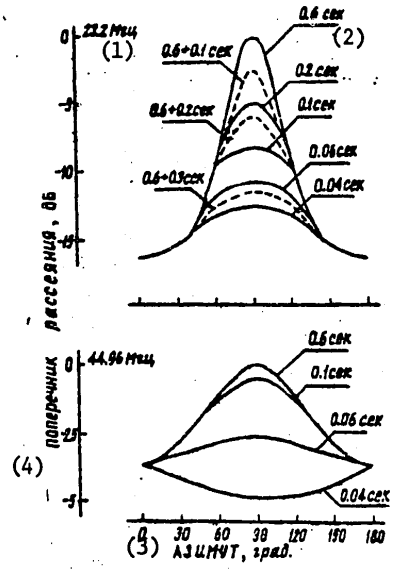

Figure 5. Reflection cross sections as a function of observation azimuth.
Solid lines -- different times of beam injection; dotted lines -- injection switched off. Observation azimuth -- angle between the vector $\vec{R}=\vec{R}_2-\vec{R}_1$ and the plane passing through the vectors $\vec{B}$ and $\vec{V}_B$.

Key:
1. megahertz
2. sec
3. Azimuth, degrees
4. Scattering cross section, decibels

Estimation of the Background Concentration of the Ionosphere Plasma. The maximum reflection amplitude on the frequency of 23.2 megahertz has been observed at 303.7 seconds of flight (see Fig 6). This clearly does not correspond to the zero value of the aspect angle. In addition, the latter function was calculated for the current altitude of the rocket although the flare is located somewhat lower. The dotted lines, the upper solid line in the upper part of Fig 6, indicate the values of the aspect angle expected for the point 2 km below the rocket. Thus, the noncorrespondence between the maximum amplitude and the zero value of the aspect angle increases to 0.7°, which can be explained by the ionospheric refraction which distorts the trajectory of the radio beam almost before the "encounter" with the flare itself. A significant argument in favor of the refraction distortion is the positive sign of the rotation of the beam which is characteristic of ionospheric refraction (on the lower edge of the ionosphere). Inasmuch as the angle of refraction rotation of the beam does not depend on the

concentration profile but is determined only by the initial and final values of the refraction coefficient, here we obtain the possibility of the inverse calculation of the background concentration directly next to the flare.

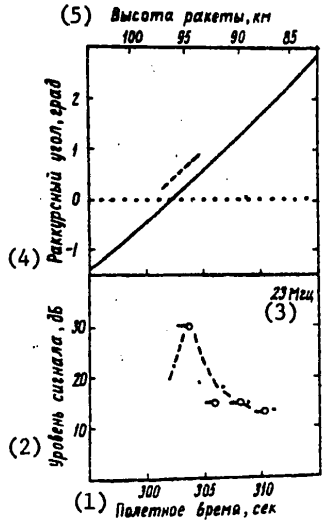

Figure 6. Variation of the aspect angle and amplitude of the 23.2 megahertz signal with time.
The dots on the amplitude curve are the short injection pulses, and the circles with dots are the long injection pulses.

Key:
1. Flight time, sec
2. Signal level, decibels
3. 23 megaherts
4. Aspect angle, degrees
5. Rocket altitude, km

For known coordinates of the transmitter, the receiver and the reflection point calculation presents no theoretical complexity. If a_x, a_y, a_z are the unit vectors of the vector $\vec{K}$ at the reflection point, and b_x, b_y, b_z are the unit vectors of the magnetic line of force, the angle between the vectors $\psi=\arccos(a_xb_x+a_yb_y+a_zb_z)$. For some concentration near the flare, each of the beams changes angle to the horizontal plane at the reflection point in accordance with Snell's law $n_2\cos\alpha_1^*=\cos\alpha_1$. Here α_1 is the beam angle with respect to the horizontal plane neglecting refraction; α_1^* is the beam angle considering refraction. The refraction coefficient is calculated from the ordinary expression

$$n_2=\left[1-\frac{4\pi e^2 n_e}{m(\omega^2+\nu^2)}\right]^{0.5},$$

e and m are the electron charge and mass, ν is the effective frequency of the collisions; outside the ionosphere it is assumed that $n_1=1$. Calculating the distortions of each of the beams in accordance with the values of $\alpha_1(t)$ and $\alpha_1(r)$, we find the new unit vectors a'_x, a'_y, a'_z and the angle ψ'. The indexes t and r refer to the beams from the transmitter and the

receiver, respectively. With the same accuracy with which we can know the position of the magnetic line of force, we find that the background concentration $n_\phi = 5 \cdot 10^4$ cm^{-3}. For an altitude of 92-93 km in the middle latitudinal ionosphere at night this turns out to be somewhat high. It is most probable that this is caused by the error of 0.15-0.2° in the data on the position of the line of force (basically its inclination). With an increase in the inclination by 0.15° the concentration becomes $4 \cdot 10^4$ cm^{-3}. When determining the background concentration by independent means the discussed procedure permits highly accurate determination of the actual position (inclination) of the line of force directly next to the flare.

Spectral Observations of the Motion of the Flare. As was noted, the Doppler shifts of the reflections with beam switched off are solved. Fig 7 shows the altitude behavior of the drift velocity component along the direction of the vector K constructed by the data from simultaneous measurements using two radars. In contrast to the above-noted effects during operation of the beam, here the Doppler shifts are mutually joined satisfactorily. The altitude of the measurements was taken equal to the rocket altitude. The obtained velocity distribution can be interpreted as the altitude profile of the ionospheric wind. In addition, here we are dealing with "strong" nonuniformities in which the concentration is appreciably greater than the background concentration. The dimensions of the nonuniformities are tens and hundreds of meters. The quite complete solution of the problem of the movement of such nonuniformities in the D-region is unknown to the authors. However, on the part of the wind measurements and the behavior of the "strong" nonuniformities the situation is similar to that which occurs when observing the overdense ionized meteor trails. In addition, the actual values of the wind velocity and the altitude gradients of the velocity [5] confirm our hypothesis of a wind nature of the altitude behavior of the Doppler shift.

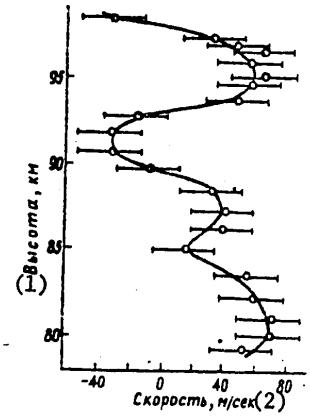

Figure 7. Altitude section of the wind velocity projection in the direction of the vector $\vec{K}=\vec{K}_2-\vec{K}_1$.

Key:
1. Altitude, km
2. Velocity, m/sec

In conclusion, the authors express their appreciation to Yu. G. Miroshnikov, Yu. P. Dukosyak, P. I. Yakovlev and G. S. Stepanov, who prepared and performed the observations, Ye. Ye. Timofeyev for participation in the calculations, and Yu. L. Sverdlov for attention to the work and for cooperation in the performance of it. The authors are grateful to A. Kh. Pyatsi and Yu. F. Zarnitskiy for offering the possibility of using the observation data from Prudovyy, and Yu. F. Zarnitskiy also for discussion of the topic.

BIBLIOGRAPHY

1. Cambou, P.; Dokukin, V. S.; Ivchenko, V. N. Managadze, G. G.; Migulin, V. V.; Nazarenko, G. K.; Nesmyanovitch, A. T.; Pyatsi, A. Kh.; Sagdeev, R. Z.; Zhulin, I. A. "The Zarnitsa Rocket Experiment on Electron Injection," 18th Plenary meeting of COSPAR (program and abstracts), Brazil, 1974, paper 11.1.7, SPACE RESEARCH, XV, Academie-Verlag, Berlin, 1975, pp 491-500.

2. Dokukin, V. S. "Zarnitsa Experiment (Problems, Composition, Basic Results)," DINAMIKA KOSMICHESKOY PLAZMY [Dynamics of Cosmic Plasma], Moscow, izd. IZMIRAN, 1976, pp 136-144.

3. Watt, T. M.; Newkirk, L. L.; Shelley, E. G. "Joint Radar-Satellite Determination of Effective Recombination Coefficient in the Auroral E-region," JGR, Vol 79, No 31, 1974, pp 4725-4731.

4. Gershman, B. N. DINAMIKA IONOSFERNOY PLAZMY [Dynamics of the Ionospheric Plasma], Moscow, Nauka, 1974, pp 130-138.

5. Spizzikino, A. "Wind Measurement Using Radar Observation of Meteor Trails over Europe," TERMOSFERYNAYA TSIRKULYATSIYA [Thermospheric Circulation], Moscow, Mir, 1975, pp 120-177.

[8144/1072-10845]

10845
CSO: 8144/1072

SURFACE RADIOPHYSICAL OBSERVATIONS OF THE LEAKAGE OF PARTICLES IN A MAGNETICALLY CONJUGATE REGION IN THE NORTHERN HEMISPHERE IN THE SOVIET-FRENCH 'ARAKS' EXPERIMENT

Apatity ISSLEDOVANIYA PROTSESSOV V AVRORAL'NOY IONOSFERE METODAMI AKTIVNOGO VOZDEYSTVIYA in Russian 1978 pp 89-96

[Article by Yu. F. Zarnitskiy, A. Kh. Pyatsi, Yu. L. Sverdlov]

[Text] The ground observations in the experiment with artificial injection of high-energy electrons into the ionosphere ("Zarnitsa" experiment) demonstrated that the meteor-range pulse radar can be used successfully to record the intrusion of these electrons into the E-region of the ionosphere. However, the detection of the signals reflected by the region of the ionosphere subjected to the effect of the intruding particles (and, hence, intrusion detection), is possible only under the condition that the aspect effect characteristic of the scattering of radio waves analogous to the aspect effect observed during auroral scattering at high latitude is taken into account when organizing the observations: the backscattering of the radio waves is most intense when the radio beam is orthogonal to the earth's magnetic field.

Fig 1 shows the position of the pulse radar, and the zones plotted in which intrusion of the electrons was expected during the periods of the first and second rocket launches in the "Araks" experiment. The same figure shows the isolines of the aspect angles (the angles of the deviations from the normal to the magnetic field of the earth of the radar beam at an altitude of 110 km) calculated without considering refraction.

The width of the antenna radiation pattern in the horizontal plane with respect to the 3 decibel level was 12°, which made it possible to cover in practice the entire region of the expected particle intrusion on the first launch. During this launch (26 January 1975), the radar antenna was oriented along the 12.5° azimuth (indicated by the arrow in Fig 1). During the period of the second launch (15 February 1975), rotation of the antennas to the east by 5° was planned. Up to 195 seconds after launch it was oriented along the 21.5° azimuth, and after 195.2 sec, along the 26.5° azimuth.

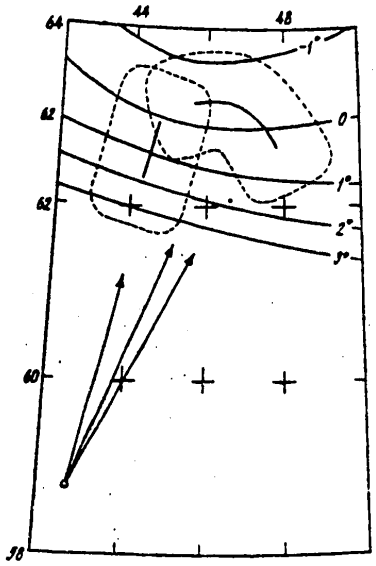

Figure 1. Position of the pulse radar with respect to the zones of expected particle intrusion in the northern hemisphere during the periods of the northern and eastern launches. The solid lines represent the isolines of the equal angles at the deviation from the normal to the magnetic field of the earth of the radio beams at an altitude of 110 km calculated without considering refraction. The arrows indicate the direction of the antenna in the horizontal plane.

For the observations the pulse radar was used with the following parameters: operating frequency 43.8 megahertz, duration of the sounding pulses 8 microseconds, frequency of their repetition 100 pulses/sec, power of the transmitter per pulse 80 kilowatts. The direction in which the gain of the antenna in the vertical plane is maximum was such as to insure optimal conditions for the reception of reflections from an altitude of 110 km from the zones of the expected particle intrusion. In order to insure continuity of the recording, use was made of the brightness display on the oscillograph screen which was photographed by a movie camera with continuous winding of the film, and the antenna was left stationary.

During the first and second launches, the occurrence of reflecting formations was recorded in the regions of expected intrusion of the particles. The evolution of these reflecting formations in time and their displacements in space were clearly connected with the nature of the operation of the guns on board the "Eridan" rockets and with the movement of the rockets themselves.

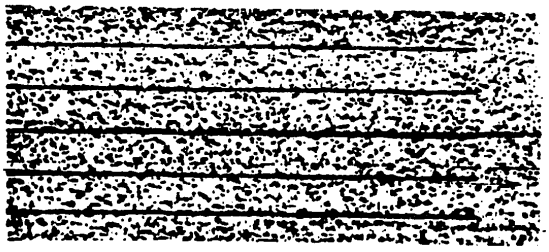

Figure 2. Example of the recording of a reflected signal during the first launch

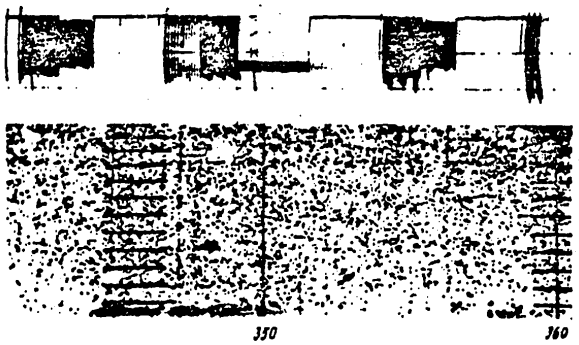

Figure 3. Example of recording of a reflected signal on the second launch.

An example of recording the reflected signal during the first launch is presented in Fig 2, and the second launch, in Fig 3.

The signal was more intense during the first launch. This is connected primarily with the fact that the region of intrusion of the particles on this launch was closer than in the second launch. Therefore the characteristics of the particle eruptions in the northern hemisphere and their relation to the operation of the gun can be discovered by the results of the radiophysical observation during the first launch (26 January 1975).

Fig 4 shows the slant range to the reflecting formations as a function of time reckoned from the time of launching the rocket during the first launch period. A more detailed relation of the reflection characteristics to the gun operation is seen in Fig 5. This figure shows the variation in time of the slant range to the reflecting formations occurring in the 14 operating cycle of the gun (13 kev), and the dependence of the reflected signal level on time obtained by photometric recording of a movie film with brightness

recording of the signal. The echo in this cycle occurred initially at a slant range of 432.8±1 km with a delay with respect to the beginning of the injection upward (along the axis of the rocket) of 2.6 sec. During the time equal to approximately the total injection time on the rocket axis -- 3.84 sec -- a tendency toward a decrease in the slant range was observed. Then this trend stopped, and the reflections continued with breaks approximately for 13 seconds out of the range interval equal to displacement of the rocket across the earth's magnetic field for 3.84 seconds. The value of this slant range fluctuated very rapidly within the limits of this interval (2.3 km).

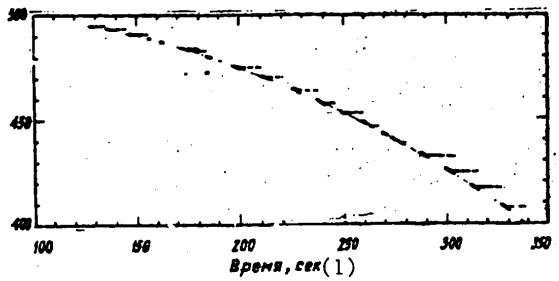

Figure 4. Slant range to the reflecting formations occurring as a result of operation of the gun as a function of time reckoned from the time the rocket was launched to the first firing peiod.

Key: (1) time, sec

Approximately 2.5 sec after the beginning of injection along the rocket axis in the next (15th) cycle the reflecting formation occurred on a range of 425.8 km, that is, for the period approximately equal to the injection cycle -- 12.8 seconds -- the slant range to the region of intrusion of the particles decreased by 7 km, which corresponds to displacement of the rocket across the magnetic field for 12.8 seconds. No reflections which could be related to the injection at an angle of 70° to the rocket axis were observed on the 14th cycle. It must be noted that for the injection of particles with an energy of 13 kv in general no such reflections were detected. For injection of the particles with an energy of 27 kev on the ascending part of the trajectory (during the period of the first few cycles), reflections were recorded which could be related to the injection at an angle of 70° to the rocket axis.

The data on the delay of the occurrence of the reflecting formations in the northern hemisphere with respect to the injection times on board the "Eridan" rocket are presented in Fig 6. For the injection time, the total injection time in the given direction with respect to the rocket axis was used. In cases, for example, where there were no breakdowns of the gun and the given injection mode was completely satisfied, the injection time of the rocket axis was made up of the injection time of 32 short pulses (1.28 seconds) and a long unmodulated pulse (2.56 sec), that is, it was 3.84 seconds.

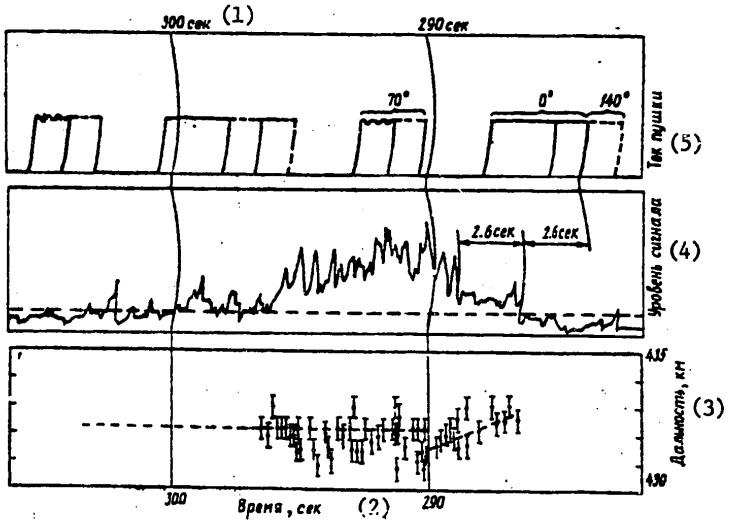

Figure 5. Slant range to the reflecting formatons and reflected signal level as a function of time during the 14th injection cycle. A diagram of the gun current is presented above.

Key:

1. sec
2. Time, sec
3. Range, km
4. Signal level
5. Gun current

During the period of injection of electrons with an energy of 27 kev the gun operated without breakdowns in practice for only one (II) cycle. The delay in this cycle was approximately 2.3 seconds. On the 14th, 15th and 16th cycles (13 kev) the delay was 2.52 to 2.64 seconds. The plasmogenerator was switched off before the 17th cycle. Obviously, this is connected with an increase in the delay to 3.5 seconds.

As a result of breakdowns of the gun in the electron injection mode with an electron energy of 27 kev there were cases where the injection time turned out to be less than 1 sec: 0.1 to 0.7 sec. In these cases delays were observed of 0.7 to 1.0 seconds.

Thus, it turned out that on injection of the electron beams with the parameters used in the "Araks" experiment the particle eruptions in the magnetically conjugate region occurred with anomalously large delays. It should be expected that on electron injection along the rocket axis, that is, with pitch angles of 10°, the particle eruption in the northern hemisphere had to occur with delays of about 0.6 and 0.8 sec, respectively, for particles with energies of 27 and 15 kev. However, with the exception of several cases of the injection of short pulses as a result of breakdowns of the gun, the delays turned out to be greater than expected by an amount somewhat exceeding the bounce period of the injected particles.

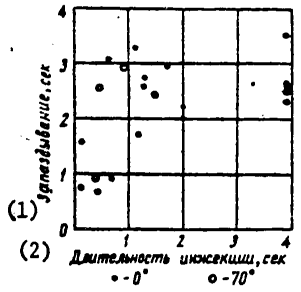

Figure 6. Delay in the occurrence of reflections (eruptions of particles) in the northern hemisphere with respect to the injection times on board the "Eridan" rocket in the northerly launch. 0° and 70° -- injection on the rocket axis and at an angle of 70° respectively.

Key:
1. Delay, seconds
2. Injection time, sec

In addition to the anomalously large delay, also a type of "aftereffect" was observed -- particle eruption from tubes of force disturbed during the injection time continued appreciably longer than the injection time -- by 10 or more seconds. Thus, on the 14th cycle the reflections from the range interval of 430.5 to 434 km during which the particles were injected along the rocket axis for 3.84 seconds, continued with some interruption for 16.8 sec. It is noteworthy that no particle eruptions from the range interval of 427.5 to 429 km, that is, from the tubes of force in which the particle injection was realized at an angle of 70° to the rocket axis, was detected in practice.

The observed cases of quite rapid variation of the slant range to the reflecting formation are of significant interest. For example, in the time interval of 286.8 to 286.92 sec (Fig 7) a short-term increase in the slant range by 3.5 km occurred. This variation of the slant range indicates that there are quite fast shifts in the region of intrusion of the particles perpendicularly to the earth's magnetic field. Indeed, in all probability the dispersion of the radiowaves connected with the particle eruptions with an energy of 13 kev occurs at an altitude of 110 km. The results of the observations during the first launch demonstrated that when the calculated deviation of the radio beam from the normal to the earth's magnetic field exceeded 2.5°, the intensity of the echo decreased below the detection threshold of the equipment. If we propose that the observed variation of the slant range is connected with variation of the position of the scattering region along the magnetic field (along the line of force) and not across it, this leads to an increase in deviation of the radio beam from the normal to the magnetic field to 14.5° and variation of the altitude (an increase in it) by 55 km.

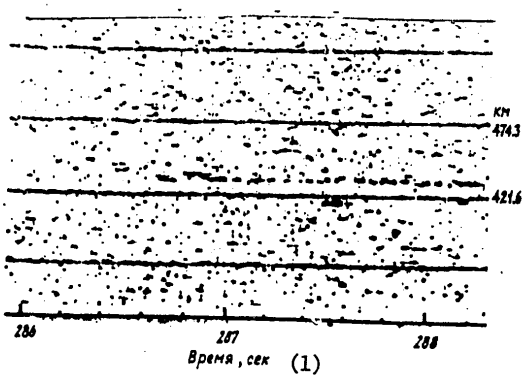

Figure 7. Example of the short fast variation of the slant range to the particle eruption region.
In 60 milliseconds the reflecting region at an altitude of about 110 km was shifted perpendicularly to the earth's magnetic field by 3.5 km to the north, and then at the same time it returned to the initial position.

Key:
1. Time, sec

The probability of recording the scattering of the radiowaves with such deviations from orthogonalness is negligible.[1] In addition, the auroral scattering under natural conditions occurs below 135 km. Thus, the case presented in Fig 7 indicates that from 286.8 to 286.92 seconds brief displacement of the region of intrusion of the particles across the magnetic field was observed with a velocity reaching 58 km/sec in the northerly direction at an altitude of 110 km: the reflecting region shifted in 60 milliseconds at an altitude of 110 km to the north by 3.5 km, and then in the same time it returned to the initial position.

The experimentally observed, quite fast shift of the reflecting formations across the magnetic field, which is of independent interest, permits some conclusion to be drawn about the aftereffects. From the case presented in Fig 7, it is obvious that the reflecting formation, shifting to the north, occurs at each point in time at a new place. In the old location it can disappear after 20 milliseconds. Thus, the aftereffect is connected more with the fact that the particle eruption from the tubes of force disturbed previously as a result of operation of the gun continues with interruptions for some time, and it is not connected with the large lifetime of the dispersing formations.

[8144/1072-10845]

[1] A. Kh. Pyatsi, "Auroral Scattering of Radio Waves," RADIOAVRORA (Radio Aurora), Moscow, Nauka, pp 260-298, 1974.

10845
CSO: 8144/1072

-END-